ON THE FLOW INDUCED IN A THERMALLY STRATIFIED FLUID BY A SOURCE OF HEAT

by

Robert A. Knox

A.B., Amherst College
(1964)

SUBMITTED IN PARTIAL FULFILLMENT OF THE
REQUIREMENTS FOR THE DEGREE OF
DOCTOR OF PHILOSOPHY

at the

MASSACHUSETTS INSTITUTE OF TECHNOLOGY

and the

WOODS HOLE OCEANOGRAPHIC INSTITUTION

June, 1971

Signature of Author.....
Joint Program in Oceanography,
Massachusetts Institute of Technology-
Woods Hole Oceanographic Institution,
and Department of Earth and Planetary
Sciences, and Department of Meteorology,
Massachusetts Institute of Technology,
June, 1971

Certified by.....
Thesis Supervisor

Accepted by.....
Chairman, Joint Oceanography Committee
in the Earth Sciences, Massachusetts
Institute of Technology - Woods Hole
Oceanographic Institution

Lindgren
WITHDRAWN
MASS. INST. TECH.
JUN 6 1971
FROM
LIBRARIES

On the Flow Induced in a Thermally Stratified Fluid by a Source of Heat

by

Robert A. Knox

Submitted to the Joint Oceanographic Committee in the Earth Sciences, Massachusetts Institute of Technology and Woods Hole Oceanographic Institution, on May 7, 1971, in partial fulfillment of the requirements for the degree of Doctor of Philosophy.

ABSTRACT

The flow produced by an infinitely long horizontal heated strip in a thermally stratified fluid is examined theoretically. For strong stratification a long flat convection cell or tongue results. Profiles of velocity and temperature anomaly are displayed and contrasted with the profiles which would obtain if the temperature anomaly were only a passive tracer. The effects of small nonlinearities are computed by perturbation methods and the profile alterations thus produced are discussed.

A laboratory experiment set up to demonstrate the major features of this circulation is described. Qualitative agreement between theory and experiment is obtained, and certain of the predicted nonlinear effects are observed.

Thesis Supervisor..... Henry Stommel

Professor of Oceanography, Department of Meteorology, Massachusetts Institute of Technology

To Muff

for her steadfastness and much more

Acknowledgements

The list of people who have assisted me in this work is very long, and I hope I shall be forgiven if I forget to mention some of them. First and foremost I owe sincere thanks to Professor Henry Stommel. Most oceanographers know of his abundant scientific talent; perhaps fewer have had the benefit, as I have had, of his infectious enthusiasm, his words of encouragement in bad times, his wit and his kindness. He has been a most patient adviser, always willing to help but also always willing to let me try to do things on my own, and for this I am deeply grateful. I also wish to thank the other two members of my thesis committee, Professor Robert Beardsley and Dr. William Simmons. I have not asked them for numerous consultations nor have they pressed me, but when I wanted to talk to them they were there.

To many of my fellow graduate students, past and present, I am indebted for particular bits of aid and for general moral support. Dave Cacchione, Bruce Magnell, John Van Leer, and Chris Welch all have had useful suggestions on the design and construction of the experimental apparatus and all have given of their time to help in assembling it.

Discussions with Ants Leetmaa and Jim Sullivan clarified a number of my fuzzy mathematical notions. Dave Nergaard, while not a graduate student, has given me enough help with nuts-and-bolts matters at zero pay to qualify as one several times over.

I am grateful to the Ford Foundation for fellowship support during my first year and a half at M.I.T and to the Department of Meteorology for research assistantships thereafter. I am also thankful to the Woods Hole Oceanographic Institution for summer employment in 1965 and 1966. Funds for the thesis research came from the National Science Foundation under grants A01613 and A12773 and are gratefully acknowledged.

Finally, I would like to thank Professor Arnold Arons, now at the University of Washington, for starting all this, in a sense. When I arrived at Amherst as a freshman and began to take his introductory physics course I had no clear idea of what I wanted to study for the next four years, and as the semester wore on it became apparent that I had some very unclear ideas about physics. Unclear ideas were not treated lightly. They were invariably ferreted out in class, no matter how cleverly their owners tried to conceal them, and were banished with a swiftness that reduced some to despair. What remained were little nuggets

of solid understanding, and as these slowly accumulated and began to fit together the whole enterprise seemed more and more worth continuing, in college and beyond. If this thesis makes sense, it is in large measure due to my trying to live up to the standard of thought set before me in that classroom many years ago.

Table of Contents

	Page
Abstract	2
Acknowledgements	4
List of figures and tables	8
I. Introduction	11
II. Theory	14
III. Laboratory Experiment	76
IV. Concluding Remarks and Suggestions	105
Appendix I. Delta-function Sources	110
Appendix II. Full Linear Problem	114
Appendix III. Computer Program	120
Appendix IV. Influence of a Sidewall	124
Bibliography	128
Biographical note	130

List of Figures and Tables

Figure No.		Page
1	Geometry of the model.	15
2	Linear buoyancy layer temperature anomaly.	32
3	Linear buoyancy layer vertical velocity.	33
4	Linear buoyancy layer horizontal velocity.	35
5	Linear buoyancy layer streamlines.	36
6	Linear far field horizontal velocity.	38
7	Linear far field temperature anomaly.	39
8	Schematic profiles of $\bar{u}^{(0,1)}(s,z)$ and $\bar{u}^{(0,1)}(s+\delta s,z)$	42
9	Linear far field vertical velocity.	44
10	Linear far field streamlines and lines of constant temperature anomaly.	46
11	Nonlinear correction to buoyancy layer vertical velocity.	57
12	Nonlinear correction to buoyancy layer horizontal velocity.	59
13	Nonlinear correction to buoyancy layer temperature anomaly.	60
14	Nonlinear correction to buoyancy layer streamlines.	61
15	Nonlinear correction to far field horizontal velocity.	62
16	Total farfield horizontal velocity.	63
17	Nonlinear correction to far field temperature anomaly.	65

List of Figures and Tables (cont'd.)

Figure No.		Page
18	Total far field temperature anomaly.	66
19	Nonlinear correction to far field vertical velocity.	67
20	Nonlinear correction to far field streamlines.	68
21	Qualitative relationships between f(z) and its derivatives.	70
22	Diagram indicating choice of operating parameters.	79
23	Side view of the major pieces of apparatus.	82
24	Positions of thermocouple junctions in the upper plate.	84
25	Section through a sidewall showing construction.	87
26	Observed temperature distribution in the tank during the runs.	91
27	Observed horizontal velocity profiles for $\delta = 0.225$ and for $\delta = 0.9$.	95
28	Observed horizontal velocity profiles for $\delta = 3.6$.	96
29	Comparison between far field horizontal velocity due to $\exp(-z^2)$ source and rectangular source function.	102
30	Three profiles taken at different times after starting the forcing.	104

Table		
I	Numbers of zeroes in far field profiles.	43
II	Values of the nondimensional vertical distance between level of zero velocity and level of maximum velocity.	98

List of Figures and Tables (cont'd.)

Table		Page
III	Differences in level of zero velocity.	99
IV	Values of the maximum positive nondimensional velocity.	100

Chapter I Introduction

In descriptive oceanography, one often encounters references to "tongues," or long, thin horizontal bodies of water differing from surrounding water in some measured property, usually temperature and/or salinity. Indeed, since temperature and salinity can be measured more easily and precisely than velocity, such tongues are often taken to be evidence for the existence of similar tongues of velocity, i.e., slow flow along the axis of the observed tongue of temperature of salinity. The implicit idea is that temperature and salinity serve essentially as tracers or diffusive substances carried along by the flow but playing no part in its dynamics. If the water in the tongue is, say, saltier than the surrounding water, salt would be expected to diffuse outward, leading to a decrease in salinity in the downstream direction, and knowledge of the horizontal salinity gradient in the tongue then determines the direction of flow. Some examples of tonguelike distributions of properties calculated by assuming particular flow patterns are given by Defant (1961) and by Sverdrup, Johnson, and Fleming (1942). Many authors have made application of such ideas to field observations in attempts to determine

flow patterns. Wüst (1959, 1960, 1961) for example has given extensive descriptions of the hydrography and inferences about the flow of the Levantine Intermediate Water in the Mediterranean Sea. This is a subsurface tongue of hot, salty water emanating from the eastern basin of the Mediterranean which extends westward past Gibraltar and forms the well-known Mediterranean outflow that is observed far into the Atlantic.

On the other hand, temperature and salinity are not true tracers; these properties affect the density of seawater and thus can influence the dynamics.. One then wonders how tongues in which density diffusion is important might behave. Some work in this connection has been done. Koh (1966) considered a source of mass in a stratified fluid both theoretically and experimentally. His model balances the diffusion of density against the (linear) advection of the mean density. Because he used salt, which has extremely low diffusivity, as the stratification agent and yet let his experiments run only a very short time (5 - 10 min.) there is some doubt that a truly steady flow with dynamically important diffusion of density was actually obtained. List (1971) has given some calculations of the flows produced by sources of momentum in a weakly stratified fluid. Both Koh and List have limited their theoretical work to the linear problem. Wunsch (1970) has dissussed

flows driven in stratified fluids by boundary temperatures which differ from those in the interior. His interest has been primarily in effects near the boundary and he has focused on the properties of a nondivergent buoyancy layer at the boundary; no "tongue" is forced into the fluid interior in this case.

In this thesis we examine both theoretically and experimentally a very simple case of a tongue in which diffusion of density is of paramount importance. The mathematical model is of a thermally stratified fluid in which an infinitely long horizontal strip is heated slightly above the mean temperature. In chapter II we solve for both the linear motion and the first nonlinear corrections, presenting plots of the results in some detail and noting the ways in which the velocity and temperature anomaly profiles differ from those one would expect if temperature were a passive tracer. In chapter III we present results of a laboratory experiment set up to demonstrate this circulation. The results are rough but tend to confirm important aspects of the theory. Chapter IV contains a brief summary and some suggestions for extension of the work.

Chapter II Theory

Formulation

In this chapter we examine a very simple mathematical model of a long horizontal tongue produced in a thermally stratified fluid by a source of heat. We consider an infinitely deep, nonrotating, Boussinesq fluid bounded by a single vertical rigid wall at x = 0 as shown in figure 1. In the absence of motion a mean stable temperature T_m, linear in z, is assumed to exist:

$$T_m(z) = T_o + \gamma z \qquad \text{(II-1)}$$

where γ and T_0 are positive constants. Fluid motion introduces perturbations of this mean field, and the total temperature $T^{(t)}$ is written as the sum of T_m and an anomaly T:

$$T^{(t)} = T_m + T \qquad \text{(II-2)}$$

A two-dimensional heat source is modelled by imposing a simple boundary condition on T:

$$T(0,z) = T_s f(z) \qquad \text{(II-3)}$$

Here T_s is some positive constant and f(z) is a dimension-

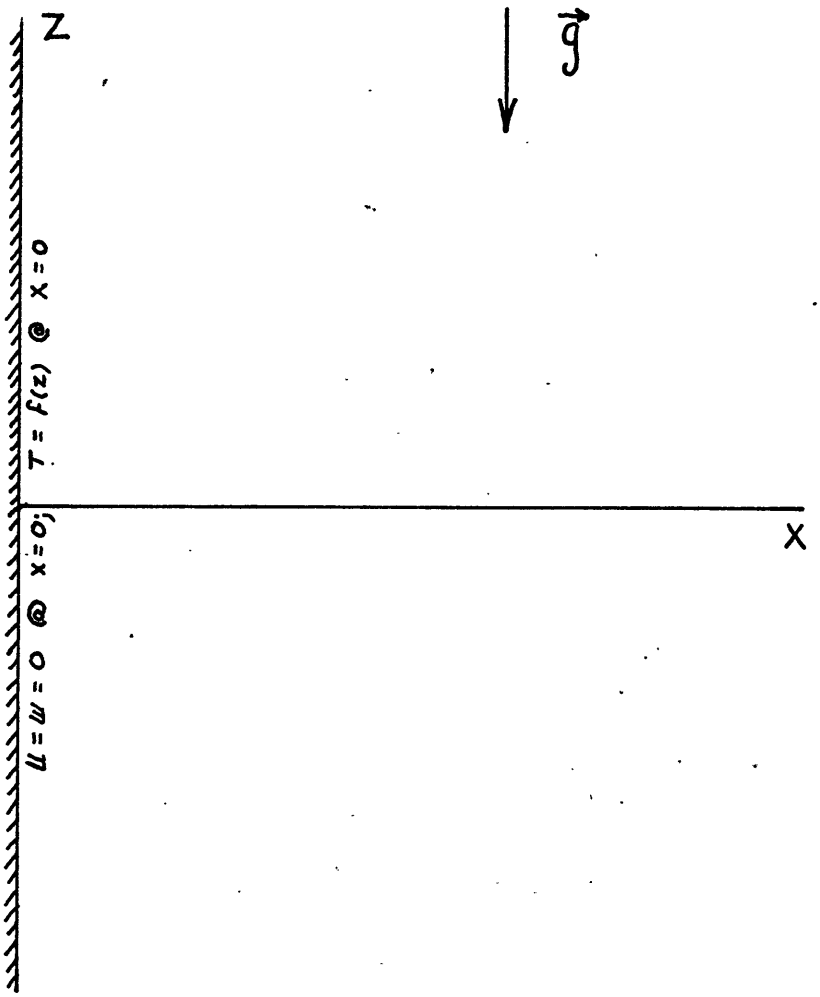


Figure 1 Geometry of the model.

less form function intended to specify a localized source. Specifically, we require of f:

$$f(z) = f(-z) \tag{II-4}$$

$$|f(0)| = 1 \tag{II-5}$$

$$\left|\int_{-\infty}^{\infty} f(z)\,dz\right| = O(1) \tag{II-6}$$

$|f|$ decays smoothly as $|z| \to \infty$ and has an e-folding length L (II-7)

Thus L is the length scale of the region over which forcing is applied to the fluid. It is the only externally imposed length in the problem and will be used to nondimensionalize the governing equations. One might expect that such a localized source would produce, at large x, the same effects as a delta-function source, i.e., a source for which

$$T(0,z) \propto \delta(z) \tag{II-8}$$

This matter is discussed in appendix I.

We assume the motion, like the source, to be steady and two-dimensional, and we assume the Boussinesq approximation to hold. The governing equations then are the x and z

momentum equations:

$$u u_x + w u_z = -\frac{1}{\rho_0} p_x^{(t)} + \nu \nabla^2 u \qquad \text{(II-9)}$$

$$u w_x + w w_z = -\frac{1}{\rho_0} p_z^{(t)} - \frac{g}{\rho_0} \rho^{(t)} + \nu \nabla^2 w \qquad \text{(II-10)}$$

the continuity equation:

$$u_x + w_z = 0 \qquad \text{(II-11)}$$

the heat equation:

$$u T_x^{(t)} + w T_z^{(t)} = \kappa \nabla^2 T^{(t)} \qquad \text{(II-12)}$$

and an equation of state:

$$\begin{aligned} \rho^{(t)} &= \rho_0 [1 - \alpha (T^{(t)} - T_0)] \\ &= \rho_0 [1 - \alpha (\gamma z + T)] \end{aligned} \qquad \text{(II-13)}$$

where:

$$\nabla^2 = \frac{\partial^2}{\partial x^2} + \frac{\partial^2}{\partial z^2} \qquad \text{(II-14)}$$

Here $p^{(t)}$ is the total pressure, $\rho^{(t)}$ the total density, ρ_0 the density at $T^{(t)} = T_0$, u and w the fluid velocities in the x and z directions respectively, g the acceleration of

gravity, ν the kinematic viscosity, κ the thermal diffusivity, and α the coefficient of thermal expansion. ρ_o, ν, κ, α, and g are assumed constant. We write $p^{(t)}$ as the sum of a hydrostatic part independent of the motion and an anomaly p:

$$p^{(t)} = -\rho_o g z + \tfrac{1}{2} g \rho_o \gamma \alpha z^2 + p \qquad \text{(II-15)}$$

We now introduce essentially the same nondimensionalization scheme used by Veronis (1967a, b) in studies of the analogy between stratified, nonrotating fluids and homogeneous, rotating fluids. We nondimensionalize x and z with L, p with a typical weight per unit volume due to density anomalies $\rho_o \alpha g L T_s$, and T with T_s. u and w are nondimensionalized with $\sqrt{\frac{T_s/L}{\gamma}}\sqrt{\frac{g\alpha L T_s \kappa}{\nu}}$. The first radicand is a measure of the source strength and the second is proportional to the pressure anomaly scale. With these scales the set of equations (II-9) - (II-13) becomes:

$$\frac{\delta}{\sigma}(u u_x + w u_z) = -p_x + \epsilon^2 \nabla^2 u \qquad \text{(II-16)}$$

$$\frac{\delta}{\sigma}(u w_x + w w_z) = -p_z + T + \epsilon^2 \nabla^2 w \qquad \text{(II-17)}$$

$$u_x + w_z = 0 \qquad \text{(II-18)}$$

$$\delta(u T_x + w T_z) = -w + \epsilon^2 \nabla^2 T \qquad \text{(II-19)}$$

In (II-16) - (II-19) and in what follows unless otherwise noted, all variables are nondimensional and all derivatives are with respect to nondimensional coordinates. The equation of state has been used to eliminate the density anomaly. The parameters appearing in the equations are:

$\delta = \frac{T_s/L}{\gamma}$ is the ratio of a typical gradient of temperature anomaly to the mean temperature gradient and is thus a measure of the source strength.

$\epsilon^2 = \left(\frac{\kappa\nu}{g\alpha\gamma L^4}\right)^{1/2}$ is the inverse square root of a Rayleigh number based on the mean temperature gradient and L.

$\sigma = \frac{\nu}{\kappa}$ is the Prandtl number.

In what follows we shall take δ and ϵ to be small and $\sigma = O(1)$. We are thus studying the motion produced by a weak source in a strongly stratified fluid with both viscosity and heat conduction acting to dissipate the flow. The boundary conditions to be satisfied are:

$$u(0,z) = w(0,z) = 0 \qquad \text{(II-20)}$$

$$T(0,z) = f(z) \qquad \text{(II-21)}$$

$$u, w, p, T \to 0 \text{ as } \sqrt{x^2 + z^2} \to \infty \qquad \text{(II-22)}$$

Linear problem

To solve (II-16) - (II-22) we adopt a perturbation scheme. We first solve the linear problem obtained by setting $\delta = 0$ and then we calculate the lowest order effects of finite nonlinearities by perturbing in δ. With $\delta = 0$ (II-16) - (II-19) can be reduced to a single equation in any of the dependent variables:

$$\left(\epsilon^4 \nabla^6 + \frac{\partial^2}{\partial x^2}\right)\begin{Bmatrix} u \\ w \\ p \\ T \end{Bmatrix} = 0 \qquad \text{(II-23)}$$

An exact solution of (II-23), valid for any finite value of ϵ, can be obtained by Fourier techniques. The result is unwieldy and we present only a brief sketch of this approach in appendix II. List (1971) has used a combination of Fourier analysis, contour integration, and numerical computation to solve a similar problem and present results for ϵ of order 1. In our case ϵ is small and boundary layer techniques yield more readily interpretable results with less effort. We rescale the x coordinate to reveal the various possible balances between the several terms of (II-23). Let θ stand for any of the dependent variables and let:

$$X = \epsilon^n \lambda \quad ; \quad \frac{\partial}{\partial x} = \epsilon^{-n} \frac{\partial}{\partial \lambda} \tag{II-24}$$

Then (II-23) becomes:

$$\epsilon^4 \left\{ \underbrace{\frac{\partial^6 \theta}{\partial z^6}}_{a} + \underbrace{3\epsilon^{-2n} \frac{\partial^6 \theta}{\partial z^4 \partial \lambda^2}}_{b} + \underbrace{3\epsilon^{-4n} \frac{\partial^6 \theta}{\partial z^2 \partial \lambda^4}}_{c} + \underbrace{\epsilon^{-6n} \frac{\partial^6 \theta}{\partial \lambda^6}}_{d} \right\} + \underbrace{\epsilon^{-2n} \frac{\partial^2 \theta}{\partial \lambda^2}}_{e} = 0 \tag{II-25}$$

The only possible balances are:

1. For n = 1 term d balances term e.
2. For n = -2 term a balances term e.

Other balances are ruled out as follows. A balances of any two of the terms a, b, c, and d requires n = 0. But then these terms are $O(\epsilon^4)$ while term e is O(/) and must therefore vanish by itself. Thus

$$\theta = C_1(z)\lambda^2 + C_2(z)\lambda + C_3(z) \tag{II-26}$$

and to have θ decay as $\sqrt{x^2 + z^2} \to \infty$ we must take $c_1 = c_2 = c_3 = 0$. The only remaining possibilities are to balance term e with either term b or term c. A balance with b requires $-2n = -2n + 4$, which is impossible. A balance with c requires n = 2. But then term d is the largest term, $O(\epsilon^{-8})$, and must itself vanish. This leads

to

$$\theta = \sum_{j=1}^{6} a_j(z)\, x^j \qquad \text{(II-27)}$$

and as in (II-26) the a_j must vanish. Thus all balances except 1 and 2 are impossible.

Balance 1 obtains when θ varies by O(1) over the short horizontal distance $x = O(\epsilon)$ and is commonly known as a buoyancy layer. We can expect such a balance to be important near the source in adjusting the dependent variables to their prescribed values at $x = 0$. Balance 2, in which θ varies by O(1) over the large horizontal distance $x = O(\epsilon^{-2})$, governs the flow far from the source and we refer to this region as the far field. More formally, we write any dependent variable as the sum of a buoyancy layer component and a far field component, denoted by a caret and by an overbar, respectively:

$$\theta = \hat{\theta}(\xi, z) + \bar{\theta}(s, z) \qquad \text{(II-28)}$$

where

$$\xi = \frac{x}{\epsilon} \quad ; \quad s = x\epsilon^2 \qquad \text{(II-29)}$$

Introducing (II-28) and (II-29) into (II-16) - (II-19) (with $\delta = 0$) the equations for the buoyancy layer components in the linear problem are:

$$0 = -\frac{1}{\epsilon}\hat{p}_{\xi}^{(0)} + \hat{u}_{\xi\xi}^{(0)} + \epsilon^2 \hat{u}_{zz}^{(0)} \qquad \text{(II-30)}$$

$$0 = -\hat{p}_{z}^{(0)} + \hat{T}^{(0)} + \hat{w}_{\xi\xi}^{(0)} + \epsilon^2 \hat{w}_{zz}^{(0)} \qquad \text{(II-31)}$$

$$0 = \frac{1}{\epsilon}\hat{u}_{\xi}^{(0)} + \hat{w}_{z}^{(0)} \qquad \text{(II-32)}$$

$$0 = -\hat{w}^{(0)} + \hat{T}_{\xi\xi}^{(0)} + \epsilon^2 \hat{T}_{zz}^{(0)} \qquad \text{(II-33)}$$

where the superscript 0 indicates that these are fields of order zero in δ. Similarly, we have the far field equations:

$$0 = -\bar{p}_{s}^{(0)} + \bar{u}_{zz}^{(0)} + \epsilon^4 \bar{u}_{ss}^{(0)} \qquad \text{(II-34)}$$

$$0 = -\bar{p}_{z}^{(0)} + \bar{T}^{(0)} + \epsilon^2 \bar{w}_{zz}^{(0)} + \epsilon^6 \bar{w}_{ss}^{(0)} \qquad \text{(II-35)}$$

$$0 = \epsilon^2 \bar{u}_{s}^{(0)} + \bar{w}_{z}^{(0)} \qquad \text{(II-36)}$$

$$0 = -\bar{w}^{(0)} + \epsilon^2 \bar{T}_{zz}^{(0)} + \epsilon^6 \bar{T}_{ss}^{(0)} \qquad \text{(II-37)}$$

The boundary conditions on (II-30) - (II-37) are:

$$\hat{u}^{(0)}(0,z) + \bar{u}^{(0)}(0,z) = \hat{w}^{(0)}(0,z) + \bar{w}^{(0)}(0,z) = 0 \qquad \text{(II-38)}$$

$$\hat{T}^{(0)}(0,z) + \bar{T}^{(0)}(0,z) = f(z) \qquad \text{(II-39)}$$

$$\hat{u}^{(0)}, \bar{u}^{(0)}, \hat{w}^{(0)}, \bar{w}^{(0)}, \hat{T}^{(0)}, \bar{T}^{(0)}, \hat{p}^{(0)}, \bar{p}^{(0)} \to 0 \text{ as } \sqrt{x^2+z^2} \to \infty \qquad \text{(II-40)}$$

We begin with the buoyancy layer equations. We expand each dependent variable in a power series in ϵ:

$$\hat{\theta}^{(0)} = \hat{\theta}^{(0,0)} + \epsilon \hat{\theta}^{(0,1)} + \epsilon^2 \hat{\theta}^{(0,2)} + \cdots \quad \text{(II-41)}$$

Then collecting coefficients of like powers of ϵ we find

terms in $\frac{1}{\epsilon}$

$$\hat{p}_{\zeta}^{(0,0)} = 0 \quad \text{(II-42)}$$

$$\hat{u}_{\zeta}^{(0,0)} = 0 \quad \text{(II-43)}$$

Then (II-42) and (II-43) together with (II-40) imply:

$$\hat{p}^{(0,0)} = \hat{u}^{(0,0)} = 0 \quad \text{(II-44)}$$

terms in ϵ^0

$$0 = -\hat{p}_{\zeta}^{(0,1)} + \hat{u}_{\zeta\zeta}^{(0,0)} \quad \text{(II-45)}$$

$$0 = -\hat{p}_{z}^{(0,0)} + \hat{T}^{(0,0)} + \hat{w}_{\zeta\zeta}^{(0,0)} \quad \text{(II-46)}$$

$$0 = \hat{u}_{\zeta}^{(0,1)} + \hat{w}_{z}^{(0,0)} \quad \text{(II-47)}$$

$$0 = -\hat{w}^{(0,0)} + \hat{T}_{\zeta\zeta}^{(0,0)} \quad \text{(II-48)}$$

Since $\hat{p}^{(0,0)} = 0$, (II-46) and (II-48) combine to give a

single equation in $\hat{w}^{(0,0)}$ or $\hat{T}^{(0,0)}$:

$$\left(\frac{\partial^4}{\partial \xi^4} + 1\right)\begin{Bmatrix}\hat{w}^{(0,0)} \\ \hat{T}^{(0,0)}\end{Bmatrix} = 0 \qquad \text{(II-49)}$$

(II-49) will be recognized as the Ekman equation. The solutions which decay in ξ and satisfy (II-46) and (II-48) are:

$$\hat{T}^{(0,0)} = e^{-\xi/\sqrt{2}}\left[F^{(0,0)}(z)\cos\xi/\sqrt{2} + G^{(0,0)}(z)\sin\xi/\sqrt{2}\right] \qquad \text{(II-50)}$$

$$\hat{w}^{(0,0)} = e^{-\xi/\sqrt{2}}\left[F^{(0,0)}(z)\sin\xi/\sqrt{2} - G^{(0,0)}(z)\cos\xi/\sqrt{2}\right] \qquad \text{(II-51)}$$

The functions $F^{(0,0)}$ and $G^{(0,0)}$ are to be determined. (II-47) gives the horizontal velocity required by continuity:

$$\hat{u}^{(0,1)} = -\int_0^{\xi} \hat{w}_z^{(0,0)}(\xi', z)\, d\xi' + \hat{u}^{(0,1)}_{(0,z)} \qquad \text{(II-52)}$$

Next we turn to the far field equations, (II-34) - (II-37). Making a power series expansion in ϵ as before we find:

terms in ϵ^0

$$0 = -\bar{p}_s^{(0,0)} + \bar{u}_{zz}^{(0,0)} \qquad \text{(II-53)}$$

$$0 = -\bar{p}_z^{(0,0)} + \dot{\bar{T}}^{(0,0)} \qquad \text{(II-54)}$$

$$0 = \bar{w}_z^{(0,0)} \qquad \text{(II-55)}$$

$$0 = \bar{w}^{(0,0)} \tag{II-56}$$

(II-53) and (II-54) give:

$$\bar{u}^{(0,0)}_{zzz} = \bar{\tau}_s^{(0,0)} \tag{II-57}$$

terms in ϵ^1

$$0 = -\bar{p}_s^{(0,1)} + \bar{u}^{(0,1)}_{zz} \tag{II-58}$$

$$0 = -\bar{p}_z^{(0,1)} + \bar{\tau}^{(0,1)} \tag{II-59}$$

$$0 = w_z^{(0,1)} \tag{II-60}$$

$$0 = \bar{w}^{(0,1)} \tag{II-61}$$

(II-58) and (II-60) give:

$$\bar{u}^{(0,1)}_{zzz} = \bar{\tau}_s^{(0,1)} \tag{II-62}$$

terms in ϵ^2

$$0 = -\bar{p}_s^{(0,2)} + \bar{u}^{(0,2)}_{zz} \tag{II-63}$$

$$0 = -\bar{p}_z^{(0,2)} + \bar{\tau}^{(0,2)} \tag{II-64}$$

$$0 = \bar{u}_s^{(0,0)} + \bar{w}_z^{(0,2)} \tag{II-65}$$

$$0 = -\bar{w}^{(0,2)} + \bar{T}_{zz}^{(0,0)} \qquad \text{(II-66)}$$

where (II-56) has been used to obtain (II-64). (II-65) and (II-66) give:

$$\bar{T}_{zzz}^{(0,0)} = -\bar{u}_s^{(0,0)} \qquad \text{(II-67)}$$

while (II-63) and (II-64) give:

$$\bar{u}_{zzz}^{(0,2)} = \bar{T}_s^{(0,2)} \qquad \text{(II-68)}$$

terms in ϵ^3

$$0 = -\bar{p}_s^{(0,3)} + \bar{u}_{zz}^{(0,3)} \qquad \text{(II-69)}$$

$$0 = -\bar{p}_z^{(0,3)} + \bar{T}^{(0,3)} \qquad \text{(II-70)}$$

$$0 = \bar{u}_s^{(0,1)} + \bar{w}_z^{(0,3)} \qquad \text{(II-71)}$$

$$0 = -\bar{w}^{(0,3)} + \bar{T}_{zz}^{(0,1)} \qquad \text{(II-72)}$$

where (II-61) has been used to obtain (II-70). (II-71) and (II-72) give:

$$\bar{T}_{zzz}^{(0,1)} = -\bar{u}_s^{(0,1)} \qquad \text{(II-73)}$$

Now from (II-57), (II-62), (II-67), and (II-73) we can derive:

$$\left(\frac{\partial^6}{\partial z^6} + \frac{\partial^2}{\partial s^2}\right) \begin{Bmatrix} \bar{T}^{(0,0)} \\ \bar{u}^{(0,0)} \\ \bar{T}^{(0,1)} \\ \bar{u}^{(0,1)} \end{Bmatrix} = 0 \qquad \text{(II-74)}$$

which is the form referred to as a far field balance above. Elementary solutions of (II-74) which tend to zero at large s are in the form of products of a decaying exponential in s and a trigonometric function in z, and these can be summed in Fourier integrals. We expect the temperature anomaly to be symmetric in z in view of the boundary condition at x = 0, hence $\bar{u}^{(0,0)}$ and $\bar{u}^{(0,1)}$ should be anti-symmetric, from (II-67) and (II-73). We can therefore work with half-range Fourier integrals and write the solutions of (II-74) satisfying (II-57), (II-62), (II-67), and (II-73) as:

$$\bar{T}^{(0,0)} = \int_0^\infty \mathcal{T}^{(0,0)}(k) e^{-k^3 s} \cos kz \, dk \qquad \text{(II-75)}$$

$$\bar{u}^{(0,0)} = \int_0^\infty \mathcal{T}^{(0,0)}(k) e^{-k^3 s} \sin kz \, dk \qquad \text{(II-76)}$$

$$\bar{T}^{(0,1)} = \int_0^\infty \mathcal{T}^{(0,1)}(k) e^{-k^3 s} \cos kz \, dk \qquad \text{(II-77)}$$

$$\bar{u}^{(0,1)} = \int_0^\infty \mathcal{T}^{(0,1)}(k) e^{-k^3 s} \sin kz \, dk \qquad \text{(II-78)}$$

Finally, we expand the boundary conditions (II-38) and (II-39) in power series in ϵ, which leads simply to:

$$\hat{u}^{(0,j)}(0,z) + \bar{u}^{(0,j)}(0,z) = \hat{w}^{(0,j)}(0,z) + \bar{w}^{(0,j)}(0,z) = 0, \quad j = 0,1,2,\ldots \tag{II-79}$$

$$\hat{T}^{(0,0)}(0,z) + \bar{T}^{(0,0)}(0,z) = f(z) \tag{II-80}$$

$$\hat{T}^{(0,\ell)}(0,z) + \bar{T}^{(0,\ell)}(0,z) = 0, \quad \ell = 1,2,3,\ldots \tag{II-81}$$

Now from (II-76):

$$\mathcal{I}^{(0,0)}(k) = \frac{2}{\pi}\int_0^\infty \bar{u}^{(0,0)}(0,z)\sin kz\, dz$$

But from (II-44) $\hat{u}^{(0,0)} = 0$ and thus to satisfy (II-79) $\bar{u}^{(0,0)}(0,z) = 0$. Hence:

$$\mathcal{I}^{(0,0)} = \bar{u}^{(0,0)} = \bar{T}^{(0,0)} = 0 \tag{II-82}$$

and the far field is not affected in any respect by the source to this order in ϵ. Then $\hat{w}^{(0,0)}$ and $\hat{T}^{(0,0)}$ must satisfy (II-79) and (II-80) by themselves, so that in (II-50) and (II-51):

$$G^{(0,0)} = 0 \; ; \; F^{(0,0)} = f(z) \qquad \text{(II-}$$

and thus (II-51) and (II-52) give:

$$\hat{u}^{(0,1)} = \frac{1}{\sqrt{2}} f'(z)\, e^{-\xi/\sqrt{2}} \left(\sin \xi/\sqrt{2} + \cos \xi/\sqrt{2}\right) \qquad \text{(II-83)}$$

Then from (II-78) and (II-79):

$$\int_0^\infty \mathcal{J}^{(0,1)}(k) \sin kz \, dk + \frac{1}{\sqrt{2}} f'(z) = 0$$

or

$$\mathcal{J}^{(0,1)}(k) = -\frac{\sqrt{2}}{\pi} \int_0^\infty f'(z) \sin kz \, dz \qquad \text{(II-84)}$$

Thus if f(z) is specified we have all the expressions needed to calculate the lowest order (in ϵ) terms of the linear buoyancy layer and the linear far field. We collect these expressions for convenience of reference:

$$\hat{T}^{(0,0)} = f(z)\, e^{-\xi/\sqrt{2}} \cos \xi/\sqrt{2} \qquad \text{(II-85)}$$

$$\hat{w}^{(0,0)} = f(z)\, e^{-\xi/\sqrt{2}} \sin \xi/\sqrt{2} \qquad \text{(II-86)}$$

$$\hat{u}^{(0,1)} = \frac{1}{\sqrt{2}} f'(z)\, e^{-\xi/\sqrt{2}} \left(\sin \xi/\sqrt{2} + \cos \xi/\sqrt{2}\right) \qquad \text{(II-87)}$$

$$T^{(0,1)} = \int_0^\infty \mathcal{J}^{(0,1)}(k)\, e^{-k^3 s} \cos kz \, dk \qquad \text{(II-88)}$$

$$\bar{u}^{(0,1)} = \int_0^\infty \mathcal{F}^{(0,1)}(k) e^{-k^3 s} \sin kz \, dk \qquad \text{(II-89)}$$

$$\bar{w}^{(0,3)} = \bar{T}_{zz}^{(0,1)} = -\int_0^\infty k^2 \mathcal{F}^{(0,1)}(k) e^{-k^3 s} \cos kz \, dk \qquad \text{(II-90)}$$

Computations for a particular f(z)

To illustrate the results just derived, profiles of the various fields have been computed and plotted for the simple source function:

$$f(z) = e^{-z^2} \quad ; \quad \mathcal{F}^{(0,1)}(k) = \frac{1}{\sqrt{2\pi}} k e^{-k^2/4} \qquad \text{(II-91)}$$

The integrals involved in the expressions (II-88) - (II-90) were computed using a trapezoidal routine; the program is given in appendix III. This program also computes the buoyancy layer components and the nonlinear corrections in both buoyancy layer and far field; these corrections are discussed in the next section. In all the plots, only the region $z \geq 0$ is shown, since each field is either symmetric or antisymmetric in z. Figure 2 shows vertical profiles of $\hat{T}^{(0,0)}$ and figure 3 shows horizontal profiles of $\hat{w}^{(0,0)}$. We see that the hot source produces a rising motion confined to a thin layer ($x \cong 4\epsilon$) and that at the outer edge of this buoyancy layer the temperature anomaly tends to zero, to this order in ϵ. Figure 4 shows vertical profiles of the

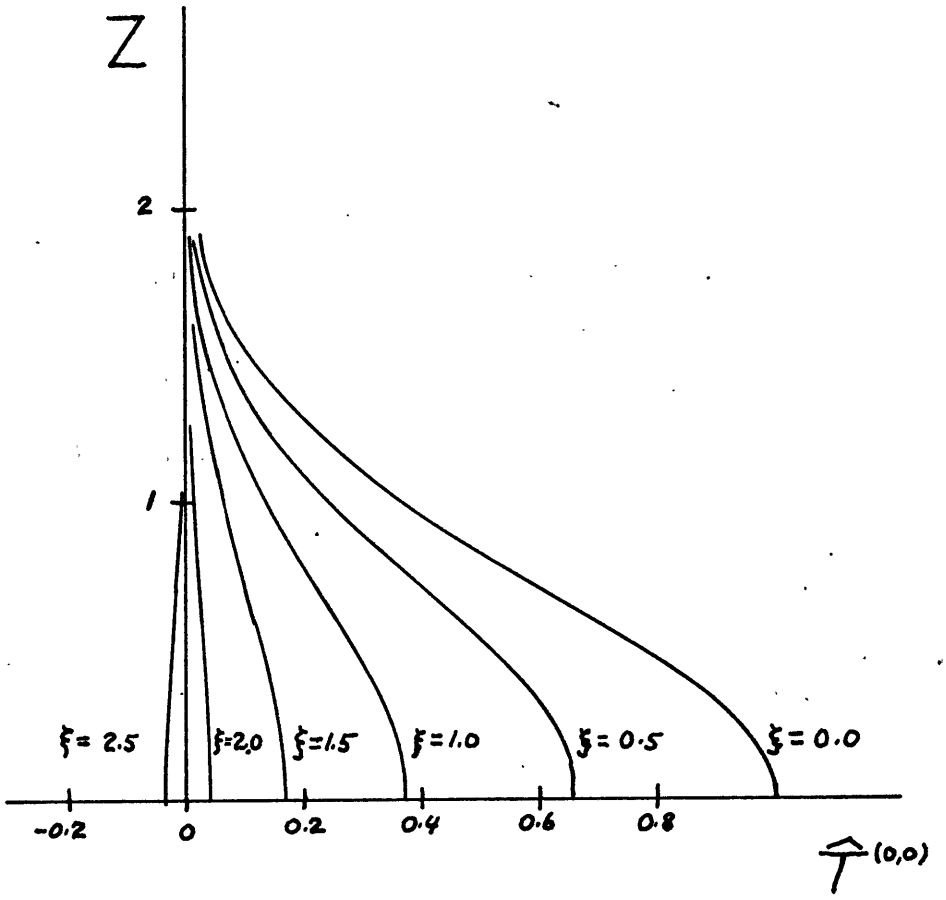


Figure 2 Linear buoyancy layer temperature anomaly.

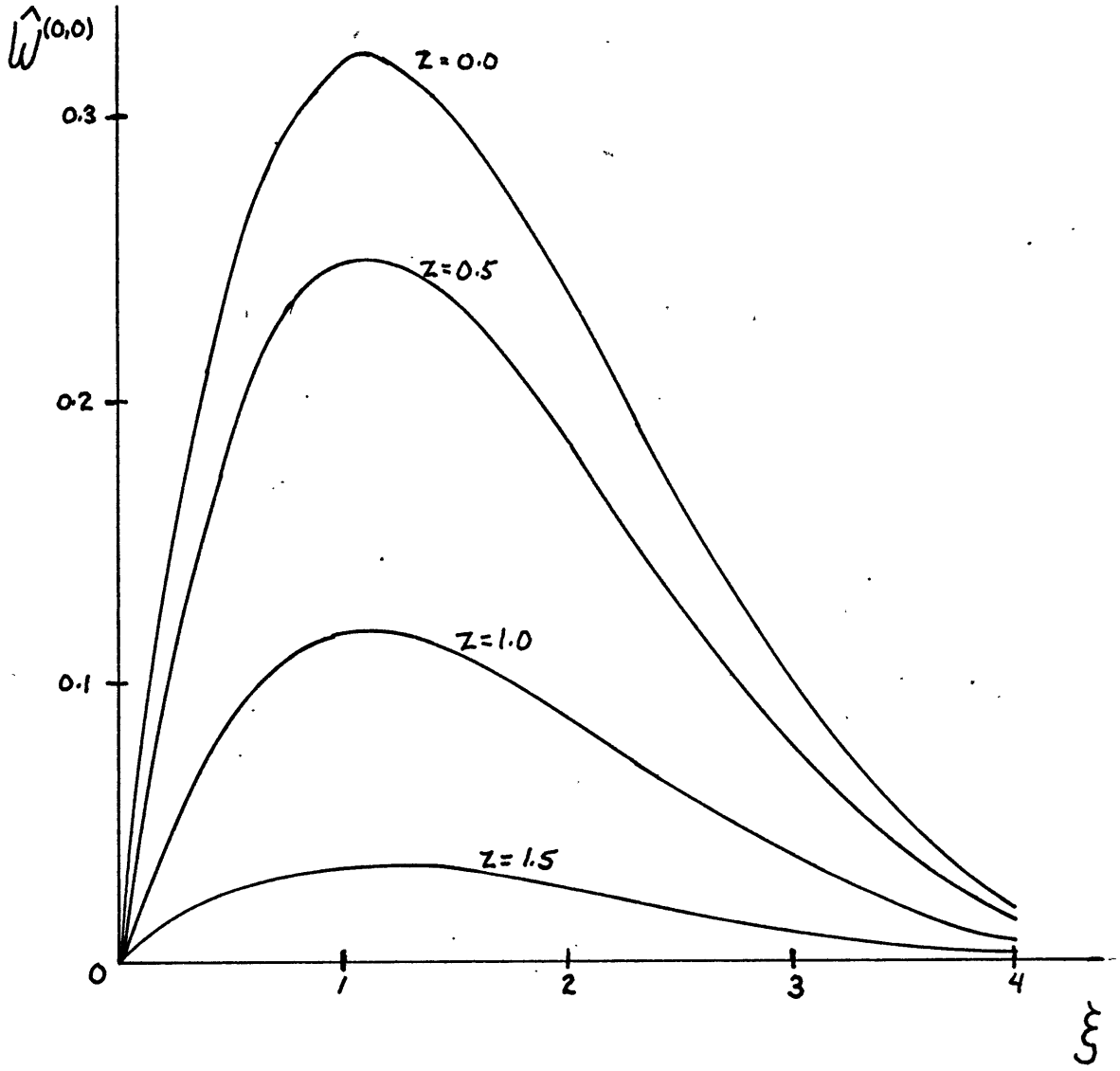


Figure 3 Linear buoyancy layer vertical velocity.

quantity

$$\hat{u}^{(0,1)}(\xi,z) + \bar{u}^{(0,1)}(0,z) \qquad \text{(II-92)}$$

For $x = O(\epsilon)$, i.e., for stations in the buoyancy layer, this is a good approximation of the quantity

$$\hat{u}^{(0,1)}(\xi,z) + \bar{u}^{(0,1)}(s,z) \qquad \text{(II-93)}$$

which is the total horizontal velocity, to order ϵ. We have chosen to plot (II-92) rather than $\hat{u}^{(0,1)}$ alone in order to exhibit the actual velocity. We see that the motion is toward the source in the region $z < 0$ and away from it for $z > 0$ and that the motion is confined to a range in depth of about 4 scale lengths L. The z-dependence of the horizontal velocity is that of the temperature anomaly gradient, from (II-87), and this is apparent in the figures. Thus the zero of velocity coincides with the maximum of temperature anomaly, and we shall see that this holds in the far field, as it must from (II-88) and (II-89). Streamlines of the motion in the buoyancy layer region are shown in figure 5. The streamfunction is defined by:

$$-\hat{\psi}_z^{(0,1)} = \hat{u}^{(0,1)}(\xi,z) + \bar{u}^{(0,1)}(0,z)$$

$$\hat{\psi}_\xi^{(0,1)} = \hat{w}^{(0,0)} \qquad \text{(II-94)}$$

so that the streamlines are distorted in x. If one imagines

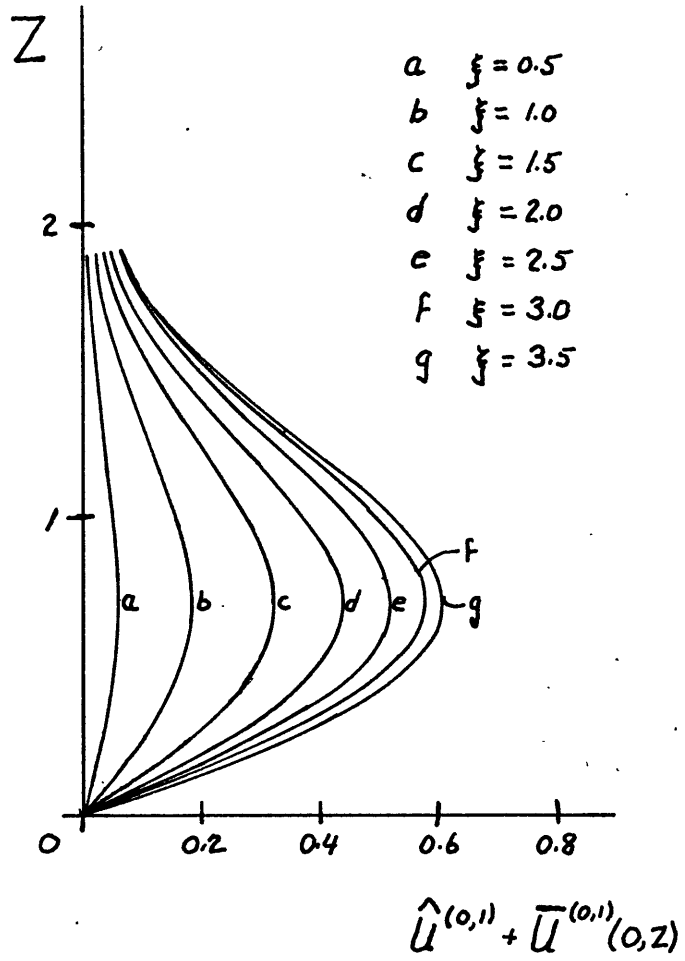


Figure 4 Linear buoyancy layer horizontal velocity.

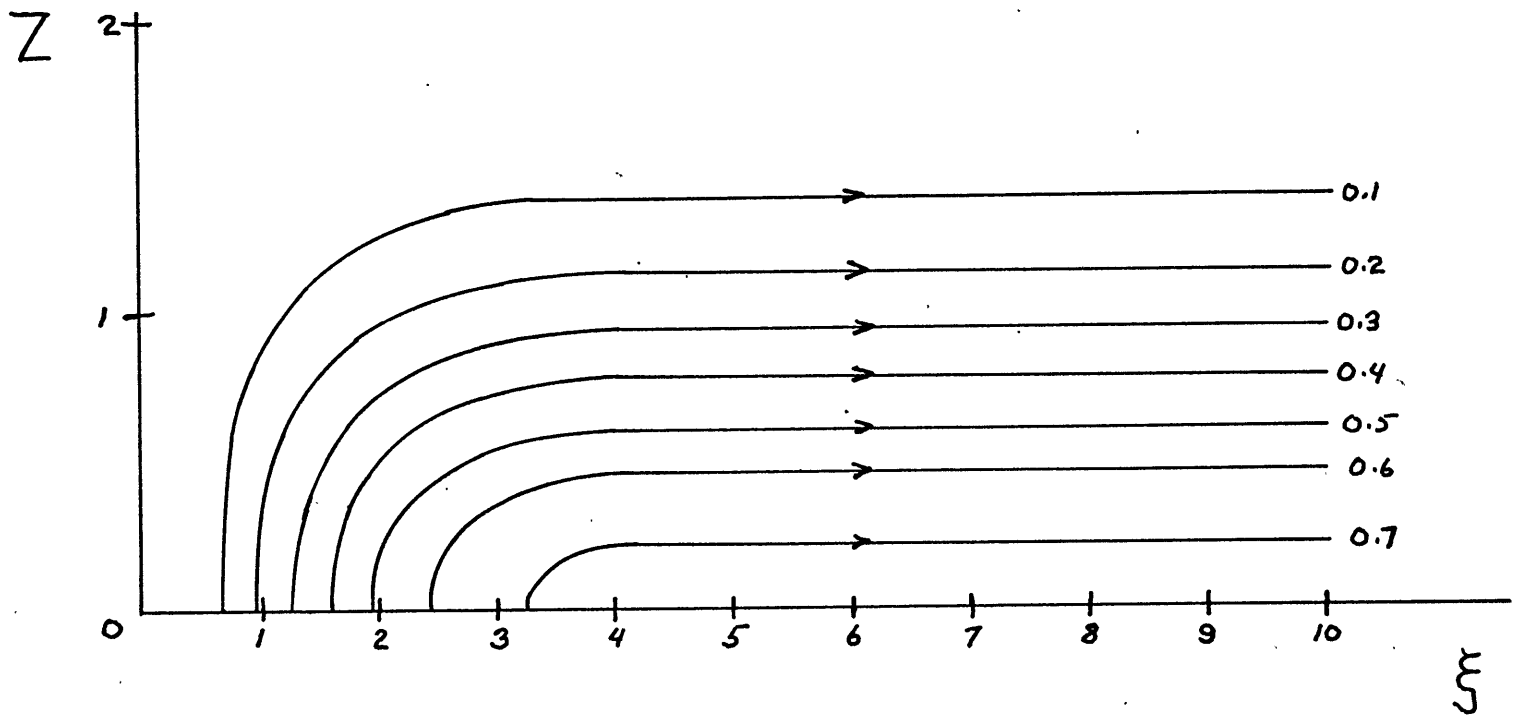


Figure 5 Linear buoyancy layer streamlines.

compressing the figure in the x direction by the factor ϵ, one has the picture of the streamlines in (x,z) space. Explicitly, from (II-86) and (II-87):

$$\hat{\psi}^{(0,1)} = \frac{1}{\sqrt{2}} f(z)\left[1 - e^{-\zeta/\sqrt{2}}\left(\cos\zeta/\sqrt{2} + \sin\zeta/\sqrt{2}\right)\right]$$

Figure 6 shows the far field horizontal velocity $\bar{u}^{(0,1)}$ at several different values of s. We see that the profile nearest the origin, that at s = 0.0078, is quite similar to the profile at ζ = 3.5 in figure 4. As s increases the profiles retain their basic shape while broadening in z and decreasing in amplitude. Figure 7 shows profiles of the temperature anomaly $\bar{T}^{(0,1)}$. Note that this quantity is not the far field extension of the buoyancy layer temperature anomaly $\hat{T}^{(0,0)}$ plotted in figure 2 but is one order higher in ϵ. An $O(\epsilon)$ buoyancy layer component- not discussed here- exists to adjust $\bar{T}^{(0,1)}$ to zero at x = 0. In figure 7 we again see the broadening and decrease of amplitude with increasing s. The central core is warmer than the mean temperature at each level, but there are relatively cooler layers above and below this core. The maximum of $\bar{T}^{(0,1)}$ lies at the level of zero horizontal velocity, z = 0. Contrast this situation with the usual pattern in a tongue identified by a dynamically unimportant tracer subject to advection and diffusion; in that case

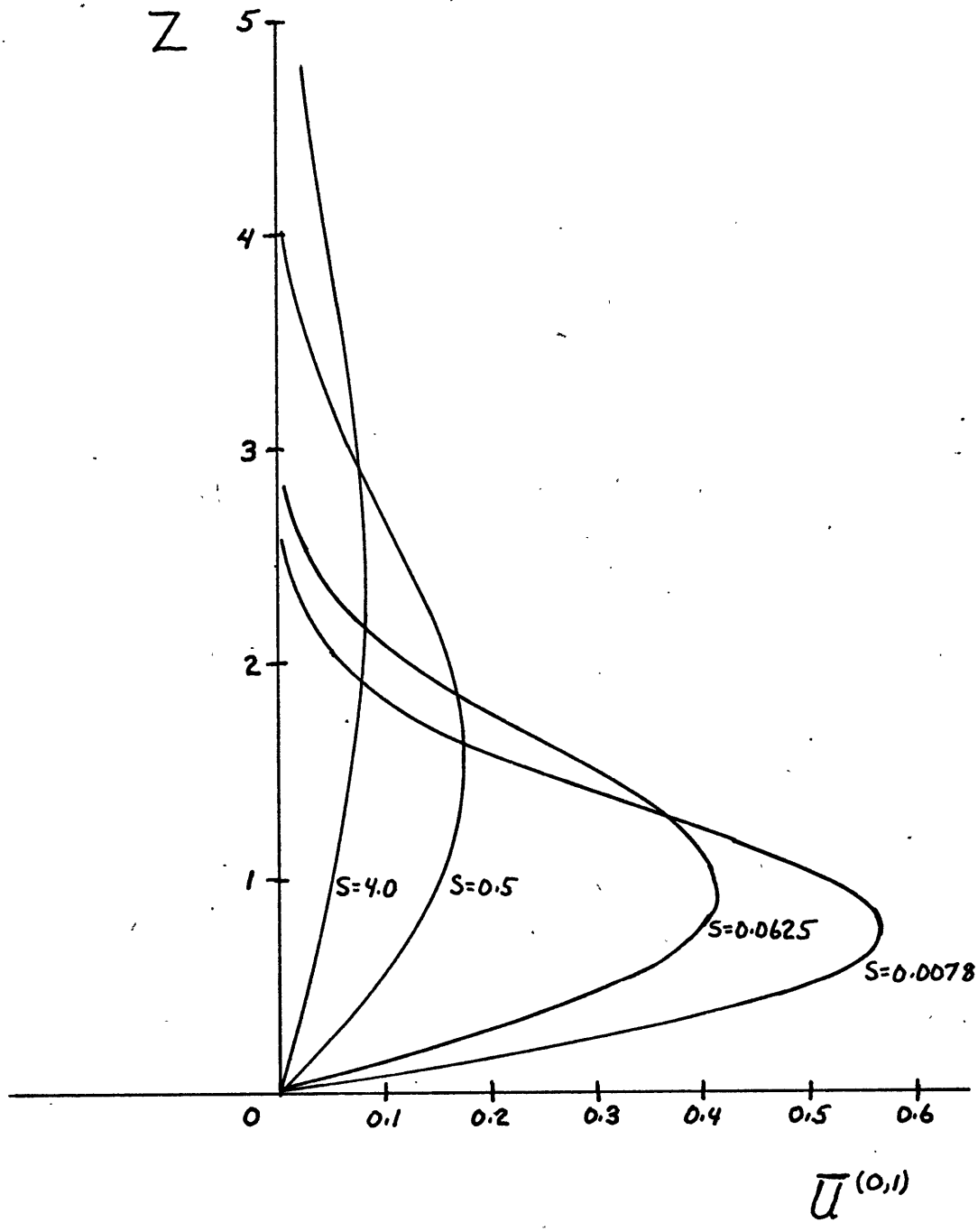


Figure 6 Linear far field horizontal velocity.

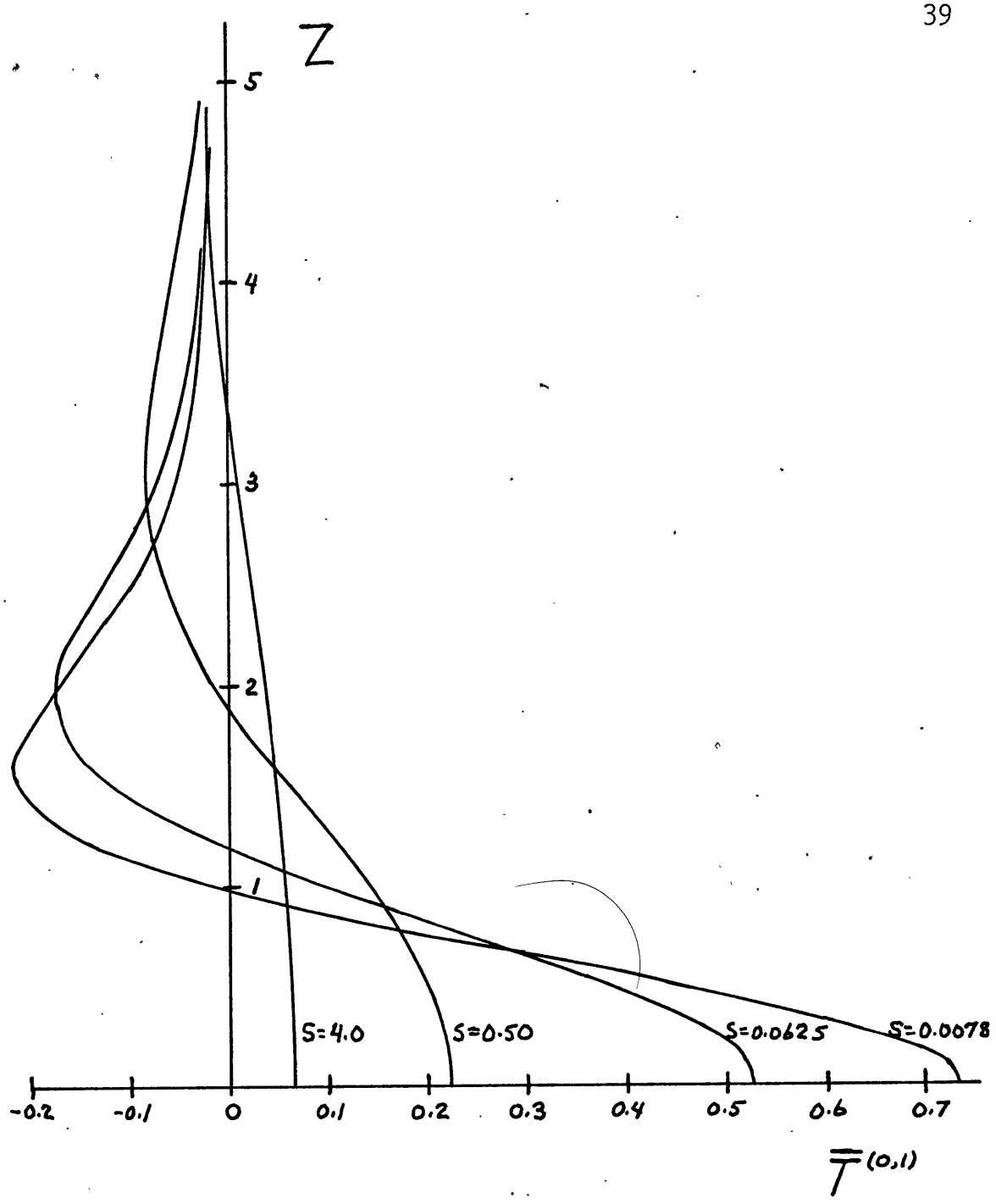


Figure 7 Linear far field temperature anomaly.

maxima of velocity and tracer concentration coincide(e.g., Sverdrup, Johnson, and Fleming, pp. 503 ff).

The existence of the relatively cooler layers may seem odd. They are not due to numerical error, for in fact all these far field profiles have an infinite number of zero crossings in z, as the following argument indicates. Consider $\bar{u}^{(0,1)}$; from (II-89) we can see that at large s the factor $e^{-k^3 s}$ decays rapidly in k and for purposes of the integration $\oint^{(0,1)}$ may be replaced by the first non-vanishing term of its Taylor series about k = 0. (II-84) shows that this term is just

$$\frac{\sqrt{2}}{\pi} k \int_0^\infty f(z)\, dz \qquad \text{(II-95)}$$

so

$$\bar{u}^{(0,1)} \simeq \frac{\sqrt{2}}{\pi} \int_0^\infty f(z) dz \cdot \int_0^\infty k e^{-k^3 s} \sin kz\, dk$$

Let $\phi = k^3 s$. Then

$$\bar{u}^{(0,1)} \simeq \frac{\sqrt{2}}{\pi} \int_0^\infty f(z) dz \cdot \frac{1}{3 s^{2/3}} \int_0^\infty \phi^{-1/3} e^{-\phi} \sin q\phi^{1/3} d\phi \qquad \text{(II-96)}$$

$$= V(\tau) s^{-2/3}$$

where

$$\tau \equiv z/s^{1/3} \qquad \text{(II-97)}$$

Thus a line along which $\bar{u}^{(0,1)} = 0$ must be a line of $V = 0$, i.e., a line of constant τ, say $\tau = \tau_0$ or

$$Z = \tau_0 S^{1/3} \tag{II-98}$$

If there are several such lines they clearly spread farther apart as s increases, so the spacing between zeroes of $\bar{u}^{(0,1)}$ increases. Similarly, lines for which $\bar{u}_z^{(0,1)} = 0$ are lines of constant τ; these lines connect points at which $|\bar{u}^{(0,1)}|$ reaches a maximum in z. Let τ_c be the value of τ on such a line; then on this line

$$|\bar{u}^{(0,1)}| = V(\tau_c)\, S^{-2/3} \tag{II-99}$$

i.e., $|\bar{u}^{(0,1)}|$ decreases along the line as s increases. In short, we have shown analytically what we have already seen in the computations, that as s increases the spacing between zeroes increases and the amplitude decreases.

Now suppose that the $\bar{u}^{(0,1)}$ profile in fact has some number N of zeroes; the case N = 5 is shown in figure 8. At a slightly larger value of s the profile will have broadened and decreased in amplitude as indicated by the dotted lines in figure 8. Thus $\bar{u}_s^{(0,1)}$ has either N or N + 2 zeroes depending on whether one draws the outermost lobes of the profile as in figure 8a or 8b. The zeroes of $\bar{u}_s^{(0,1)}$

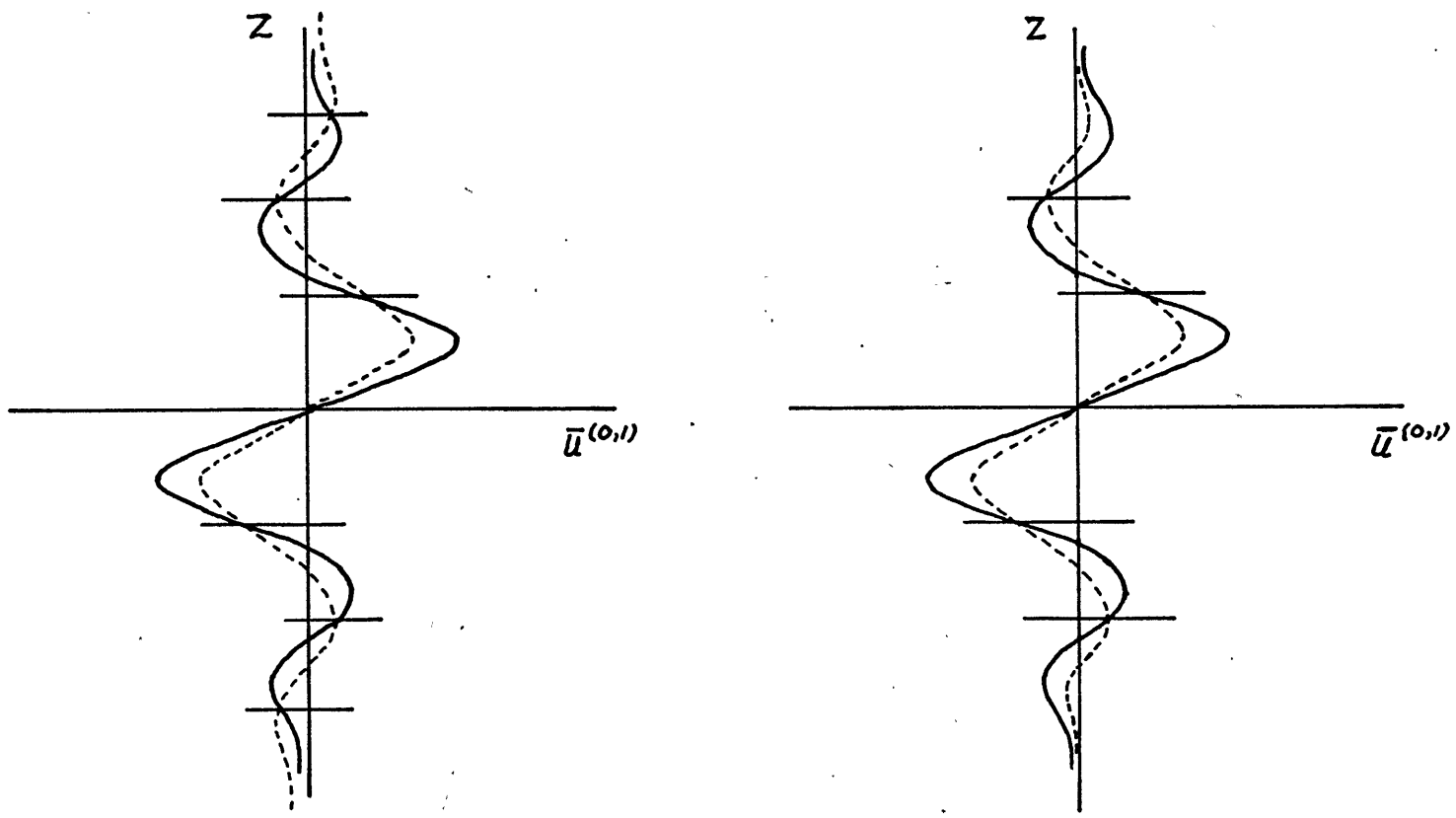


Figure 8 Schematic profiles of $\bar{u}^{(0,1)}(s,z)$ (solid lines) and of $\bar{u}^{(0,1)}(s + \delta s,z)$ (dotted lines). Zeroes of $\bar{u}^{(0,1)}_s$ are indicated by horizontal lines.

are indicated by the horizontal marks in figure 8. Furthermore, a profile gains one zero by each differentiation in z. Such considerations used in conjunction with the far field equations lead in sequence to the entries in table 1.

Table 1

Numbers of zeroes in far field profiles starting with assumption of 5 zeroes in $u^{(0,1)}$

Variable	N
$\bar{u}^{(0,1)}$	5
$\bar{u}^{(0,1)}_{zz}$	7
$\bar{u}^{(0,1)}_{s} \equiv -\bar{w}^{(0,3)}_{z}$	5 or 7
$\bar{w}^{(0,3)} = \bar{T}^{(0,1)}_{zz}$	4 or 6
$\bar{T}^{(0,1)} = \bar{p}^{(0,1)}_{z}$	2 or 4
$\bar{p}^{(0,1)}$	1 or 3
$\bar{p}^{(0,1)}_{s} = \bar{u}^{(0,1)}_{zz}$	1 or 3 3 or 5

Any choice of the last entry contradicts the second entry and the contradiction arises for any finite value of N. We conclude that N must be infinite.

Figure 9 shows profiles of the vertical velocity $\bar{w}^{(0,3)}$. Along the s axis the velocity is everywhere downward and is of the correct amount to recirculate the upward flux of

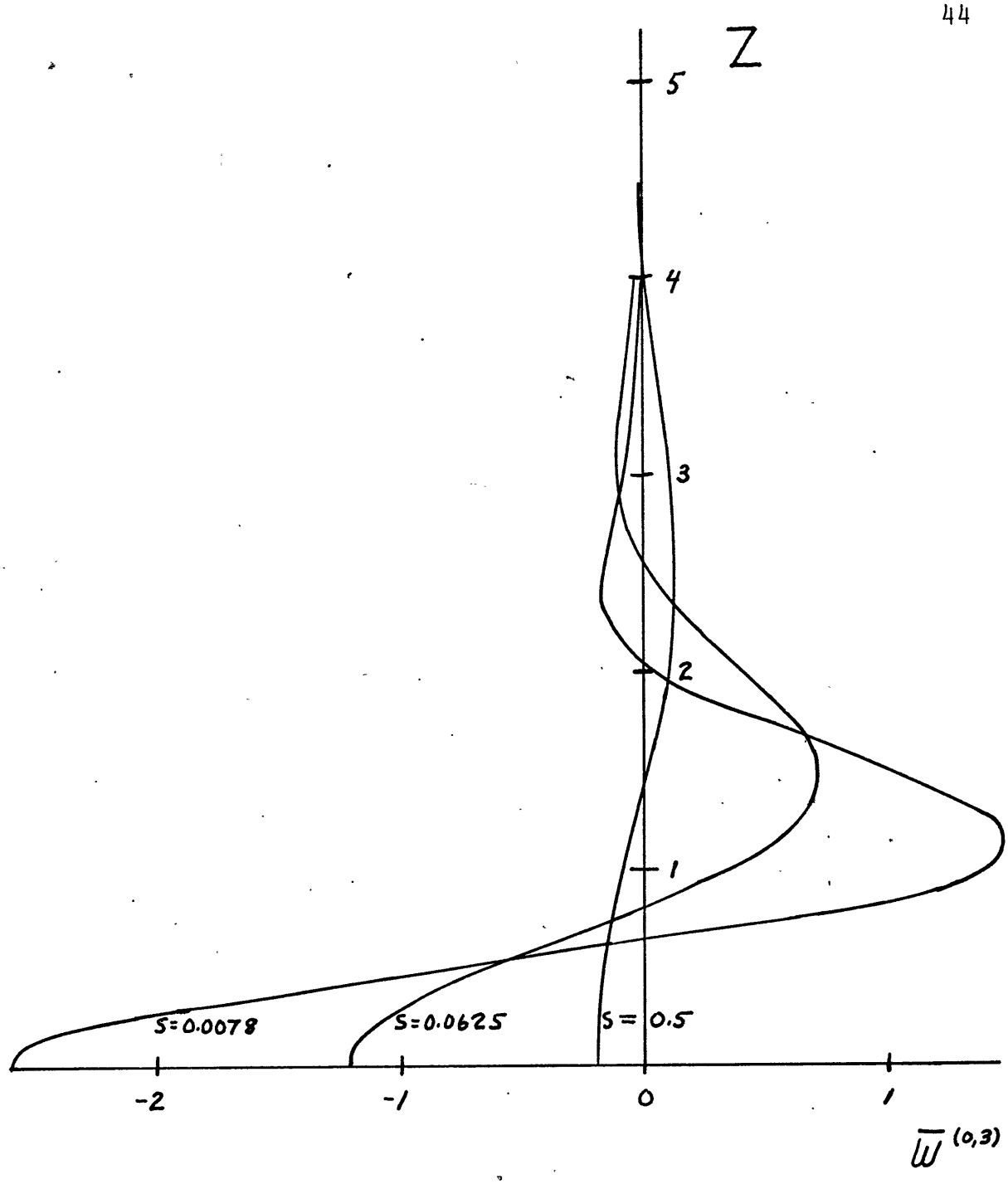


Figure 9 Linear far field vertical velocity.

fluid in the buoyancy layer:

$$\int_0^\infty w^{(0)}(x,0)\,dx = \text{, to lowest order in } \epsilon,$$

$$\int_0^\infty \left(\hat{w}^{(0,0)}(\xi,0) + \epsilon^3 \bar{w}^{(0,3)}(s,0)\right) dx$$

$$= \epsilon\left\{ \int_0^\infty \hat{w}^{(0,0)}(\xi,0)\,d\xi + \int_0^\infty \bar{w}^{(0,3)}(0,s)\,ds \right\} \qquad \text{(II-100)}$$

$$= \epsilon\left\{ \int_0^\infty e^{-\xi/\sqrt{2}} \sin \xi/\sqrt{2}\, d\xi + \int_0^\infty ds \int_0^\infty -\frac{1}{\sqrt{2\pi}} k^3 e^{-k^2/4} e^{-k^3 s}\, dk \right\} = 0$$

Note that this velocity is very small- two orders in ϵ less than the horizontal velocity. Qualitatively, because the fluid is strongly stratified in the vertical only a slight vertical motion is needed to produce an advective change of heat content in balance with that given by conduction. Comparing figures 9 and 7 we see that this central region of sinking fluid is associated with the region of anomalously warm temperatures. Above and below are regions of rising motion which are regions of conductive heat gain.

The streamlines of the far field motion are drawn in figure 10, where the streamfunction is defined by:

$$-\bar{\psi}_z^{(0,1)} = \bar{u}^{(0,1)}$$

$$\bar{\psi}_s^{(0,1)} = \bar{w}^{(0,3)}$$

If one stretches this plot in the horizontal by the factor ϵ^{-2} one has the picture of the streamlines in (x,z) space. The flow is thus in the form of a very long cell of limited

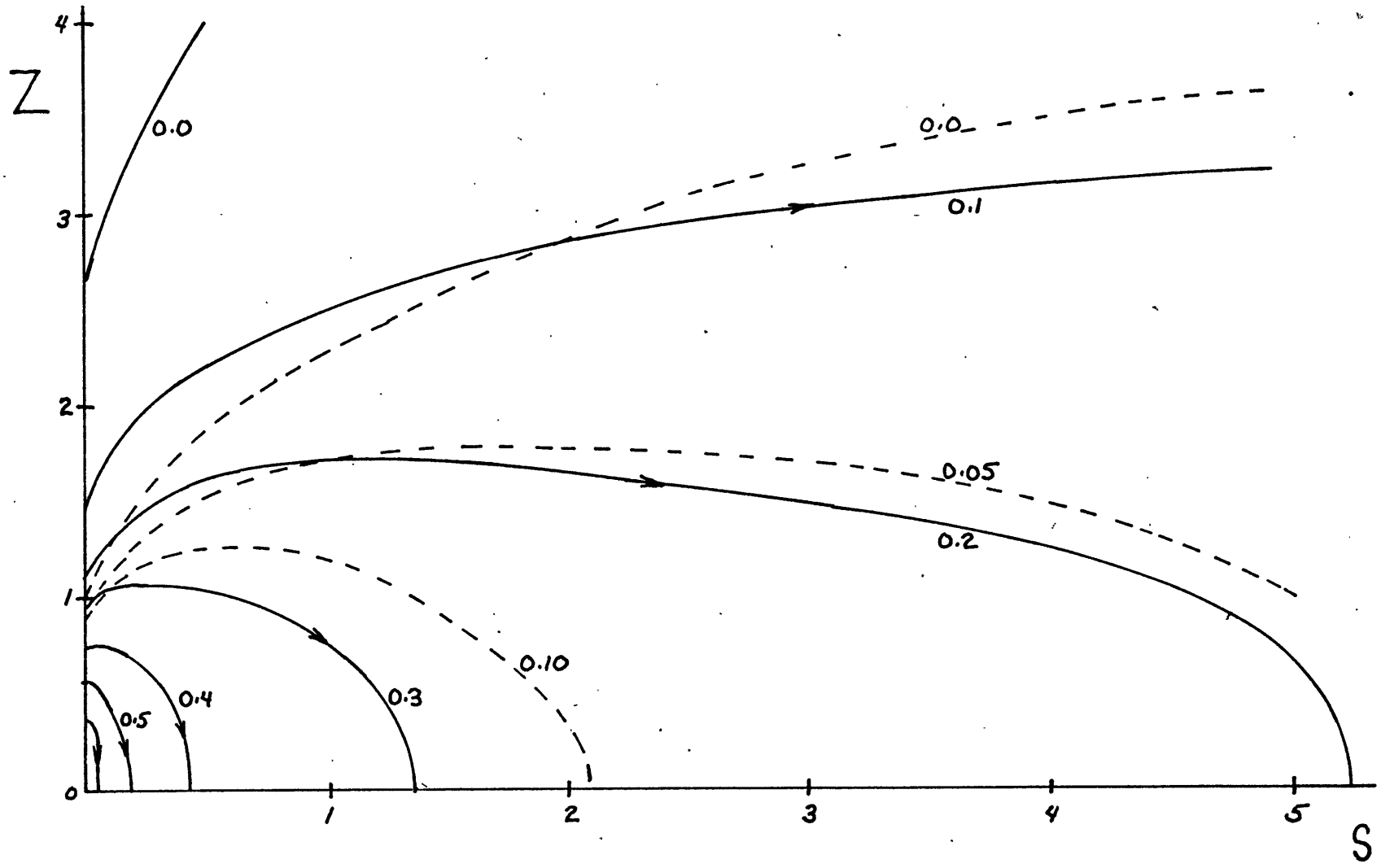


Figure 10 Linear far field streamlines (solid lines) and lines of constant temperature anomaly (dotted lines).

vertical extent, with much weaker cells above and below. For example, if $\epsilon = 0.1$ the ratio of length to height of the loop formed by the 0.20 streamline is about 200. In figure 10 are also drawn a few lines of constant $\bar{T}^{(0,1)}$ so that the course of a fluid particle through the field of temperature anomaly can be seen. We see that in the main cell particles gradually become relatively warm as their paths lose the upward slope imparted on leaving the buoyancy layer, become horizontal, and finally bend downwards, becoming vertical at z = 0.

Nonlinear corrections

We next turn to calculating the effects of small but finite nonlinearities on this flow. We write any dependent variable θ as the sum of its linear part, calculated in the previous section, and a nonlinear correction term of $O(\delta)$:

$$\theta = \left(\hat{\theta}^{(0)} + \bar{\theta}^{(0)}\right) + \delta\,\theta^{(1)} \qquad \text{(II-101)}$$

In the basic equations (II-16), (II-17), and (II-19) the nonlinear terms on the left sides are all multiplied by δ while the right sides have δ^0 as coefficient. Substitution of (II-101) leads to terms of the form

$$\delta\left(\hat{u}^{(0)}+\bar{u}^{(0)}\right)\frac{\partial}{\partial x}\left(\hat{u}^{(0)}+\bar{u}^{(0)}\right) \qquad \text{(II-102)}$$

on the left sides, while the unknown correction fields and their derivatives, multiplied by δ, appear on the right sides. We suppose that these corrections may be expanded in power series in ϵ and split into buoyancy layer and far field components, just like the linear fields. First superscript 1 indicates nonlinear correction:

$$\theta^{(1)} = \hat{\theta}^{(1,0)}(\xi, z) + \epsilon\hat{\theta}^{(1,1)}(\xi, z) + \cdots + \bar{\theta}^{(1,0)}(s, z) + \epsilon\bar{\theta}^{(1,1)}(s, z) + \cdots \tag{II-103}$$

Making such substitutions in (II-16) - (II-19) we have:

$$\frac{1}{\sigma}\left(\epsilon\hat{u}^{(0,1)} + \epsilon^2\hat{u}^{(0,2)} + \cdots + \epsilon\bar{u}^{(0,1)} + \epsilon^2\bar{u}^{(0,2)} + \cdots\right)\frac{\partial}{\partial x}\left(\epsilon\hat{u}^{(0,1)} + \cdots + \epsilon\bar{u}^{(0,1)} + \cdots\right)$$
$$+\frac{1}{\sigma}\left(\hat{w}^{(0,0)} + \epsilon\hat{w}^{(0,1)} + \cdots + \epsilon^3\bar{w}^{(0,3)} + \epsilon^4\bar{w}^{(0,4)} + \cdots\right)\frac{\partial}{\partial z}\left(\epsilon\hat{u}^{(0,1)} + \cdots + \epsilon\bar{u}^{(0,1)} + \cdots\right)$$
$$= -\frac{\partial}{\partial x}\left(\hat{p}^{(1,0)} + \epsilon\hat{p}^{(1,1)} + \cdots + \bar{p}^{(1,0)} + \epsilon\bar{p}^{(1,1)} + \cdots\right) + \epsilon^2\nabla^2\left(\hat{u}^{(1,0)} + \cdots + \bar{u}^{(1,0)} + \cdots\right) \tag{II-104}$$

$$\frac{1}{\sigma}\left(\epsilon\hat{u}^{(0,1)} + \epsilon^2\hat{u}^{(0,2)} + \cdots + \epsilon\bar{u}^{(0,1)} + \epsilon^2\bar{u}^{(0,2)} + \cdots\right)\frac{\partial}{\partial x}\left(\hat{w}^{(0,0)} + \cdots + \epsilon^3\bar{w}^{(0,3)} + \cdots\right)$$
$$+\frac{1}{\sigma}\left(\hat{w}^{(0,0)} + \epsilon\hat{w}^{(0,1)} + \cdots + \epsilon^3\bar{w}^{(0,3)} + \epsilon^4\bar{w}^{(0,4)} + \cdots\right)\frac{\partial}{\partial z}\left(\hat{w}^{(0,0)} + \cdots + \epsilon^3\bar{w}^{(0,3)} + \cdots\right)$$
$$= -\frac{\partial}{\partial z}\left(\hat{p}^{(1,0)} + \epsilon\hat{p}^{(1,1)} + \cdots + \bar{p}^{(1,0)} + \epsilon\bar{p}^{(1,1)} + \cdots\right) + \hat{T}^{(1,0)} + \epsilon\hat{T}^{(1,1)} + \cdots + \bar{T}^{(1,0)} + \epsilon\bar{T}^{(1,1)} + \cdots \tag{II-105}$$
$$+\epsilon^2\nabla^2\left(\hat{w}^{(1,0)} + \epsilon\hat{w}^{(1,1)} + \cdots + \bar{w}^{(1,0)} + \epsilon\bar{w}^{(1,1)} + \cdots\right)$$

$$\frac{\partial}{\partial x}\left(\hat{u}^{(1,0)} + \epsilon\hat{u}^{(1,1)} + \cdots + \bar{u}^{(1,0)} + \epsilon\bar{u}^{(1,1)} + \cdots\right) + \frac{\partial}{\partial z}\left(\hat{w}^{(1,0)} + \epsilon\hat{w}^{(1,1)} + \cdots + \bar{w}^{(1,0)} + \epsilon\bar{w}^{(1,1)} + \cdots\right) \tag{II-106}$$
$$= 0$$

$$\left(\epsilon\hat{u}^{(0,1)} + \epsilon^2\hat{u}^{(0,2)} + \cdots + \epsilon\bar{u}^{(0,1)} + \epsilon^2\bar{u}^{(0,2)} + \cdots\right)\frac{\partial}{\partial x}\left(\hat{T}^{(0,0)} + \epsilon\hat{T}^{(0,1)} + \cdots + \epsilon\bar{T}^{(0,1)} + \cdots\right)$$
$$+\left(\hat{w}^{(0,0)} + \epsilon\hat{w}^{(0,1)} + \cdots + \epsilon^3\bar{w}^{(0,3)} + \epsilon^4\bar{w}^{(0,4)} + \cdots\right)\frac{\partial}{\partial z}\left(\hat{T}^{(0,0)} + \epsilon\hat{T}^{(0,1)} + \cdots + \epsilon\bar{T}^{(0,1)} + \cdots\right) \tag{II-107}$$
$$= -\left(\hat{w}^{(0,0)} + \epsilon\hat{w}^{(1,1)} + \cdots + \bar{w}^{(1,0)} + \epsilon\bar{w}^{(1,1)} + \cdots\right)$$
$$+\epsilon^2\nabla^2\left(\hat{T}^{(1,0)} + \epsilon\hat{T}^{(1,1)} + \cdots + \bar{T}^{(1,0)} + \epsilon\bar{T}^{(1,1)} + \cdots\right)$$

In (II-104) - (II-107) we have left out fields such as $\bar{w}^{(0,0)}$ known to be zero from the linear calculations. Performing

the indicated differentiations we obtain:

$$\frac{1}{\sigma}(\epsilon\hat{u}^{(0,1)}+\cdots+\epsilon\bar{u}^{(0,1)}+\cdots)(\hat{u}_{\xi}^{(0,1)}+\cdots+\epsilon^3\bar{u}_{s}^{(0,1)}+\cdots)+\frac{1}{\sigma}(\hat{w}^{(0,0)}+\cdots+\epsilon^3\bar{w}^{(0,3)}+\cdots)(\epsilon\hat{u}_{z}^{(0,1)}+\cdots+\epsilon\bar{u}_{z}^{(0,1)}+\cdots)$$
$$=-\left(\frac{1}{\epsilon}\hat{p}_{\xi}^{(1,0)}+\hat{p}_{\xi}^{(1,1)}+\cdots+\epsilon^2\bar{p}_{s}^{(1,0)}+\epsilon^3\bar{p}_{s}^{(1,1)}+\cdots\right)+\epsilon^2\left[\frac{1}{\epsilon^2}\hat{u}_{\xi\xi}^{(1,0)}+\frac{1}{\epsilon}\hat{u}_{\xi\xi}^{(1,1)}+\cdots\right.$$
$$\left.+\epsilon^4\bar{u}_{ss}^{(1,0)}+\epsilon^5\bar{u}_{ss}^{(1,1)}+\cdots+\hat{u}_{zz}^{(1,0)}+\cdots+\bar{u}_{zz}^{(1,0)}+\cdots\right] \qquad \text{(II-108)}$$

$$\frac{1}{\sigma}(\epsilon\hat{u}^{(0,1)}+\cdots+\epsilon\bar{u}^{(0,1)}+\cdots)(\frac{1}{\epsilon}\hat{w}_{\xi}^{(0,0)}+\cdots+\epsilon^5\bar{w}_{s}^{(0,3)}+\cdots)+\frac{1}{\sigma}(\hat{w}^{(0,0)}+\cdots+\epsilon^3\bar{w}^{(0,3)}+\cdots)(\hat{w}_{z}^{(0,0)}+\cdots+\epsilon^3\bar{w}_{z}^{(0,3)}+\cdots)$$
$$=-(\hat{p}_{z}^{(1,0)}+\cdots+\bar{p}_{z}^{(1,0)}+\cdots)+\hat{\tau}^{(1,0)}+\cdots+\bar{\tau}^{(1,0)}+\cdots+\epsilon^2\left[\frac{1}{\epsilon^2}\hat{w}_{\xi\xi}^{(1,0)}+\frac{1}{\epsilon}\hat{w}_{\xi\xi}^{(1,1)}+\cdots\right.$$
$$\left.+\epsilon^4\bar{w}_{ss}^{(1,0)}+\epsilon^5\bar{w}_{s\xi}^{(1,1)}+\cdots+\hat{w}_{zz}^{(1,0)}+\cdots+\bar{w}_{zz}^{(1,0)}+\cdots\right] \qquad \text{(II-109)}$$

$$\frac{1}{\epsilon}\hat{u}_{\xi}^{(1,0)}+\hat{u}_{\xi}^{(1,1)}+\cdots+\epsilon^2\bar{u}_{s}^{(1,0)}+\epsilon^3\bar{u}_{s}^{(1,1)}+\cdots+\hat{w}_{z}^{(1,0)}+\cdots+\bar{w}_{z}^{(1,0)}+\cdots=0 \qquad \text{(II-110)}$$

$$(\epsilon\hat{u}^{(0,1)}+\cdots+\epsilon\bar{u}^{(0,1)}+\cdots)(\frac{1}{\epsilon}\hat{\tau}_{\xi}^{(0,0)}+\cdots+\epsilon^3\bar{\tau}_{s}^{(1,1)}+\cdots)$$
$$+(\hat{w}^{(0,0)}+\cdots+\epsilon^3\bar{w}^{(0,3)}+\cdots)(\hat{\tau}_{z}^{(0,0)}+\cdots+\epsilon\bar{\tau}_{z}^{(0,1)}+\cdots)$$
$$=-(\hat{w}^{(1,0)}+\cdots+\bar{w}^{(1,0)}+\cdots)+\epsilon^2\left[\frac{1}{\epsilon^2}\hat{\tau}_{\xi\xi}^{(1,0)}+\frac{1}{\epsilon}\hat{\tau}_{\xi\xi}^{(1,1)}+\cdots\right. \qquad \text{(II-111)}$$
$$\left.+\epsilon^4\bar{\tau}_{ss}^{(1,0)}+\epsilon^5\bar{\tau}_{ss}^{(1,1)}+\cdots+\hat{\tau}_{zz}^{(1,0)}+\cdots+\bar{\tau}_{zz}^{(1,0)}+\cdots\right]$$

Since the linear temperature anomaly has already satisfied the only inhomogeneous boundary condition in the problem, (II-80), all these nonlinear corrections must satisfy homogeneous conditions at all orders in ϵ, i.e.:

$$\hat{u}^{(1,j)}(0,z)+\bar{u}^{(1,j)}(0,z)=\hat{w}^{(1,j)}(0,z)+\bar{w}^{(1,j)}(0,z)$$
$$=\hat{\tau}^{(1,j)}(0,z)+\bar{\tau}^{(1,j)}(0,z)=0 \qquad \text{(II-112)}$$
$$j=0,1,2,\cdots$$

and of course all must tend to zero as $\sqrt{x^2+z^2}\to\infty$.

For large x all buoyancy layer fields decay rapidly to zero and the far fields alone must satisfy (II-108) -

(II-111) by themselves. We assume that they do so for all x. Collecting coefficients of like powers of ϵ we then have:

terms in ϵ^0

$$0 = -\bar{p}_s^{(1,0)} + \bar{u}_{zz}^{(1,0)} \tag{II-113}$$

$$0 = -\bar{p}_z^{(1,0)} + \bar{T}^{(1,0)} \tag{II-114}$$

$$0 = -\bar{w}_z^{(1,0)} \tag{II-115}$$

$$0 = \bar{w}^{(1,0)} \tag{II-116}$$

and thus:

$$\bar{u}_{zzz}^{(1,0)} = \bar{T}_s^{(1,0)} \tag{II-117}$$

terms in ϵ^1

$$0 = -\bar{p}_s^{(1,1)} + \bar{u}_{zz}^{(1,1)} \tag{II-118}$$

$$0 = -\bar{p}_z^{(1,1)} + \bar{T}^{(1,1)} \tag{II-119}$$

$$0 = -\bar{w}_z^{(1,1)} \tag{II-120}$$

$$0 = \bar{w}^{(1,1)} \tag{II-121}$$

and thus:

$$\bar{u}_{zzz}^{(1,1)} = \bar{T}_s^{(1,1)} \tag{II-122}$$

terms in ϵ^2

$$\frac{1}{\sigma}\left[\bar{u}^{(0,1)}\bar{u}_s^{(0,1)} + \bar{w}^{(0,3)}\bar{u}_z^{(0,1)}\right] = -\bar{p}_s^{(1,2)} + \bar{u}_{zz}^{(1,2)} \tag{II-123}$$

$$0 = -\bar{p}_z^{(1,2)} + \bar{T}^{(1,2)} \tag{II-124}$$

$$0 = \bar{u}_s^{(1,0)} + \bar{w}_z^{(1,2)} \tag{II-125}$$

$$0 = -\bar{w}^{(1,2)} + \bar{T}_{zz}^{(1,0)} \tag{II-126}$$

where (II-116) has been used to obtain (II-124). From (II-125) and (II-126):

$$\bar{T}_{zzz}^{(1,0)} = -\bar{u}_s^{(1,0)} \tag{II-127}$$

terms in ϵ^3

$$\frac{1}{\sigma}\left[\bar{u}^{(0,1)}\bar{u}_s^{(0,2)} + \bar{u}^{(0,2)}\bar{u}_s^{(0,1)} + \bar{w}^{(0,3)}\bar{u}_s^{(0,2)} + \bar{w}^{(0,4)}\bar{u}_s^{(0,1)}\right] \tag{II-128}$$
$$= -\bar{p}_s^{(1,3)} + \bar{u}_{zz}^{(1,3)}$$

$$0 = -\bar{p}_z^{(1,3)} + \bar{T}^{(1,3)} \tag{II-129}$$

$$0 = \bar{u}_s^{(1,1)} + \bar{w}_z^{(1,3)} \tag{II-130}$$

$$0 = -\bar{w}^{(1,3)} + \bar{T}_{zz}^{(1,1)} \tag{II-131}$$

where (II-121) has been used to obtain (II-129). From (II-130) and (II-131):

$$T_{zzz}^{(1,1)} = -\bar{u}_s^{(1,1)} \qquad \text{(II-132)}$$

From (II-117), (II-122), (II-127), and (II-132) we have:

$$\left(\frac{\partial^6}{\partial z^6} + \frac{\partial^2}{\partial s^2}\right) \begin{Bmatrix} \bar{T}^{(1,0)} \\ \bar{u}^{(1,0)} \\ \bar{T}^{(1,1)} \\ \bar{u}^{(1,1)} \end{Bmatrix} = 0 \qquad \text{(II-133)}$$

(II-133) is of exactly the same form as (II-74), so these nonlinear correction fields are governed by the same dynamics as the basic linear fields. In (II-104), (II-105), and (II-107) we can establish the symmetry properties of the left sides by referring to the linear results (II-85) - (II-90). On the left side of (II-104) is the expression:

$$\frac{1}{\sigma}\left\{\left(\hat{u}^{(0)}+\bar{u}^{(0)}\right)\frac{\partial}{\partial x}\left(\hat{u}^{(0)}+\bar{u}^{(0)}\right) + \left(\hat{w}^{(0)}+\bar{w}^{(0)}\right)\frac{\partial}{\partial z}\left(\hat{u}^{(0)}+\bar{u}^{(0)}\right)\right\} \qquad \text{(II-134)}$$

Since $\hat{u}^{(0)}$ and $\bar{u}^{(0)}$ are odd in z while $\hat{w}^{(0)}$ and $\bar{w}^{(0)}$ are even, the entire expression is even, so that on the right side of (II-104) we can expect $\hat{u}^{(1)}$, $\bar{u}^{(1)}$, $\hat{p}^{(1)}$, and $\bar{p}^{(1)}$ to be even. Similar considerations in (II-105) and (II-107) show that $\hat{T}^{(1)}$, $\bar{T}^{(1)}$, $\hat{w}^{(1)}$, and $\bar{w}^{(1)}$ are odd. In short, each nonlinear correction field has the opposite symmetry to its linear counterpart. With this information we can write the solutions of (II-133) satisfying (II-117), (II-122), (II-127), and (II-132) as:

$$\bar{T}^{(1,0)} = \int_0^\infty \mathcal{T}^{(1,0)}(k) e^{-k^3 s} \sin kz \, dk \tag{II-135}$$

$$\bar{u}^{(1,0)} = \int_0^\infty -\mathcal{T}^{(1,0)}(k) e^{-k^3 s} \cos kz \, dk \tag{II-136}$$

$$\bar{T}^{(1,1)} = \int_0^\infty \mathcal{T}^{(1,1)}(k) e^{-k^3 s} \sin kz \, dk \tag{II-137}$$

$$\bar{u}^{(1,1)} = \int_0^\infty -\mathcal{T}^{(1,1)}(k) e^{-k^3 s} \cos kz \, dk \tag{II-138}$$

We next extract from (II-108) - (II-111) the equations governing the nonlinear corrections to the buoyancy layer fields.

terms in ϵ^{-1}

$$0 = -\hat{p}_\xi^{(1,0)} \tag{II-139}$$

$$0 = \hat{u}_\xi^{(1,0)} \tag{II-140}$$

whence by the requirement that buoyancy layer fields tend to zero as $\xi \to \infty$:

$$\hat{u}^{(1,0)} = \hat{p}^{(1,0)} = 0 \tag{II-141}$$

and the same reasoning that led to (II-82) gives:

$$\mathcal{T}^{(1,0)} = \bar{u}^{(1,0)} = \bar{T}^{(1,0)} = 0 \tag{II-142}$$

terms in ϵ^0

$$0 = \hat{p}_\xi^{(1,1)} \tag{II-143}$$

$$\frac{1}{\sigma}\left[(\hat{u}^{(0,1)} + \bar{u}^{(0,1)})\hat{\omega}_\xi^{(0,0)} + \hat{w}^{(0,0)}\hat{\omega}_z^{(0,0)}\right] = \hat{T}^{(1,0)} + \hat{\omega}_{\xi\xi}^{(1,0)} \tag{II-144}$$

$$0 = \hat{u}_\xi^{(1,1)} + \hat{w}_z^{(1,0)} \tag{II-145}$$

$$\left(\hat{u}^{(0,1)} + \bar{u}^{(0,1)}\right)\hat{T}_\xi^{(0,0)} + \hat{w}^{(0,0)}\hat{T}_z^{(0,0)} = -\hat{w}^{(1,0)} + \hat{T}_{\xi\xi}^{(1,0)} \tag{II-146}$$

(II-144) and (II-146) are just the Ekman equations with inhomogeneous terms on the left sides. On these left sides we can make the approximation:

$$\hat{u}^{(0,1)} + \bar{u}^{(0,1)} \simeq \hat{u}^{(0,1)} + \bar{u}^{(0,1)}(0,z) \tag{II-147}$$

which is good to $O(\epsilon^3)$, since the fields to be determined decay on a scale $\xi = O(1)$ or $s \doteq O(\epsilon^3)$. Using (II-84) - (II-90) (II-144) and (II-146) become:

$$\frac{1}{\sigma}\frac{d}{dz}\left(\tfrac{1}{4}f^2\right)e^{-\xi/\sqrt{2}}\left(\sin\xi/\sqrt{2} - \cos\xi/\sqrt{2} + e^{-\xi/\sqrt{2}}\right) = \hat{\omega}_{\xi\xi}^{(1,0)} + \hat{T}^{(1,0)} \tag{II-148}$$

$$\frac{d}{dz}\left(\tfrac{1}{4}f^2\right)e^{-\xi/\sqrt{2}}\left(\sin\xi/\sqrt{2} + \cos\xi/\sqrt{2} - e^{-\xi/\sqrt{2}}\right) = -\hat{w}^{(1,0)} + \hat{T}_{\xi\xi}^{(1,0)} \tag{II-149}$$

The solutions of (II-148) and (II-149) must satisfy $\hat{T}^{(1,0)}(0,z) = \hat{w}^{(1,0)}(0,z) = 0$, since $\bar{T}^{(1,0)} = \bar{w}^{(1,0)} = 0$.

These are:

$$\hat{T}^{(1,0)} = \frac{d}{dz}\left(\tfrac{1}{4}f^2\right) e^{-\sqrt{3}/\sqrt{2}}\left[\left(\tfrac{2}{5}-\tfrac{1}{5\sigma}\right)\cos\sqrt{3}/\sqrt{2} - \left(\tfrac{3}{10}-\tfrac{9}{10\sigma}\right)\sin\sqrt{3}/\sqrt{2}\right.$$

$$\left. - \tfrac{\sqrt{3}}{2\sqrt{2}}\left(1+\tfrac{1}{\sigma}\right)\cos\sqrt{3}/\sqrt{2} - \left(\tfrac{2}{5}-\tfrac{1}{5\sigma}\right)e^{-\sqrt{3}/\sqrt{2}}\right] \qquad \text{(II-150)}$$

$$\hat{w}^{(1,0)} = \frac{d}{dz}\left(\tfrac{1}{4}f^2\right) e^{-\sqrt{3}/\sqrt{2}}\left[-\left(\tfrac{1}{5}+\tfrac{2}{5\sigma}\right)\cos\sqrt{3}/\sqrt{2} - \left(\tfrac{1}{10}-\tfrac{3}{10\sigma}\right)\sin\sqrt{3}/\sqrt{2}\right.$$

$$\left. - \tfrac{\sqrt{3}}{2\sqrt{2}}\left(1+\tfrac{1}{\sigma}\right)\sin\sqrt{3}/\sqrt{2} + \left(\tfrac{1}{5}+\tfrac{2}{5\sigma}\right)e^{-\sqrt{3}/\sqrt{2}}\right] \qquad \text{(II-151)}$$

(II-145) then gives the horizontal velocity set up by the divergence of $\hat{w}^{(1,0)}$:

$$\hat{u}^{(1,1)} = \frac{1}{\sqrt{2}}\frac{d^2}{dz^2}\left(\tfrac{1}{4}f^2\right) e^{-\sqrt{3}/\sqrt{2}}\left[\left(\tfrac{1}{10}+\tfrac{7}{10\sigma}\right)\sin\sqrt{3}/\sqrt{2}\right.$$

$$-\left(\tfrac{4}{5}+\tfrac{3}{5\sigma}\right)\cos\sqrt{3}/\sqrt{2} - \tfrac{\sqrt{3}}{2\sqrt{2}}\left(1+\tfrac{1}{\sigma}\right)\sin\sqrt{3}/\sqrt{2} \qquad \text{(II-152)}$$

$$\left. - \tfrac{\sqrt{3}}{2\sqrt{2}}\left(1+\tfrac{1}{\sigma}\right)\cos\sqrt{3}/\sqrt{2} + \left(\tfrac{1}{5}+\tfrac{2}{5\sigma}\right)e^{-\sqrt{3}/\sqrt{2}}\right]$$

Using (II-152) and (II-138) to satisfy the boundary condition (II-112) we find:

$$\int_0^\infty \mathcal{J}^{(1,1)}(k)\cos kz\,dk + \frac{1}{\sqrt{2}}\left(\tfrac{3}{5}+\tfrac{1}{5\sigma}\right)\frac{d^2}{dz^2}\left(\tfrac{1}{4}f^2\right) = 0 \qquad \text{(II-153)}$$

or

$$\mathcal{J}^{(1,1)}(k) = -\frac{\sqrt{2}}{\pi}\left(\tfrac{3}{5}+\tfrac{1}{5\sigma}\right)\int_0^\infty \frac{d^2}{dz^2}\left(\tfrac{1}{4}f^2\right)\cos kz\,dz \qquad \text{(II-154)}$$

(II-154) determines $\mathcal{J}^{(1,1)}$ and hence, via (II-137) and (II-138), determines $\overline{T}^{(1,1)}$ and $\overline{u}^{(1,1)}$, the lowest order nonlinear

corrections to the horizontal velocity and temperature anomaly fields. We collect all these correction fields for convenience of reference:

$$\hat{w}^{(1,0)} = \frac{d}{dz}\left(\frac{1}{4}f^2\right)e^{-\sqrt{2}z}\left[-\left(\frac{1}{5}+\frac{2}{5\sigma}\right)\cos\sqrt{2}z - \left(\frac{1}{10}-\frac{3}{10\sigma}\right)\sin\sqrt{2}z \right.$$
$$\left. -\frac{3}{2\sqrt{2}}\left(1+\frac{1}{\sigma}\right)\sin\sqrt{2}z + \left(\frac{1}{5}+\frac{2}{5\sigma}\right)e^{-\sqrt{2}z}\right] \qquad \text{(II-155)}$$

$$\hat{T}^{(1,0)} = \frac{d}{dz}\left(\frac{1}{4}f^2\right)e^{-\sqrt{2}z}\left[\left(\frac{2}{5}-\frac{1}{5\sigma}\right)\cos\sqrt{2}z - \left(\frac{3}{10}-\frac{9}{10\sigma}\right)\sin\sqrt{2}z \right.$$
$$\left. -\frac{3}{2\sqrt{2}}\left(1+\frac{1}{\sigma}\right)\cos\sqrt{2}z - \left(\frac{2}{5}-\frac{1}{5\sigma}\right)e^{-\sqrt{2}z}\right] \qquad \text{(II-156)}$$

$$\hat{u}^{(1,1)} = \frac{1}{\sqrt{2}}\frac{d^2}{dz^2}\left(\frac{1}{4}f^2\right)e^{-\sqrt{2}z}\left[\left(\frac{1}{10}+\frac{7}{10\sigma}\right)\sin\sqrt{2}z - \left(\frac{4}{5}+\frac{3}{5\sigma}\right)\cos\sqrt{2}z \right.$$
$$\left. -\frac{3}{2\sqrt{2}}\left(1+\frac{1}{\sigma}\right)\left(\sin\sqrt{2}z+\cos\sqrt{2}z\right) + \left(\frac{1}{5}+\frac{2}{5\sigma}\right)e^{-\sqrt{2}z}\right] \qquad \text{(II-157)}$$

$$\bar{u}^{(1,1)} = -\int_0^\infty \mathcal{J}^{(1,1)}(k)e^{-k^3 s}\cos kz\, dk \qquad \text{(II-158)}$$

$$\bar{T}^{(1,1)} = \int_0^\infty \mathcal{J}^{(1,1)}(k)e^{-k^3 s}\sin kz\, dk \qquad \text{(II-159)}$$

$$\bar{w}^{(1,3)} = -\int_0^\infty k^2\mathcal{J}^{(1,1)}(k)e^{-k^3 s}\sin kz\, dk \qquad \text{(II-160)}$$

$$\mathcal{J}^{(1,1)}(k) = -\frac{\sqrt{2}}{\pi}\left(\frac{3}{5}+\frac{1}{5\sigma}\right)\int_0^\infty \frac{d^2}{dz^2}\left(\frac{1}{4}f^2\right)\cos kz\, dz \qquad \text{(II-161)}$$

Computations for a particular f(z)

Profiles of the nonlinear correction fields have been computed for the same source function $f = e^{-z^2}$ used to illustrate the linear fields. In these computations we take $\sigma = 1$. In figure 11 are plotted horizontal profiles of the vertical velocity $\hat{w}^{(1,0)}$ in the buoyancy layer. We see that the basic upward flow of the linear buoyancy

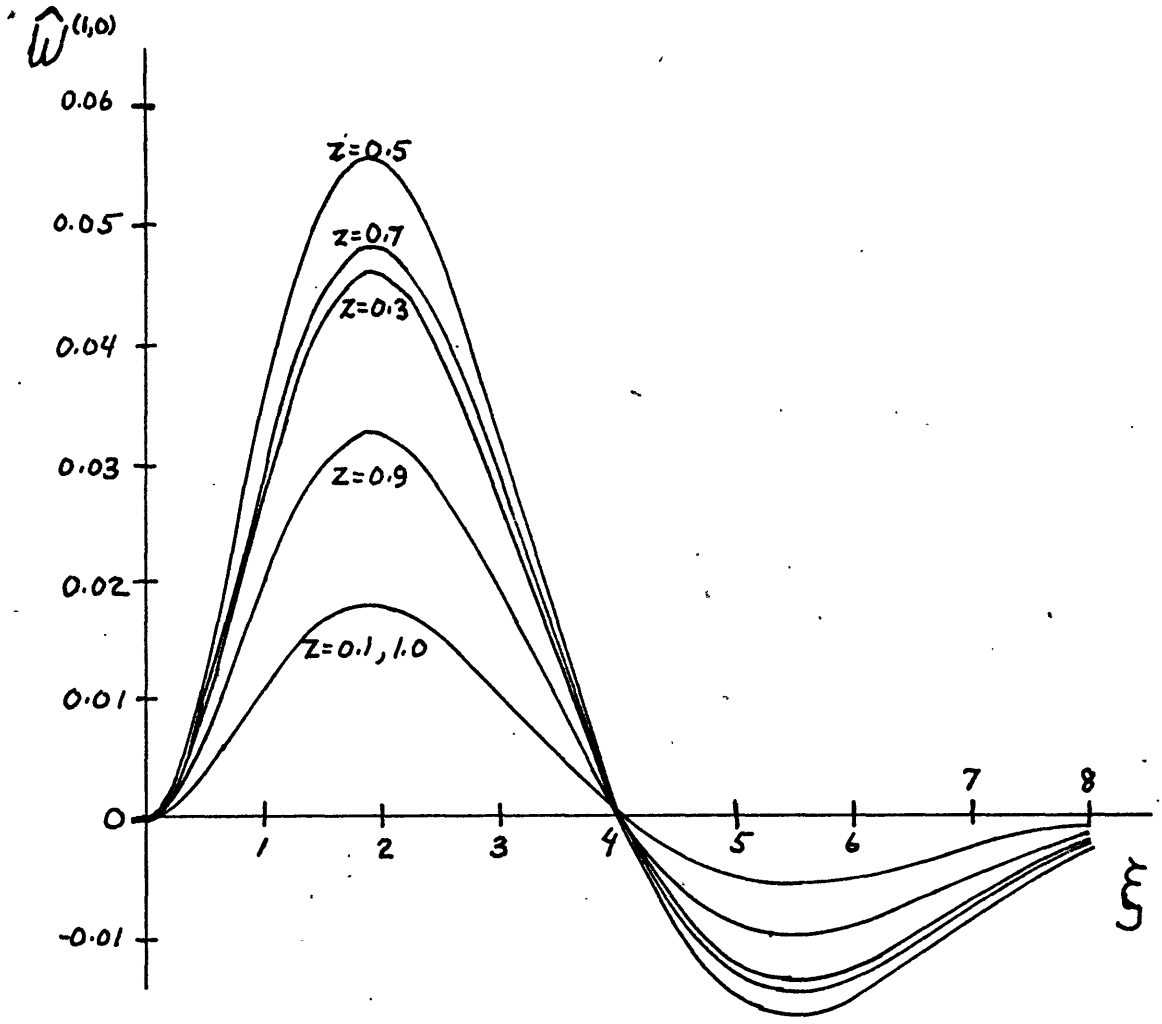


Figure 11 Nonlinear correction to buoyancy layer vertical velocity.

layer (figure 3) is enhanced by this correction for $z > 0$ and retarded for $z < 0$. The horizontal velocity which results from continuity is shown in figure 12. In similarity to (II-93) the quantity plotted is the total nonlinear correction velocity in the buoyancy layer, $\hat{u}^{(1,1)} + \bar{u}^{(1,1)}(0,z)$. Profiles of $\hat{T}^{(1,0)}$ are drawn in figure 13. For $z > 0$ there is near the wall a region of positive values and at larger ξ a region of negative values, the reverse being true for $z < 0$. The streamlines of the motion in the buoyancy layer are shown in figure 14; the streamfunction is defined similarly to (II-94).

In figure 15 profiles of the far field horizontal velocity correction $\bar{u}^{(1,1)}$ are plotted. We see the usual broadening and decrease of amplitude with increasing s. The amplitude decreases faster with s than the amplitude of the linear field $\bar{u}^{(0,1)}$, which is reasonable in view of the fact that $\bar{u}^{(1,1)}$ varies more rapidly in z and should therefore suffer dissipation by viscosity more strongly. The same comment applies to the other nonlinear correction fields. The total horizontal velocity in the far field is $\bar{u}^{(0,1)} + \delta\bar{u}^{(1,1)}$, and in figure 16 we plot this quantity for $\delta = 5/8$, a large value chosen to emphasize the nonlinear effect. We see that the profile in the region of the outflow ($z > 0$) is sharpened, the profile of the return flow is broadened, and the level of zero velocity moved up to

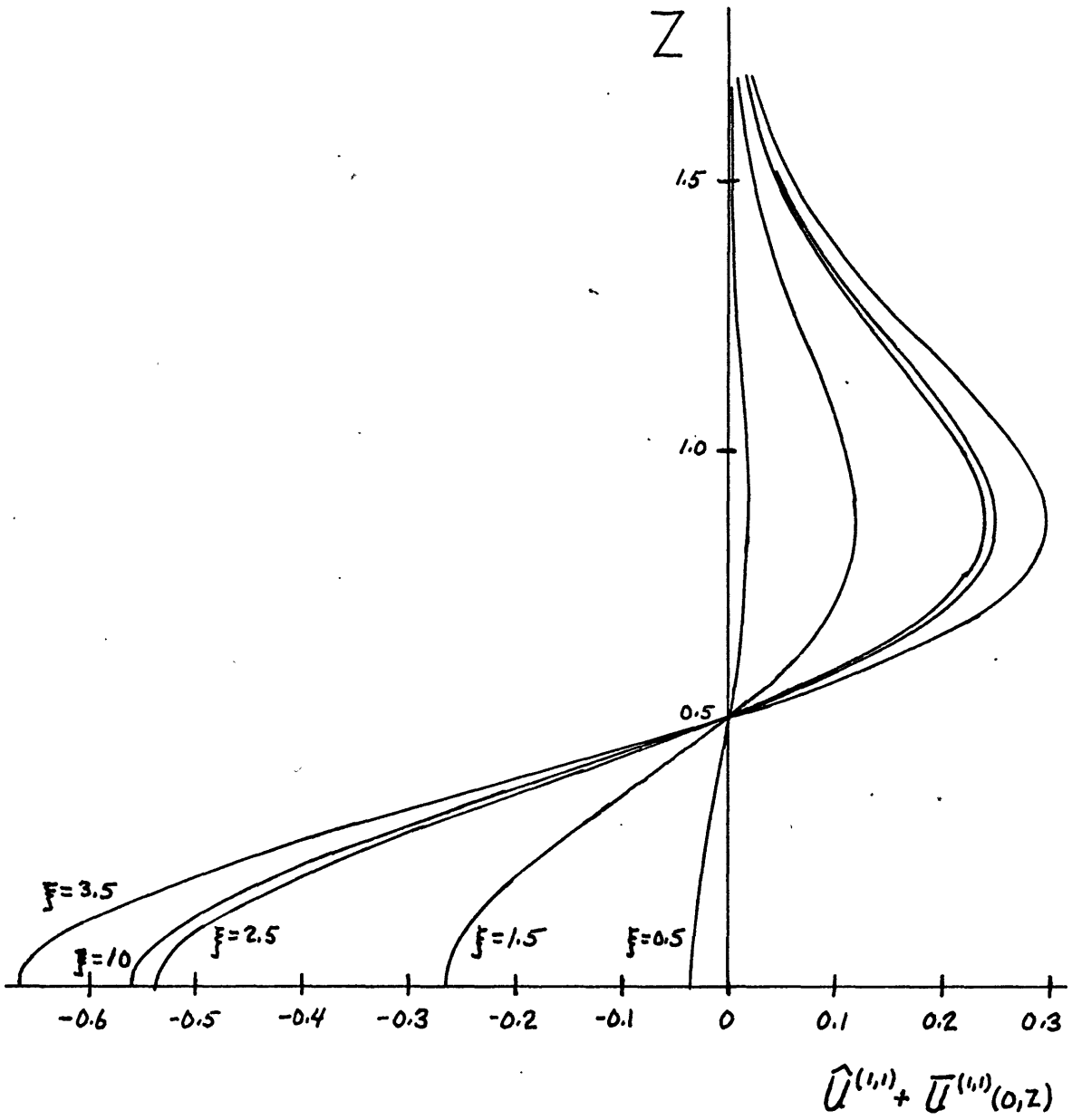


Figure 12. Nonlinear correction to buoyancy layer horizontal velocity.

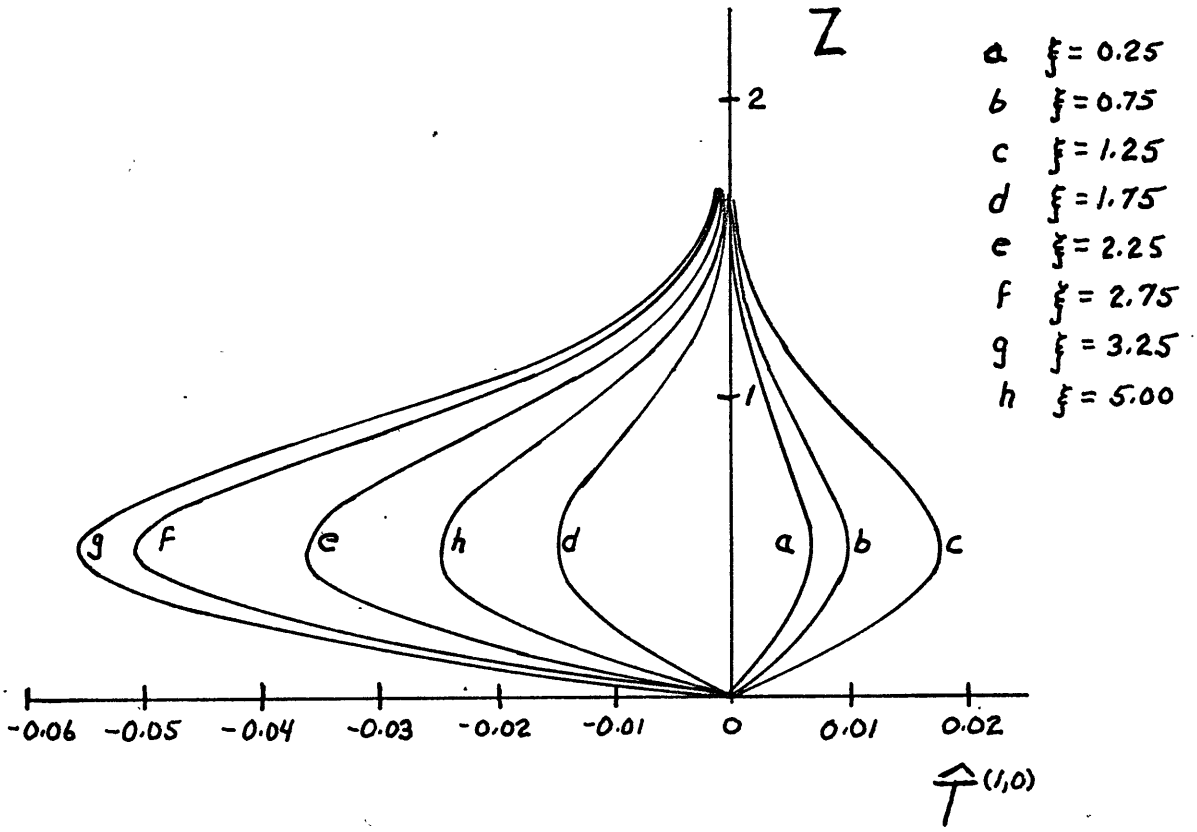


Figure 13 Nonlinear correction to buoyancy layer temperature anomaly.

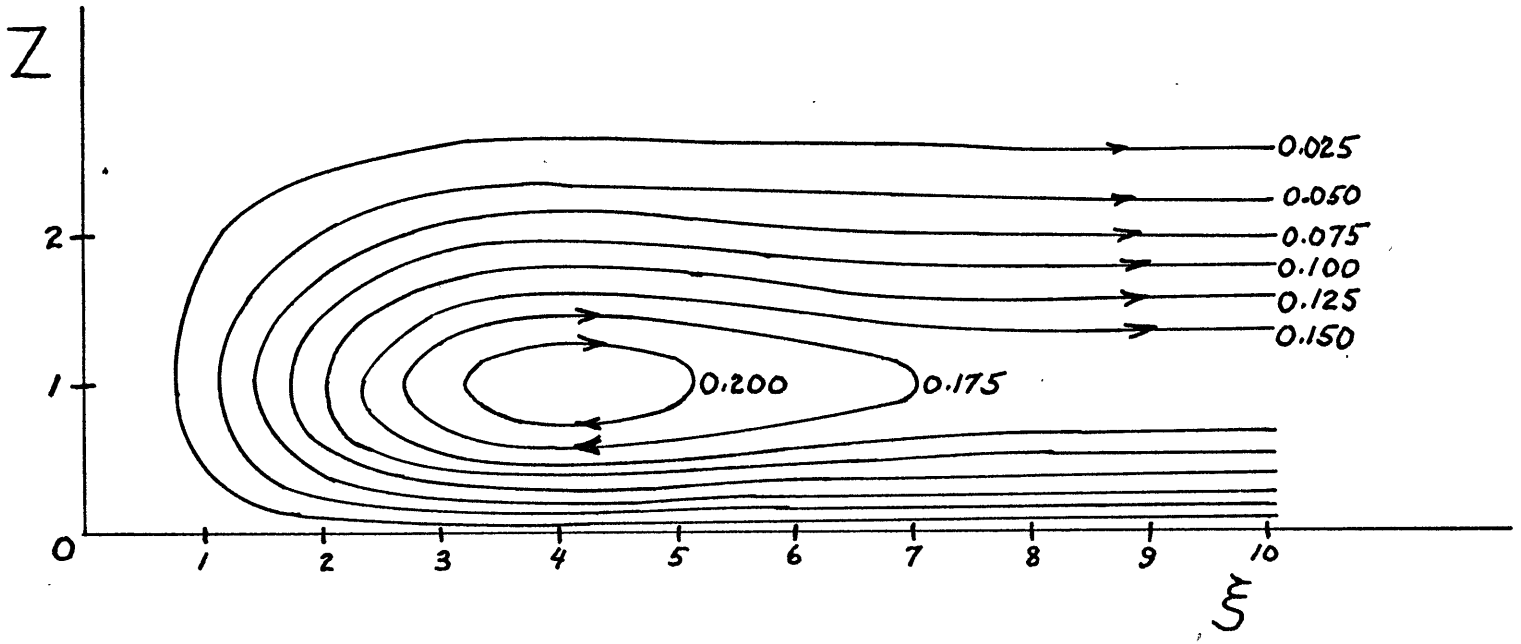


Figure 14 Nonlinear correction to buoyancy layer streamlines.

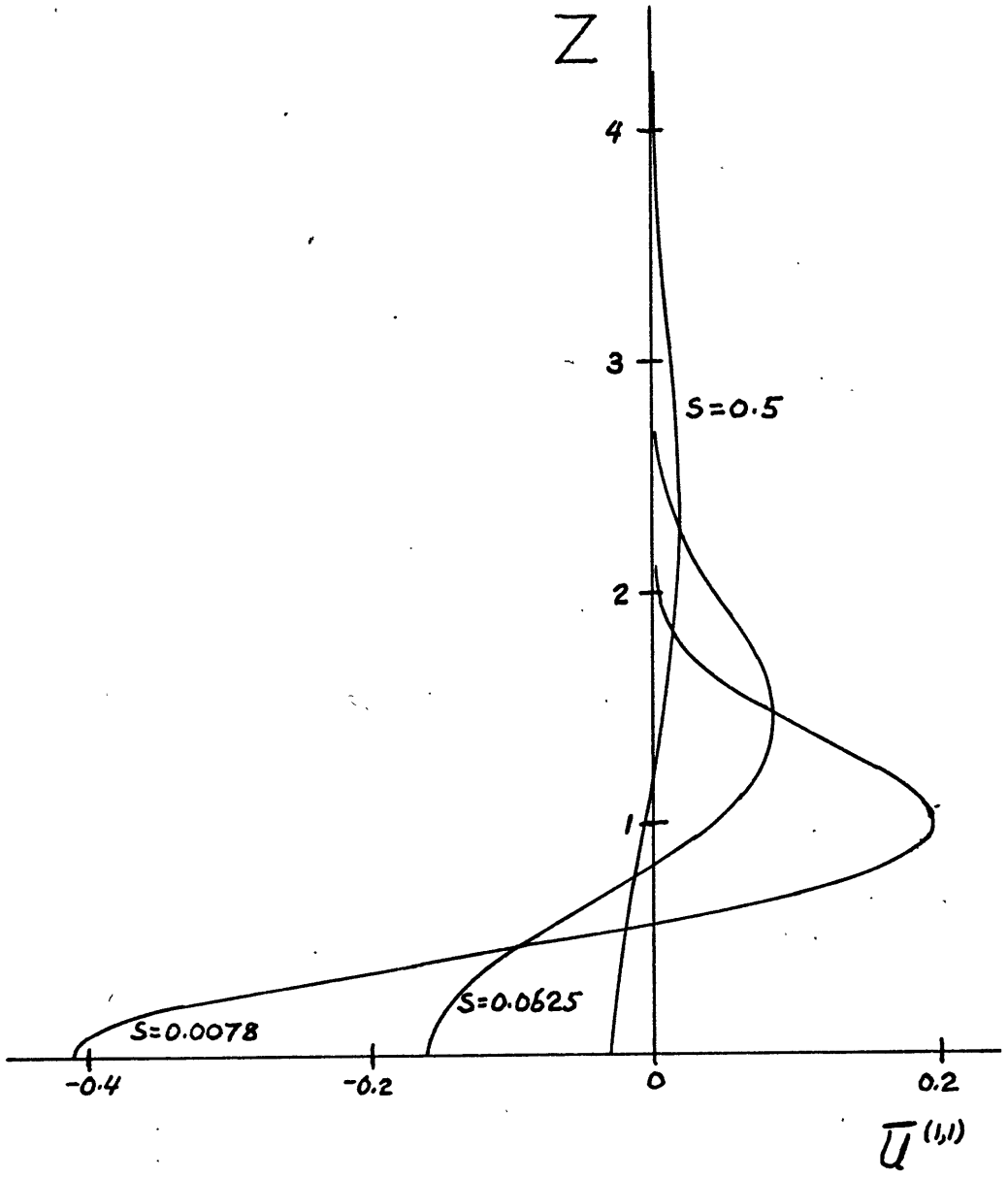


Figure 15 Nonlinear correction to far field horizontal velocity.

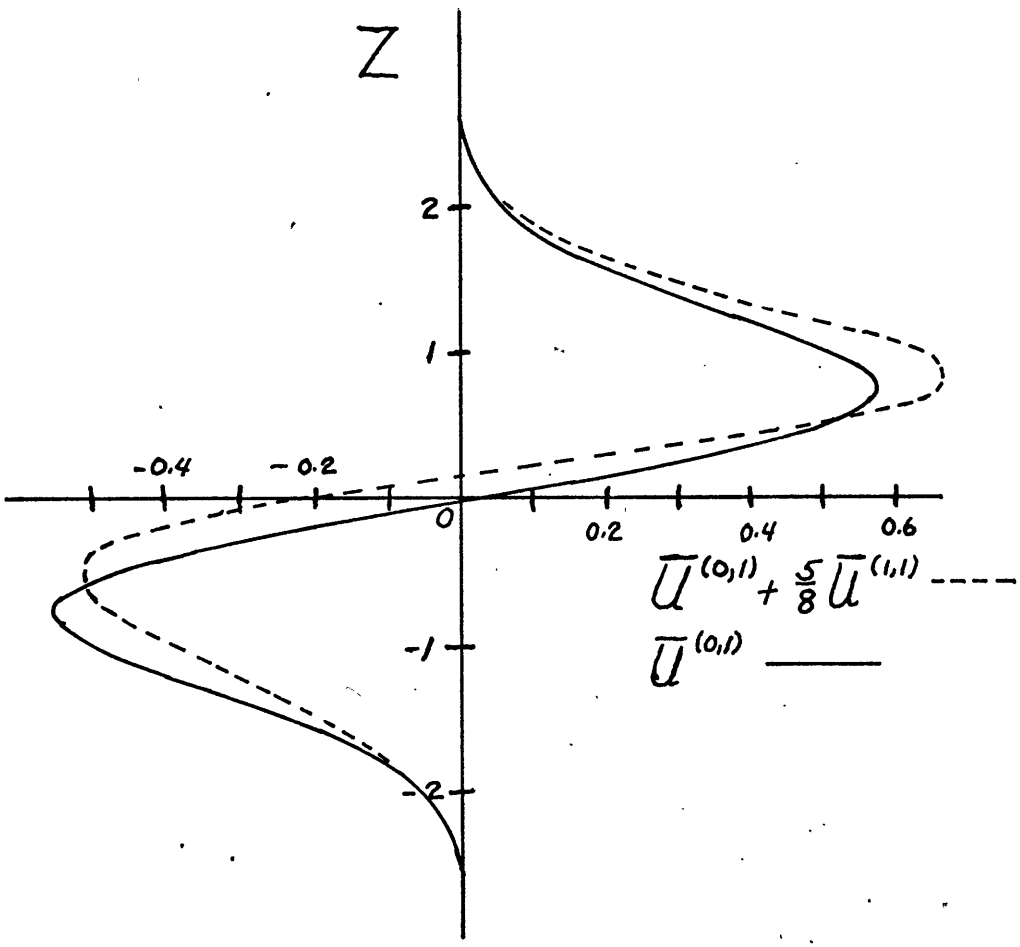


Figure 16 Total far field horizontal velocity for $\delta = 5/8$.

positive z. For a cold source the linear fields reverse sign but the nonlinear corrections, dependent on $(f(z))^2$, do not; in this case the outflow ($z < 0$) is again sharpened, the return flow broadened, and the level of zero velocity moved to negative z. The nonlinear correction to the temperature anomaly, $\bar{T}^{(1,1)}$, is plotted in figure 17 and the total temperature anomaly $\bar{T}^{(0,1)} + \delta \bar{T}^{(1,1)}$ with $\delta = 5/8$ is plotted in figure 18. The nonlinear correction leads to an elevation of the core of relatively warmer fluid; with a cold source the central core of relatively cold fluid would be depressed. The profiles of $\bar{w}^{(1,3)}$ are presented in figure 19 and the streamlines in figure 20.

The computed elevation of the maxima of horizontal velocity and of temperature anomaly is not peculiar to our e^{-z^2} source but is a general effect of the nonlinear corrections. Refer to (II-158):

$$\bar{u}^{(1,1)}(0,z) = \frac{1}{\sqrt{2}} \left(\frac{3}{5} + \frac{1}{5\sigma}\right) \frac{d^2}{dz^2} \left(\frac{1}{4} f^2\right)$$

This is the value of $\bar{u}^{(1,1)}$ at the outer edge of the buoyancy layer. Likewise from (II-84) and (II-89)

$$\bar{u}^{(0,1)}(0,z) = -\frac{1}{\sqrt{2}} f'$$

Thus the total velocity is:

$$\bar{u} = \frac{1}{\sqrt{2}} \left[-f' + \beta (f^2)'''\right], \quad \beta \equiv \frac{\delta}{4} \left(\frac{3}{5} + \frac{1}{5\sigma}\right)$$

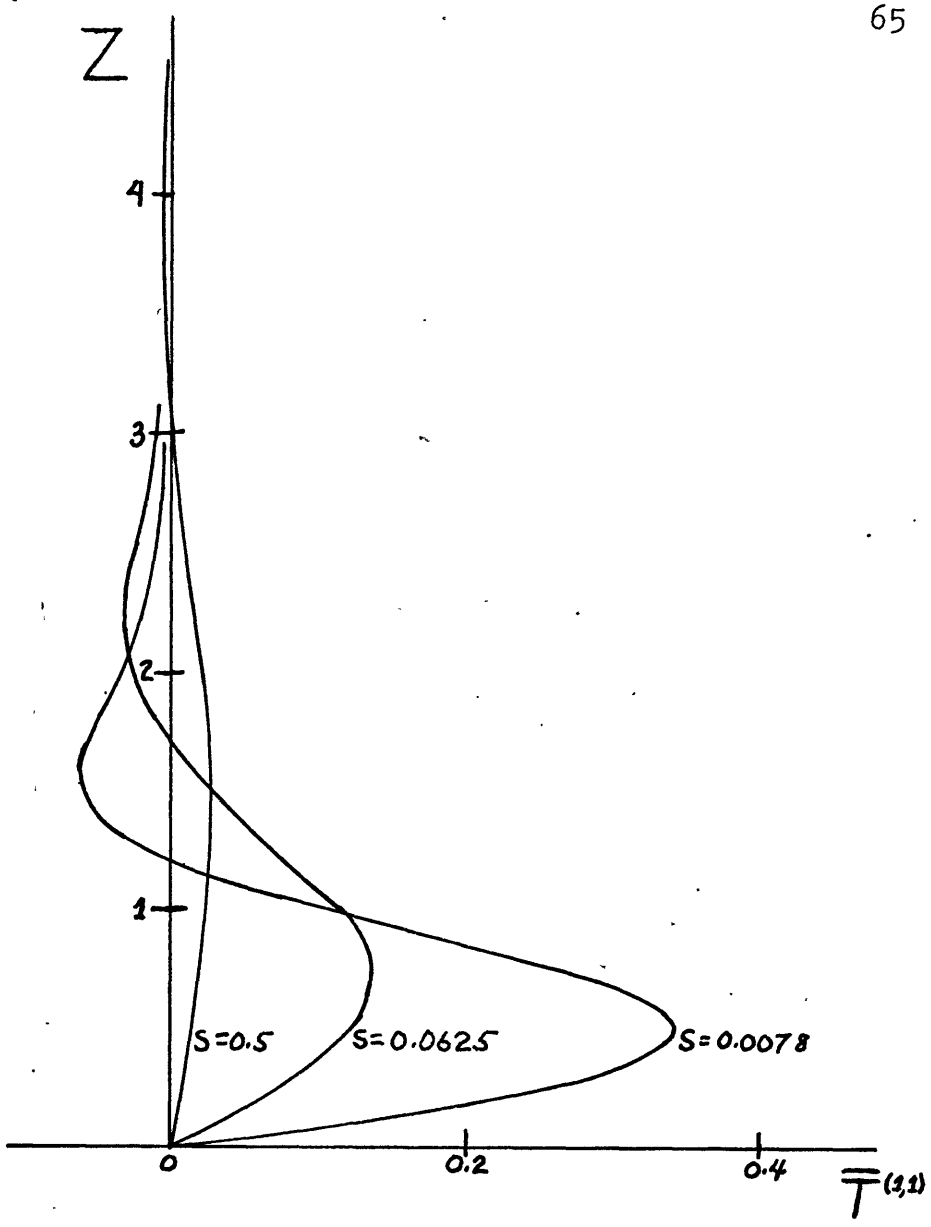


Figure 17 Nonlinear correction to far field temperature anomaly.

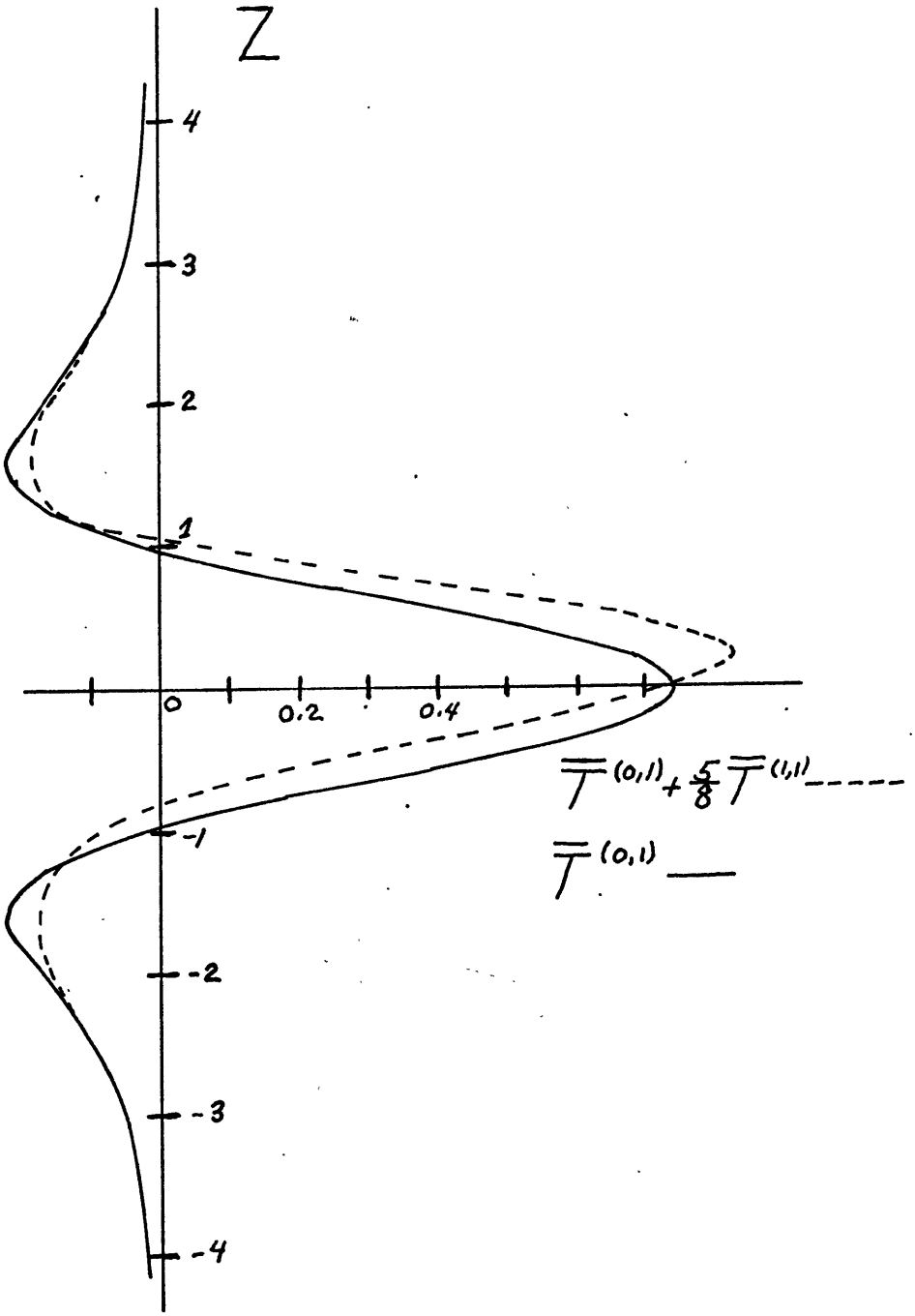


Figure 18 Total far field temperature anomaly for $\delta = 5/8$.

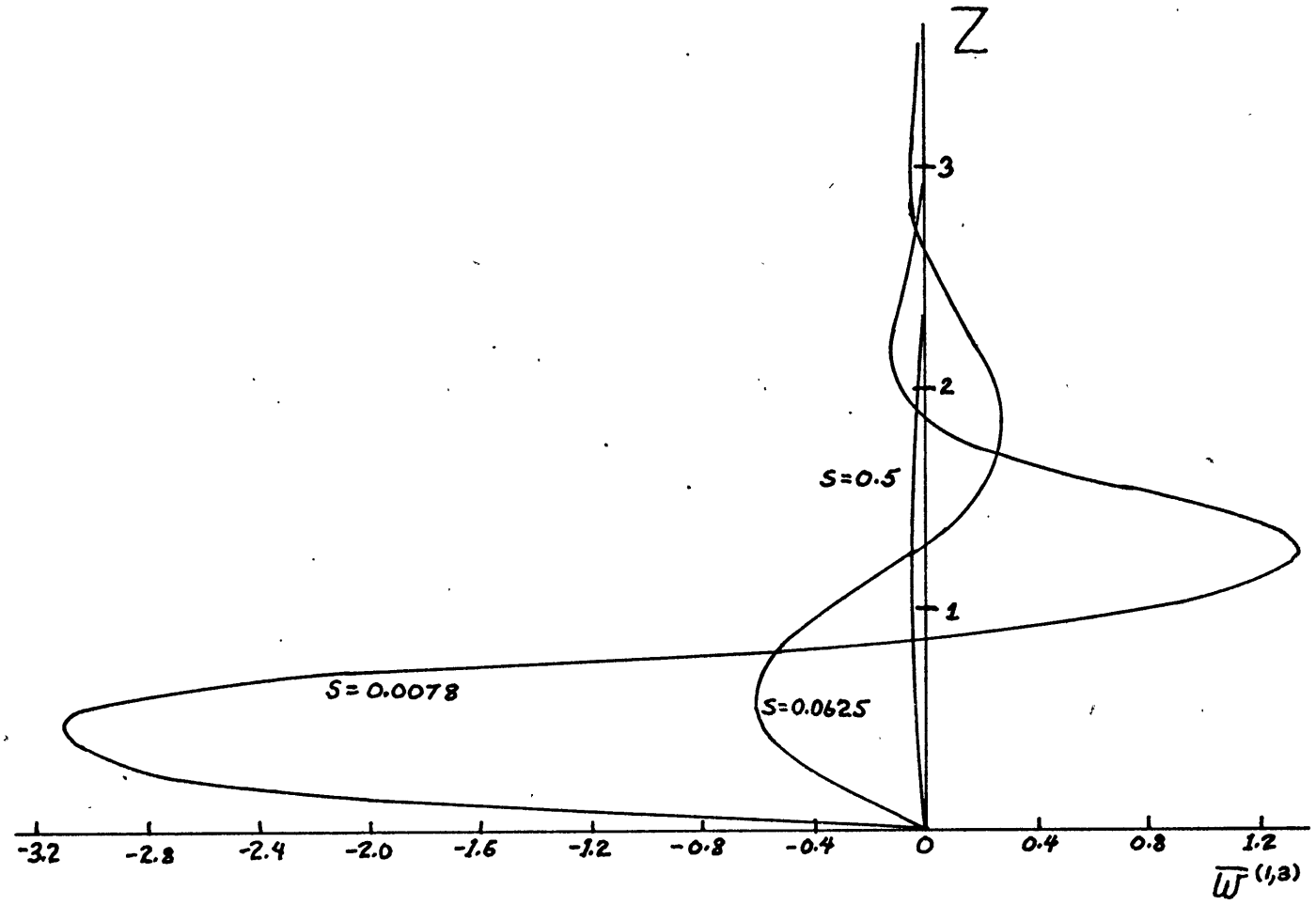


Figure 19 Nonlinear correction to far field vertical velocity.

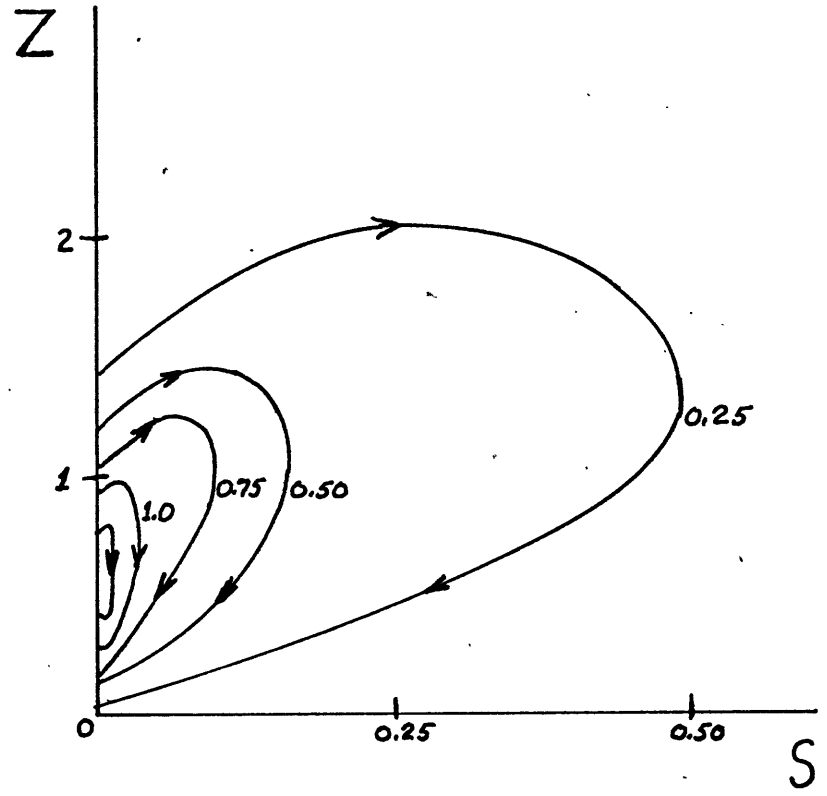


Figure 20 Nonlinear correction to far field streamlines.

Hence:

$$\bar{u}_z = \frac{1}{\sqrt{2}}\left(f'' + \beta(2ff''' + 6f'f'')\right)$$

and $\bar{u}$ therefore has its maximum at z_c such that

$$\frac{f''}{f'''} = \frac{2\beta}{1-6\beta F'}$$

Now $f > 0$ and in $z > 0$, $f' < 0$, so the ratio f''/f''' is positive at $z = z_c$. A glance at figure 21, which shows the qualitative forms of f and its derivatives, reveals that z_c must lie above z_a, which is the level of the maximum linear velocity.

Summary

The linear calculation results in a long flat convection cell or tongue containing two distinct regimes of flow. Near the source is a buoyancy layer, a region in which vertical advection of the mean temperature is balanced by horizontal heat conduction and the buoyancy of fluid parcels is balanced by the horizontal gradient of the vertical component of stress. The vertical velocity and temperature anomaly are O(1) in the power series expansion in ϵ. Variation in z of the imposed flux of heat into the fluid gives rise to z-variation of the vertical velocity, which in turn, by continuity of mass, results in a horizontal velocity of order ϵ. This horizontal

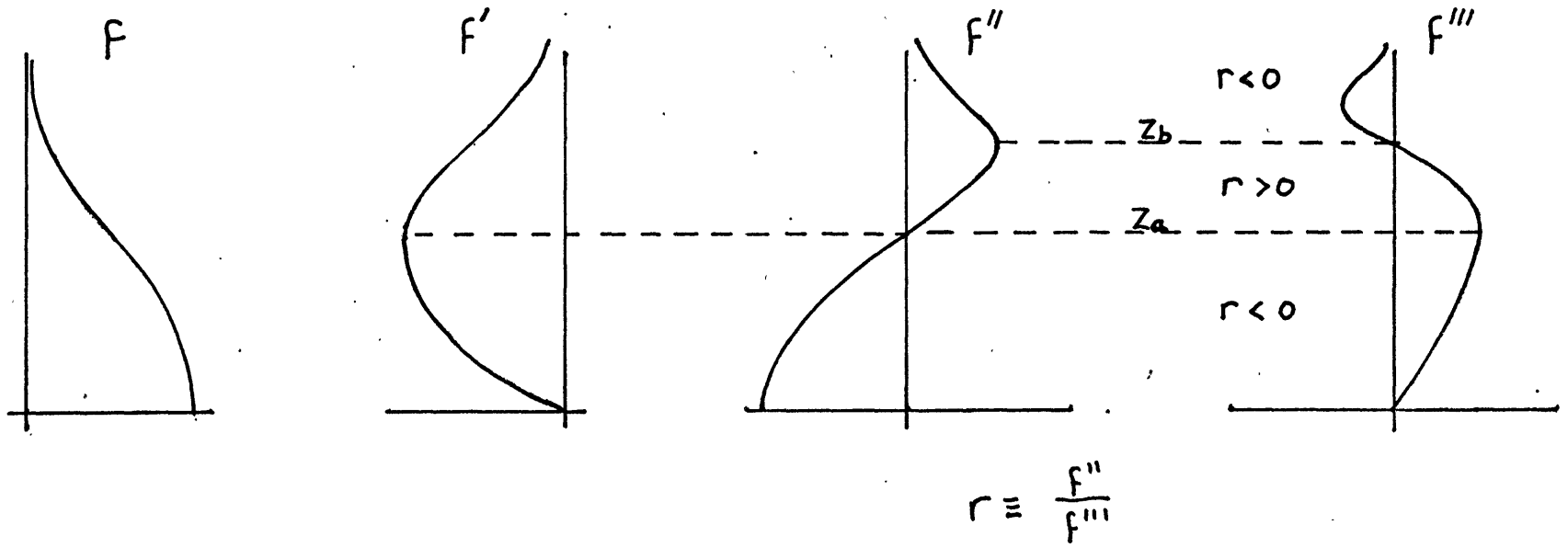


Figure 21 Qualitative relationships between f(z) and its derivatives.

velocity then extends into the second region, the far field. Here vertical advection of the mean temperature is balanced by vertical heat conduction, the horizontal pressure gradient by the vertical gradient of the horizontal component of stress, and the buoyancy force by a hydrostatic vertical gradient of pressure anomaly. The pressure and temperature anomalies in this region, like the horizontal velocity, are $O(\epsilon)$; the vertical velocity is two orders smaller.

The central feature of this tongue is that the scalar which "marks" the flow, the temperature anomaly, is not simply a tracer but also gives rise to a dynamically important force, buoyancy. Because of this, distributions of velocity and temperature anomaly bear quite different relationships to each other from those found in a tongue marked by a passive tracer.. The level of largest temperature anomaly and the level of zero horizontal velocity coincide, at the level of the center of the source. The vertical velocity in the far field is everywhere downwards at this same level.

Inclusion of the most important nonlinear terms through a perturbation expansion leads to a modification of the balance of forces in the buoyancy layer, advections of heat and of vertical momentum becoming important there. No modification of the far field balance of forces occurs,

however; this region simply accepts the now slightly altered horizontal velocity pumped out of the buoyancy layer and dissipates it and its associated temperature anomaly through viscous action and conduction. The profile shapes are altered by the addition of the nonlinear corrections, more so near the source than far from it , as the nonlinear corrections decay faster in s. For a hot source, the outflow lifts upward and intensifies, as does the central core of positive temperature anomaly.

It is instructive to trace the overall flow of heat through this system.. The net flux Q of heat (dimensional) into the fluid takes place by conduction at x = 0:

$$Q = -\rho_0 c_p K \int_{-\infty}^{\infty} \frac{\partial \hat{T}_d^{(0,0)}}{\partial x_d}\, dz_d = -\rho_0 c_p K T_s \int_{-\infty}^{\infty} \hat{T}_f^{(0,0)}\, dz$$

$$= \frac{\rho_0 c_p K T_s}{\epsilon\sqrt{2}} \int_{-\infty}^{\infty} f(z)\, dz$$

where the subscript d indicates a dimensional variable. There is no additional contribution to Q due to the vertical integral of the nonlinear correction $\hat{T}^{(1,0)}$, since this field is odd in z.

This amount of heat then enters the far field by horizontal advection with the velocity $\bar{u}^{(0,1)}$, the outflowing fluid having higher <u>mean</u> temperature than the returning fluid. That is:

$$\rho_o c_p \int_{-\infty}^{\infty} \bar{u}_d^{(0,1)}(0,z_d)\, T_m(z_d)\, dz_d$$

$$= L\rho_o c_p \delta\epsilon \sqrt{\frac{g\alpha\gamma L^2}{\sigma}} \int_{-\infty}^{\infty} \bar{u}^{(0,1)}(0,z)\,(T_o + L\gamma z)\, dz \qquad \text{(II-162)}$$

$$= \frac{\rho_o c_p K T_s}{\epsilon} \int_{-\infty}^{\infty} \bar{u}^{(0,1)}(0,z)\, z\, dz$$

$$= \frac{\rho_o c_p K T_s}{\epsilon} \int_{-\infty}^{\infty} -\frac{z f'(z)}{\sqrt{2}}\, dz \quad = Q$$

At values of s > 0 this integral decreases, vertical conduction and advection in the far field taking up part of the flux. The conductive heat flux in the horizontal is

$$-\rho_o c_p K T_s \epsilon^3 \int_{-\infty}^{\infty} \bar{T}_s^{(0,1)}\, dz = -\rho_o c_p K T_s \epsilon^3 \frac{\partial}{\partial s} \int_{-\infty}^{\infty} \bar{p}_z^{(0,1)}\, dz \qquad \text{(II-163)}$$

$$= -\rho_o c_p K T_s \epsilon^3 \frac{\partial}{\partial s}\left[\bar{p}^{(0,1)}(s,\infty) - \bar{p}^{(0,1)}(s,-\infty)\right] = 0$$

The nonlinear corrections do not contribute any net horizontal advective or conductive flux in the far field because $\bar{u}^{(1,1)}$ is even in z and $\bar{T}^{(1,1)}$ is odd and the integrals corresponding to (II-162) and (II-163) therefore vanish.

Ultimately the far field gets rid of the flux Q by vertical conduction. The conductive heat flux toward $z = +\infty$ at a level z = a is, in dimensional form:

$$-\rho_o c_p K T_s \int_0^\infty \left[\hat{\overline{T}}_z^{(0,0)}(\xi,a) + \epsilon \bar{\overline{T}}_z^{(0,1)}(s,a) \right] dx$$

$$= -\rho_o c_p K T_s \left[\epsilon \int_0^\infty \hat{\overline{T}}_z^{(0,0)}(\xi,a)\, d\xi + \frac{1}{\epsilon} \int_0^\infty \bar{\overline{T}}_z^{(0,1)}(s,a)\, ds \right]$$

$$\simeq -\frac{\rho_o c_p K T_s}{\epsilon} \int_0^\infty \bar{\overline{T}}_z^{(0,1)}(s,a)\, ds$$

Adding a like term for the flux toward $z = -\infty$ across $z = -a$ we have for the flux out of this region:

$$-\frac{2\rho_o c_p K T_s}{\epsilon} \int_0^\infty \bar{\overline{T}}_z^{(0,1)}(s,a)\, ds$$

$$= -\frac{2\rho_o c_p K T_s}{\epsilon} \int_0^\infty -k \mathcal{J}^{(0,1)}(k) \left[\int_0^\infty e^{-k^3 s}\, ds \right] \sin ka\, dk$$

$$= \frac{2\rho_o c_p K T_s}{\epsilon} \int_0^\infty \frac{\mathcal{J}^{(0,1)}(k)}{k^2} \sin ka\, dk$$

Now from (II-84)

$$\int_0^a f(z)\, dz = \sqrt{2} \int_0^\infty \frac{\mathcal{J}^{(0,1)}(k)}{k^2} \sin ka\, dk$$

so our conductive flux is

$$\frac{\rho_o c_p K T_s}{\epsilon \sqrt{2}} \int_{-a}^{a} f(z)\, dz$$

and as $a \to \infty$ this becomes just Q. There is no advective flux to $z = \pm\infty$, for

$$\lim_{a \to \infty} \int_0^\infty \bar{w}^{(0,3)}(s,a)\, T_m(a)\, ds$$

vanishes. The nonlinear corrections also give no net flux contributions, advective or conductive. Finally, all vertically integrated fluxes toward $x = +\infty$ vanish as $x \rightarrow \infty$.

Chapter III Laboratory Experiment

Description

In this section we outline the design of the laboratory experiment set up to model the thermally-driven tongue discussed theoretically in chapter II. It should be mentioned at the outset that the experiment was not expected to yield precise results over a wide range of the several parameters of the problem. Rather it was intended to demonstrate that the long flat convection cell or tongue actually exists and to exhibit some of its grosser features, and these objectives have been achieved. A more elegant apparatus, capable of yielding better data, could be built now, in the light of experience gained in this effort.

As is usually the case in designing an experiment, several compromises on dimensions, values of parameters, etc., must be made. We begin by settling on water as the working fluid because of its transparency, its O(1) Prandtl number as per the theory, and its convenience. The silicone fluids often used in convection experiments are rejected because all except the lowest viscosity ones have high Prandtl numbers, while the low viscosity ones would require a huge experimental tank in order for the

weak dissipative effects to bring the flow in the far field to zero.

Next we recall that the parameter δ, which should be kept small for the model to correspond to the theory, is $T_s/L\gamma$. It is desirable, however, to have T_s large in order that the temperature anomalies in the flow may be measurable and that they may dominate over any spurious temperature anomalies introduced at the sidewalls. Thus we want to keep $L\gamma$ large. $L\gamma$ is limited, though, since the total top-to-bottom temperature difference cannot exceed 96°C without producing either boiling at the top or instability at the bottom, and in practice a difference of 85°C seems reasonable. Thus we set

$$\gamma = 85^{\circ}C/D$$

where D is the depth of the tank in centimeters. Now L must be some small fraction of D at most so that the circulation does not feel the top and bottom of the tank, for the theory is concerned with how the flow is dissipated in the absence of boundaries. Referring to the far field profiles (e.g., figure 6) at s = 4 we see that the circulation may extend over a range in the vertical of about 10L and still retain about 10% of the amplitude present near the source. A safe choice seems to be

$$L = D/20$$

So

$$\gamma L = 4^{\circ}C \qquad \text{(III-1)}$$

Another consideration involving L is that if it is chosen too small the dye lines will be difficult to photograph and interpret. The dimensional far field horizontal velocity on linear theory is $O(\frac{\epsilon\delta}{\sqrt{\sigma}}\sqrt{g\alpha\gamma L^2})$ and hence is proportional to 1/L. If, for example, $\delta = \epsilon = 0.1$ this velocity is about $0.01\sqrt{L}$ cm/sec and to have observable displacements of a dye line before it is obliterated by diffusion it seems necessary to keep L of O(1 cm) or larger. Referring now to figure 22 we can see how limited our choices are. The curved line is the locus of points for which $\delta = \epsilon$; ideally we would like to operate in the region $\delta < \epsilon$ so that our theoretical perturbation scheme would be valid. The vertical lines denote various choices of L subject to the condition (III-1), and on account of the dye diffusion problem we would like to operate well to the left on this plot. The farther to the left we go, the smaller T_s becomes. We finally come to what is at root an ad hoc choice and select the operating point shown by the cross in the figure. This gives the following values to design around:

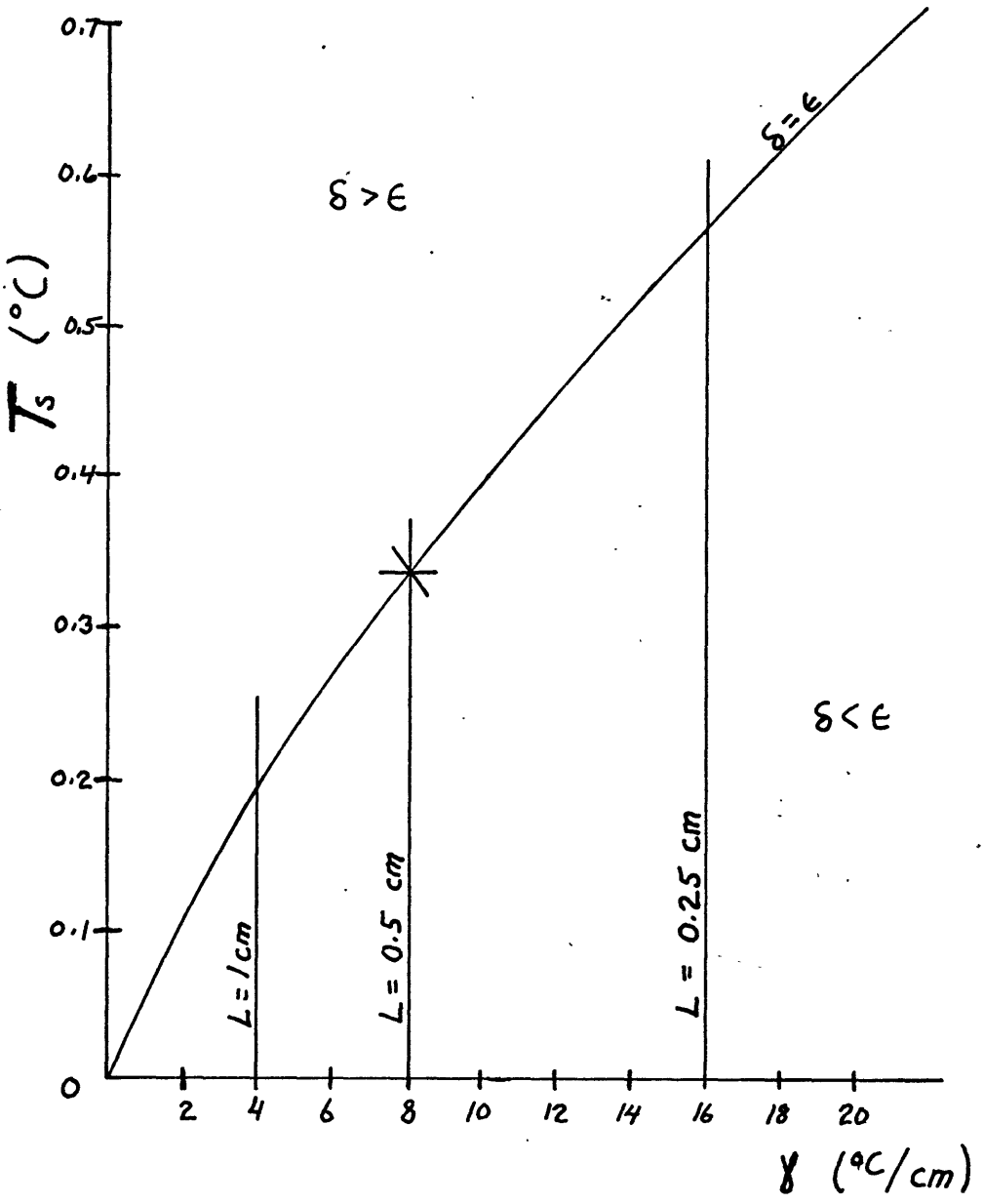


Figure 22 Diagram indicating choice of operating parameters.

$$\delta = \epsilon = 0.08$$

$$T_s = 0.33^{\circ}C$$

$$\gamma = 8^{\circ}C/cm$$

$$L = 0.5 \text{ cm}$$

$$D = 10 \text{ cm}$$

Then if we plan the tank long enough for s = 4, as seems sensible from the far field profiles, we have

$$Lx = \text{tank length} = 4L\epsilon^{-2} = 200cm$$

The choice of a width for the tank is made as follows. Ideally we would like the width much larger than any other dimension, large enough for any extraneous temperature perturbations introduced at the sidewalls to decay to zero before reaching the axis of the tank, leaving an undisturbed interior region in which to observe the flow driven by a source on one end wall. This would be a prohibitively large tank. We must therefore try to insulate the sidewalls thermally and to check that any secondary flows introduced by the presence of sidewalls are small. For a perfectly insulating, vertical sidewall there is no direct adjustment of the interior temperature field required, but there is a velocity boundary condition to be met. It is straightforward to show that there exists a viscous boundary layer

which can bring the interior horizontal velocity (the far field horizontal velocity of the theoretical two-dimensional problem) to zero and which introduces negligible alterations of the other dependent variables. This boundary layer is discussed in appendix IV. At the end of the tank opposite the source (s = 4) this boundary layer alters the flow 10 cm in from the sidewall by only about 5%. Thus a tank width of about 20 cm should suffice. With these features of the design rationalized we proceed to describe the actual hardware of the experiment.

The experimental tank and major pieces of auxiliary apparatus are shown in figure 23. The upper plate, base plate, and icebath plate were of anodized aluminum, 1", 1/2", and 1/2" in thickness, respectively. Cemented to the top surface of the upper plate was a custom-made electric heating pad (Electroflex Heat) covering the entire plate. The heating wires were spaced about 1/4" apart to give very uniform heating. A proportional temperature controller (not shown; YSI Model 72) was used to regulate the power supplied to the heating pad and hold the upper plate at a fixed temperature ($\pm$ 0.05°C). The thermister probe of this unit was placed in a blind hole in the upper plate center along with some Dow Corning heat sink grease to ensure good thermal contact between probe and plate. 16 copper-constantan thermocouple junctions, two per hole

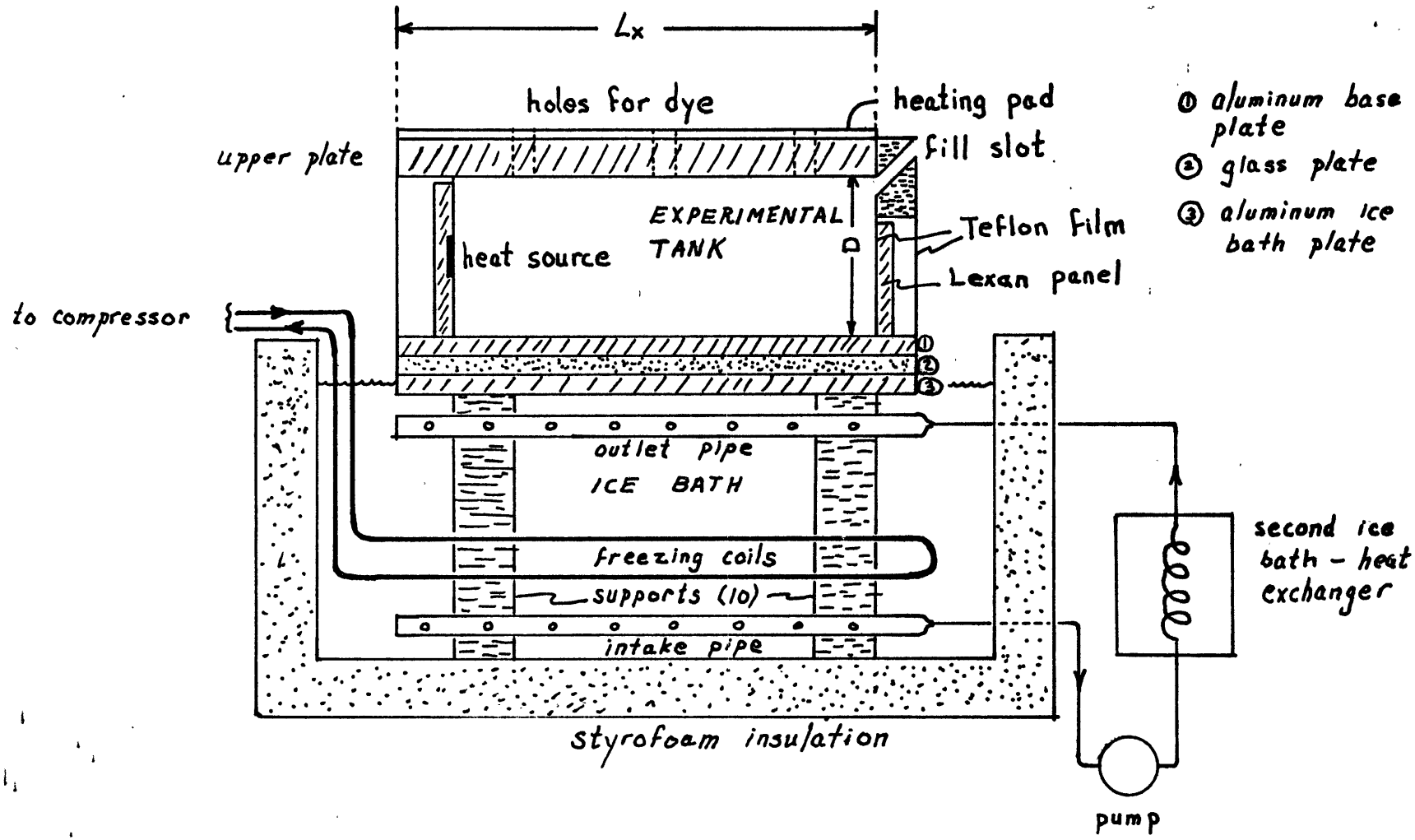


Figure 23 Side view of the major pieces of apparatus (not to scale).

to provide spares in case of damage to the fine wires (#40) were placed in 8 blind holes in the upper plate. These holes were arranged in a pattern as shown in figure 24 and were drilled from above to within 1/16' of the lower face of the upper plate; the thermocouples thus sensed very nearly the temperature at the water-aluminum boundary, for the temperature drop across 1/16" of aluminum at the planned heat flux is only about $0.004^{o}C$. The junctions were electrically insulated with a bead of Devcon 5-Minute epoxy, and the remaining space in the holes was filled with heat sink grease. An exactly similar array of junctions was placed in the baseplate; the wires were led out in fine grooves cut in the lower face of this plate. These arrays were used to check on lateral temperature differences in the plates by connecting junction #3 to any of the other junctions to form a thermocouple. Special thermocouple switches (Omega Engineering) were used for this purpose and were housed in a thermally insulated box. In addition junction # 6 of the base plate could be connected to junction #3 of the upper plate to find the temperature difference across the depth of the tank. Voltage readings were made on a Kiethley Model 149 milli-microvoltmeter. Several small holes were drilled through the upper plate to allow dye particles to be dropped; a few of these holes are indicated schematically in figure 23. The holes were plugged when not in use.

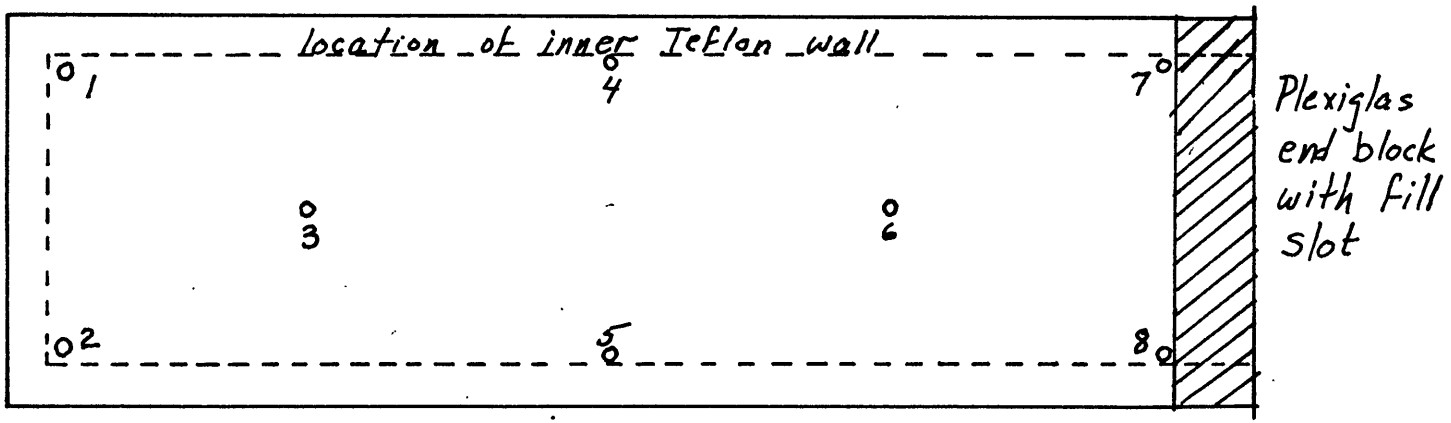


Figure 24 Positions of thermocouple junctions in the upper plate. A similar array is mounted in the base plate.

The bottom of the tank was a sandwich consisting of an aluminum base plate, a glass plate, and an aluminum icebath plate. Thin layers of heat sink grease on both sides of the glass plate ensured thermal contact. The original plan was for the icebath plate to be in contact with a reservoir of ice-water mixture and thus to be at $0^{\circ}C$. The glass would then provide enough thermal resistance so that the base plate would be at about 9 or $10^{\circ}C$, well above the $4^{\circ}C$ point. In this way it was hoped to avoid the more usual cooling system of thermostatted water circulating in channels cut in the base plate. To carry away the heat flux through the tank (about 40 cal/sec) with, say, a $0.1^{\circ}C$ temperature rise between inlet and outlet of the cooling water, would have required a flow rate of 400 cc/sec, and this flow would have had to be distributed evenly through a large number of channels. The ice-water scheme, in principle, would have solved these problems through the natural downward convection of the melt water formed underneath the icebath plate, and one day's operation would have only required the melting of about 100 lbs of ice to absorb the heat flux through the experiment. In practice, however, the ice chips clumped and remained submerged by sticking to the support columns in the bath, and enough additional heat leaked into the bath that the ice supply was depleted in half a day. The author feels, however,

that with a bit more work this technique can provide effective cooling for similar experiments much more cheaply than conventional thermostatted circulators and it is for this reason that he mentions a device which did not work.

The arrangement finally used to provide cooling is sketched in figure 23 and is essentially a circulated water system. A 1/3 hp circulating pump maintained the bath temperature uniform at about 6°C and freezer coils in the bath plus a second ice bath heat exchanger in the pump circuit provided additional cooling. Despite its make-shift look this apparatus maintained the temperature of base plate steady (change of 1°C over 30 hours) and laterally constant (< 0.25°C difference between junction #3 and nos. 4,5,6; < 0.5°C between junction #3 and nos. 1,2,7,8 which are in the extreme corners of the tank).

The tank walls were made of 0.005" Teflon FEP film, backed by 1/4" Lexan panels for strength and flatness, as shown in figure 25. The film, which can stretch slightly, was used because the upper plate elongated by about 3mm at its working temperature of 85°C. A rigid wall fixed to the upper and base plates would suffer severe stresses under these conditions; the Lexan panels were not thus clamped. A second Teflon wall 3/4" outside the panels trapped a dead air space for thermal insulation. In addition 2" thick styrofoam insulation was placed outside the

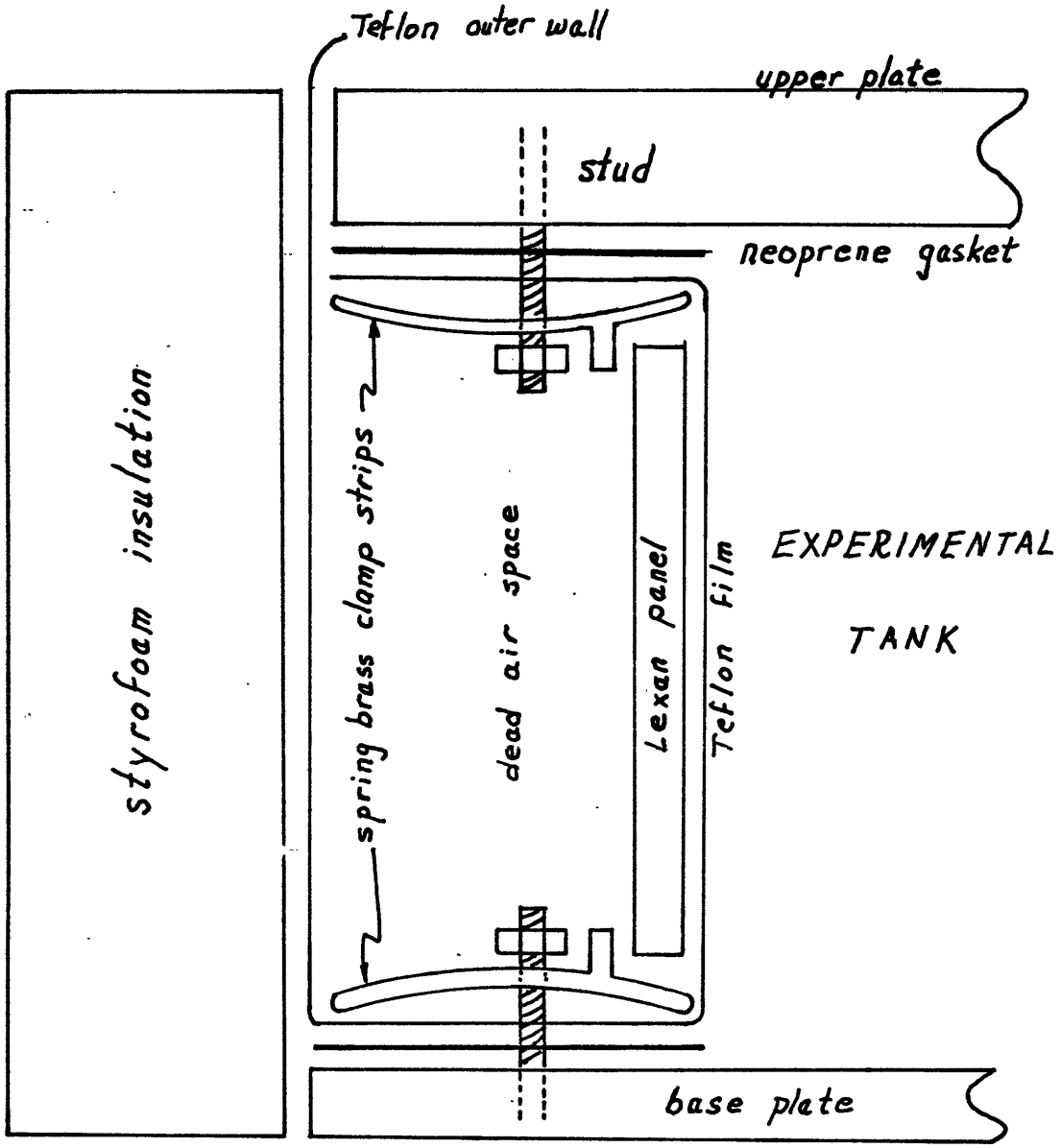


Figure 25 Section through a sidewall showing construction. Exploded view.

outer Teflon wall. Small sections of the styrofoam were removed briefly to permit photography.

The heat source was a strip of Chromel resistance ribbon 3/8" wide x 0.005" thick mounted at mid-depth on one end wall and spanning the width of the tank. The heat supplied to the fluid by the source was determined simply by measuring the electric power dissipated in it. Chromel was chosen because in water it neither corrodes nor reacts significantly with aluminum and because it is fabricated in ribbons to close tolerances.

The entire apparatus was supported on a rigid framework of 4" steel I-beams, the upper plate and the lower sandwich being independently suspended. The levels of the various plates relative to the framework were checked during runs by micrometer measurements and found not to vary observably. The overall tilt of the framework relative to a level surface (a trough of still water) was also checked. The largest effect was found to be due to the bending of the building by solar heating and amounted at most to an angle of 10^{-4} radians or a difference in level between the ends of the tank of about 0.02 cm. This is about the order of magnitude reported by Simon and Strong (1968).

Conduct of experimental runs

To begin a run the tank was filled with distilled water. A large immersion heater was inserted via the fill slot and the water was boiled for several minutes to drive out dissolved air. The heater was then removed, short vertical pipes were fitted into the dye holes, and boiled water from an outside reservoir was fed into the fill slot at a slight pressure. The temperature of the upper plate was set above boiling and thus the water being added at the fill slot boiled at the lower surface of the upper plate, the steam venting through the pipes and sweeping away residual air. After several minutes the temperature of the upper plate was lowered to its operating value of 85°C and the cooling apparatus was turned on. Residual bubbles of steam under the upper plate condensed leaving the tank very free of bubbles. The author is indebted to Mr. Bruce Magnell and to Mr. John Van Leer for suggesting this method of dealing with a mundane but most troublesome problem. The reservoir of boiled water remained connected to the fill slot to maintain the water level against the volume contraction during the cooling and stratification process. The tank was allowed about 12 hours to equilibrate to a static, stably stratified condition.

To check on the static equilibrium in the absence of forcing by the source the tank was stratified once before

the heat source was built in. All four walls were then insulators; had the metal heat source been present, even with no power supplied to it, it would have constituted a thermal short-circuit and consequently a temperature anomaly. In this fully insulated configuration dye streaks exhibited no appreciable movement, either along the length of the tank or transversely, and this was taken as evidence that the desired motionless stratified equilibrium existed in the absence of forcing. The heat source was then built into the tank and runs with forcing could be made.

The actual gathering of the data was straightforward. A value of forcing (voltage applied to the source) was set up and the flow allowed to equilibrate for about 2 hours. Then a small (0.3 mm) particle of potassium permanganate dye was dropped through one of the upper plate holes. After a few seconds to allow the flow to readjust the dye streak was photographed at two separate times, usually about one minute apart. This process was repeated at other holes and then a new value of the forcing was set up. Velocity profiles were determined from the photograph pairs simply by measuring displacements of the dye line.

Experimental results

The data obtained are now presented. The mean tem-

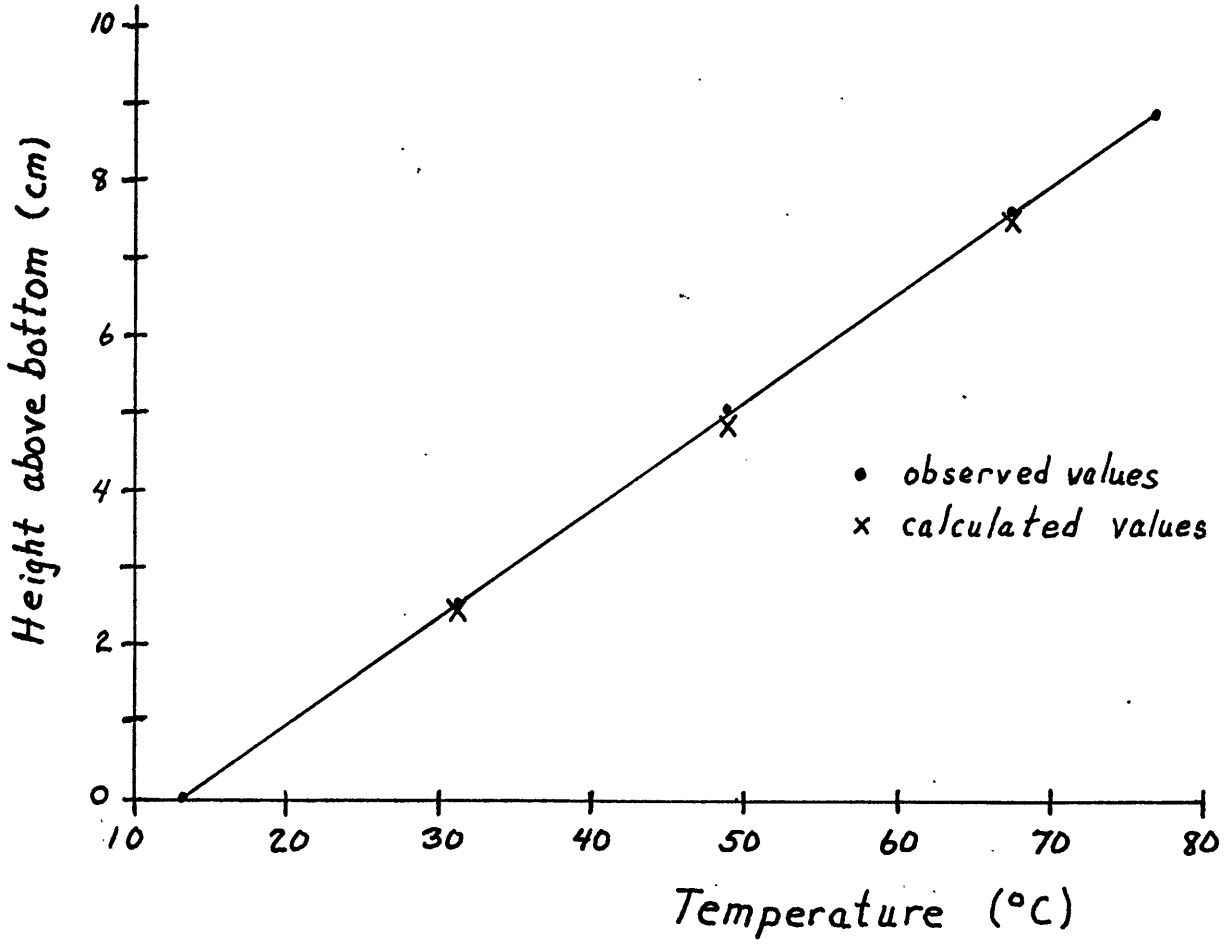


Figure 26 Observed temperature distribution in the tank during the runs. Calculated values are based on tabulated values of thermal conductivity of water (International Critical Tables, 1928).

perature profile, measured with a thermocouple probe, is shown in figure 26, and is seen to deviate only slightly from a profile based on tabulated values of the heat conductivity of water. The line in figure 26 is simply a straight line connecting the two endpoints. These measurements are far too crude to reveal any temperature anomalies due to the flow and are presented only to show that no gross departure from the equilibrium profile is present. One could, for example, have homogeneous layers with sharp interfaces. With insulating sidewalls this is a motionless state but not one in which we want to conduct experiments. From figure 26 we also determine the value of γ, 7.2°C/cm. The parameter ϵ is then calculated using L = 0.49cm (the half-width of the source strip) and values of ν, κ, α appropriate to the mid-depth temperature of 49°C; the result is ϵ = 0.08. (International Critical Tables, 1928)

The variation of the fluid properties with temperature is a significant, but hopefully not catastrophic, departure from the conditions of the theoretical model, The worst offenders are the viscosity and the thermal expansion coefficient which vary in the opposite sense with temperature and whose ratio enters into ϵ. This ratio varies between 2.06 cgs at 35°C and 0.82 at 63°C; these temperatures represent the vertical limits of the observable flow. Thus $(\nu/\alpha)^{1/4}$, to which ϵ is proportional, varies from 1.2

to 0.96 or by about 25%. Alternatively one can estimate from the observed profiles and tabulated values of ν the term νu_{zz} and compare it with the term $\nu_z u_z$ neglected in the basic equation (II-9). The neglected term is about 10% of the term retained. Certainly any attempts at more precise experiments should be compared to computer solutions of the equations with variable fluid properties and not to the constant-coefficient model developed here.

The parameter δ is determined by an approximate calculation as follows. From (II-85) the dimensional horizontal temperature gradient at x = 0 is:

$$T_x = \frac{T_s f}{\epsilon L \sqrt{z}}$$

We do not know the exact form of f in the experiment; let us suppose f = 1 over the entire source ribbon. Then the total heat flux into the fluid, Q, is:

$$Q = \rho_o c_p \kappa A T_x$$

where A is the area of the source and c_p is the specific heat of water. From this expression we have

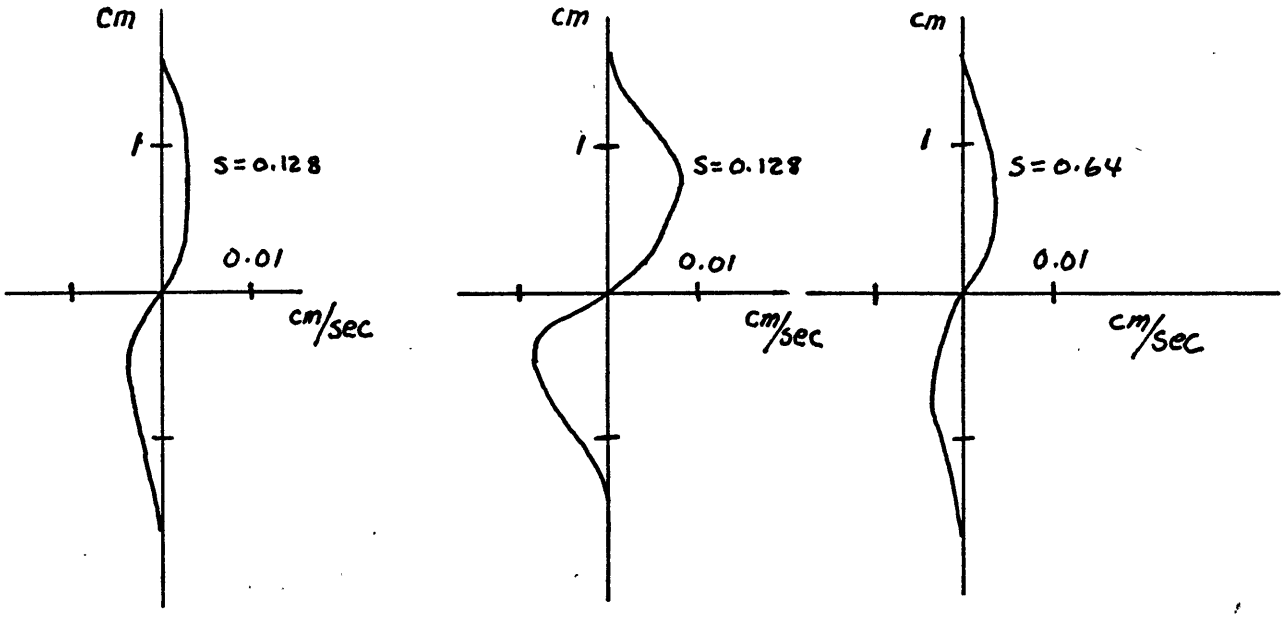
$$\delta = \frac{T_s}{\gamma L} = \frac{\epsilon Q \sqrt{z}}{\rho_o c_p \kappa A}$$

and δ is thus determined by known constants and the electric power dissipated in the source; we assume that the Lucite backing permits heat from the source to go nowhere except into the water.

The velocity profiles are presented in figures 27

and 28. In these figures the origin has been placed at the point of coincidence of the two dye traces from which the profile was determined and thus does not correspond to a fixed geometrical level. An oversight in the photographic alignment technique left the photographs devoid of a sufficiently accurate reference for such a level, but the point of dye line coincidence is unambiguous. The primary observation to be made is that the profiles do look qualitatively as expected from the theory. The decrease of amplitude with increasing s is apparent in the series of three profiles at $\delta = 3.6$ (figure 28) and in the pair of profiles at $\delta = 0.9$ (figure 27b). Dye lines were also photographed at s = 0.64, 1.28 for $\delta = 0.225$ and at s = 1.28 for $\delta = 0.9$ but the lines did not move by as much as their own width during the time allowed by dye diffusion; the velocities were thus less than about 0.002 cm/sec, and this number is a reasonable estimate of the error in the profiles in figures 27 and 28.

A few rough quantitative comparisons with theory are possible. In Table II we show three quantities. The first is the observed value of the vertical distance (nondimensionalized with L) between the velocity maximum and the velocity zero. The second is the computed value of this quantity for the e^{-z^2} source on linear theory, and the third is the computed value using both linear



27 a

27 b

Figure 27 Observed horizontal velocity profiles, for δ = 0.225 (27 a) and for δ = 0.9 (27 b).

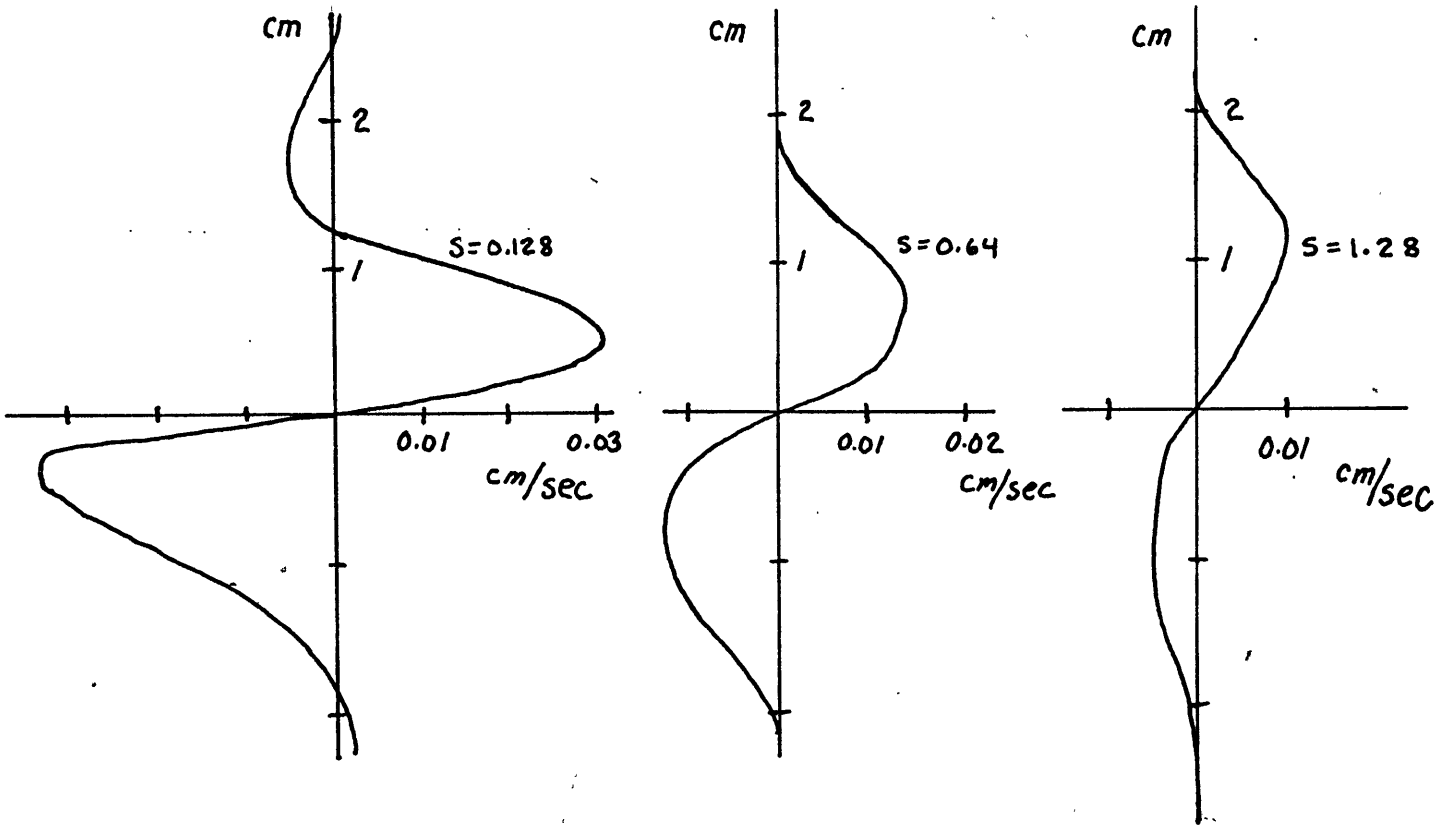


Figure 28 Observed horizontal velocity profiles for $\delta = 3.6$.

and nonlinear terms. We see that in the δ = 3.6 series (figure 28) the observed values agree rather well with the values from the full computation, better than with the purely linear computation. This indicates that the expected narrowing and intensifying of the outflow by nonlinear effects actually occurrs.

In Table III we show the difference in level of zero velocity between the value at δ = 0.225 and the values at δ = 0.9, 3.6, both observed and computed. The magnitudes do not agree well but the trend at s = 0.128 toward greater elevation of the zero level with increasing δ is observed, again indicating the presence of the calculated nonlinear effects.

In Table IV we show the values of the maximum positive (outflow) velocity, observed, computed on linear theory, and computed in full. The observations have been nondimensionalized with the velocity scale factor $\frac{\epsilon\delta}{\sqrt{\sigma}}\sqrt{g\alpha\gamma L^2}$ to make them commensurable with the theory. The agreement is not good. The δ = 3.6 series disagrees with the full computation by a factor of about 2; the δ = 0.9 series by a factor of about 1.5. Within the δ = 3.6 series and the δ = 0.9 series, though, the ratios of velocity maxima at different s values agree fairly well with computed ratios, indicating that the theoretical rate of decay of amplitude with s is observed.

Table II

Values of the nondimensional vertical distance between level of zero velocity and level of maximum velocity

	Observed	Linear computation	Nonlinear computation
δ = 3.6			
s = 0.128	1.06	1.42	0.97
0.64	1.49	1.87	1.44
1.28	2.35	2.25	1.83
δ = 0.9			
s = 0.128	1.38	1.25	1.10
s = 0.64	1.27	1.62	1.50
δ = 0.225			
s = 0.128	1.60	1.12	1.10

Table III

Differences in level of zero velocity

	Height of zero level for δ = 3.6 less height for δ = 0.225 (nondimensional distance)		Height of zero level for δ = 3.6 less height for δ = 0.9 (nondimensional distance)	
	Observed	Computed	Observed	Computed
s = 0.128	1.3	0.35	1.0	0.3
s = 0.64	---	---	0.4	0.3

Table IV

Values of the maximum positive nondimensional velocity

	Observed		Linear computation		Nonlinear computation	
$\delta = 3.6$						
s = 0.128	0.225	2.2	0.329		0.425	2.1
s = 0.64	0.102	1.4	0.179		0.200	1.5
s = 1.28	0.071		0.123		0.132	
$\delta = 0.9$						
s = 0.128	0.232	2.3	0.329		0.345	1.9
s = 0.64	0.102		0.179		0.181	
$\delta = 0.225$						
s = 0.128	0.306		0.329		0.329	
		ratio				ratio

The use of the computations for the e^{-z^2} source instead of computations based on the (unknown) experimental f(z) as a standard of comparison for the observations is not as bad a device as might be thought, for at large distances from the source the details of f(z) affect the profiles only slightly. What matters are integrated properties of f(z) such as $\int_{-\infty}^{\infty} f(z)\,dz$ (cf. (II-96) and the discussion immediately preceeding; also appendix I). In figure 29 we show the profile of $\overline{u}^{(0,1)}(s = 0.128, z)$ calculated for the e^{-z^2} source and also calculated for an extreme source function:

$$f(z) = 1, \quad -1 \leq z \leq 1$$
$$= 0 \quad \text{elsewhere}$$

This is a source function which injects delta-function horizontal velocity profiles into the far field at $z = \pm 1$. The calculation was made using some tabulated functions due to Koh (1966) and the units on the velocity axis are his nondimensional units. The point to note is that the two profiles are quite similar even at this modest value of s; the pathological profile introduced at s = 0 is quickly smoothed out. Our experimental source is undoubtedly not so pathological and thus it is a reasonably good approximation to use the computations for the e^{-z^2} source.

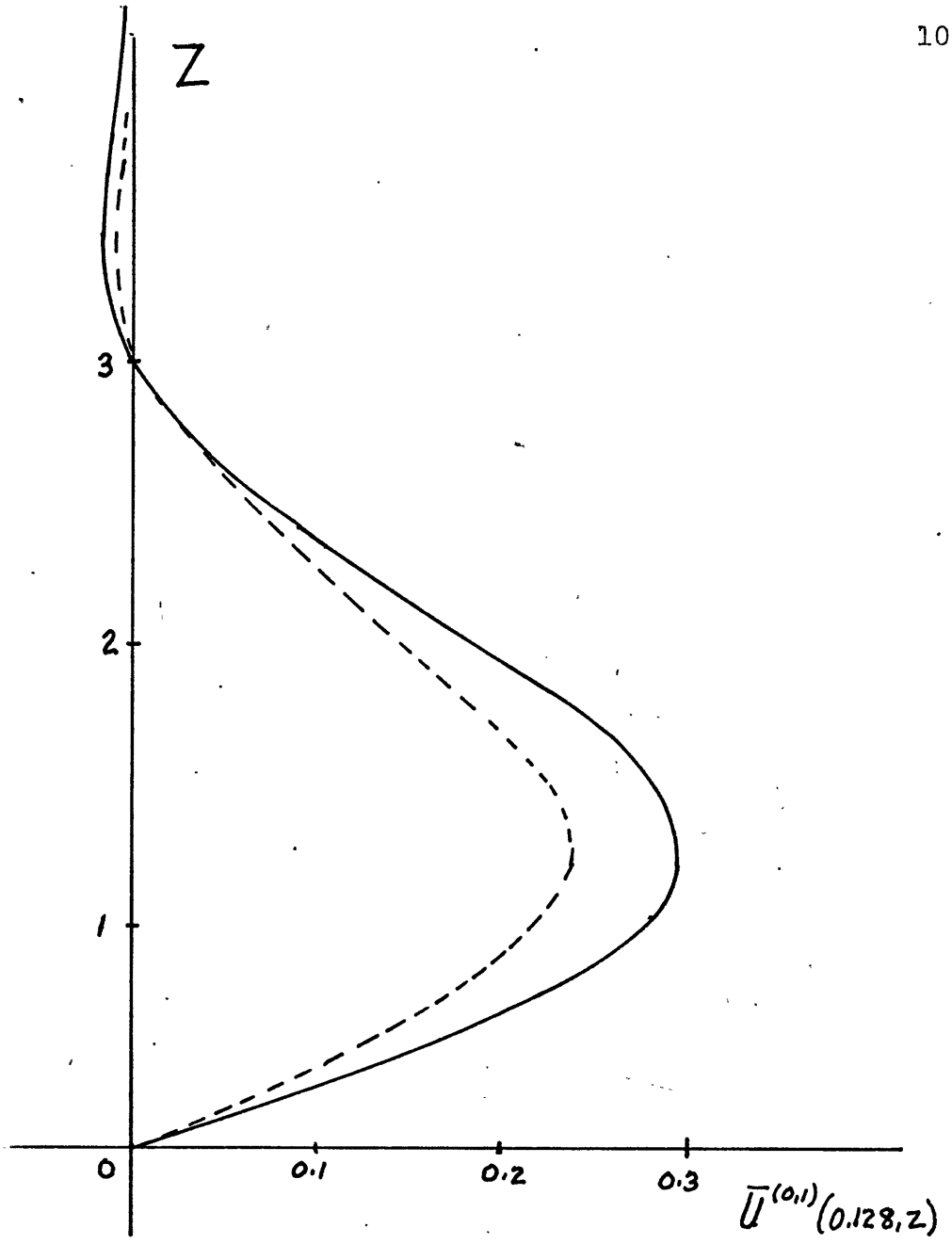


Figure 29 Comparison between far field horizontal velocity due to e^{-z^2} source (dotted line) and rectangular source function (solid line).

It should be pointed out here that some of the observed profiles appear not to conserve mass, e.g., the profile at s = 0.128, δ = 3.6 (figure 28). Errors in tracing dye lines cannot account for such a large discrepancy; moreover, there is a pronounced reversal above 1 cm which is not observed on the other profiles of the series. Some local perturbation of unknown origin is suspected, perhaps related to bubbles which had begun to form when this, the final profile, was measured.

Finally, in figure 30 we present three profiles taken with δ = 3.6, s = 0.64 at different times after the initiation of forcing. Note that there is very little difference between them; the flow was steady during this time. Thus our procedure of making photographs 2 hours after setting up the forcing seems certain to have avoided observing transient flows; there is no doubt that a dynamical balance between heating at the source and dissipation in the far field was achieved. The 2 hour wait is more than sufficient on theoretical grounds also, for the flow should become steady at least in the conductive time scale $O(L^2/\kappa$ = 160 sec).

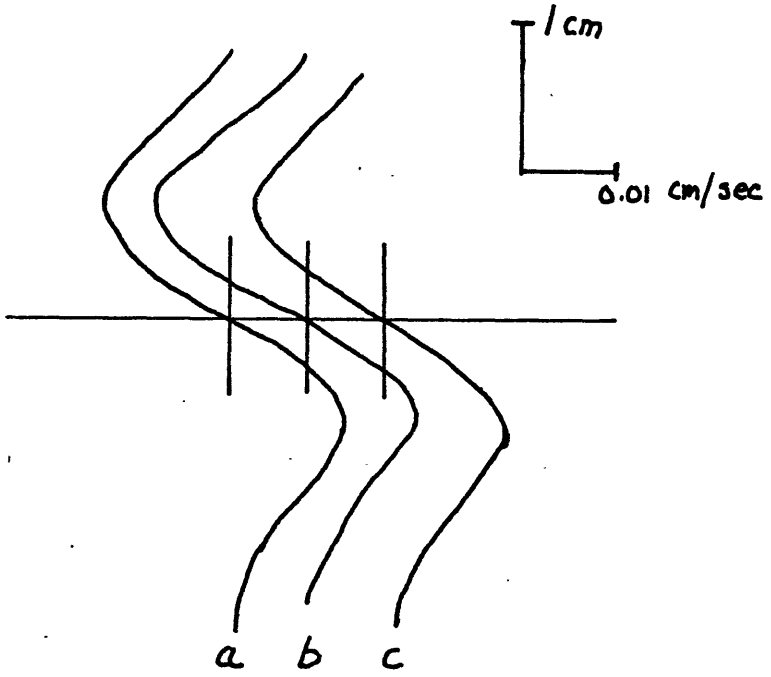


Figure 30 Three profiles taken at δ = 3.6, s = 0.64, and at 1/2 hour (a), 1 hour (b), and 2 hours (c) after starting the forcing.

Chapter IV Concluding Remarks and Suggestions

We have seen that the predicted tongue of Chapter II is in fact observed in the laboratory, and that certain of the primary effects of nonlinearities are also found. We now outline several ways in which both theory and experiment could be extended and improved.

The mathematical scheme and fluid geometry of chapter II can be used directly to solve for the flow due to other kinds of sources. We can, for example, set $u(0,z) = f(z)$, and thereby model a source of mass. If we specify $T(0,z)$ and $w(0,z)$ correctly, we can avoid having a buoyancy layer (cf. appendix I). With a symmetric $f(z)$ we will obtain in the linear solution a a symmetric u and an antisymmetric T; the highest velocity will now coincide with the zero of temperature anomaly.

The model of chapter II could be solved numerically with the actual variable fluid parameters α, κ, and ν. These are in principle functions of the total temperature but in practice, in this strongly stratified system, can be given quite accurately as functions of z alone. For small forcing we can thus obtain a linear problem again, but one with variable coefficients. Solution of this problem and of the corresponding problem for the nonlinear

corrections should be undertaken if more precise experiments are to be interpreted by such a theory.

A wide range of new theoretical problems opens up if we admit a second stratification agent, e.g., salt. We distinguish two types of such problems. There are truly laminar problems in which the greatly different diffusivities of heat and salt will be of prime importance. Thorpe, Hutt, and Soulsby (1969) have discussed what happens when a salt-stratified solution is heated uniformly from one side. If the stratification were thermal we should obtain just a nondivergent buoyancy layer, but the salt stratification leads to a double-diffusive instability and a series of flat cells which gradually push out into the interior. Such effects are likely to be central to any theory of source flows in such a fluid.

On the other hand, if we interpret the heat and salt diffusivities as eddy coefficients, with an eye to examining larger scale flows, and suppose them to be equal, we can combine the heat and salt conservation equations to get a similar conservation equation for density anomaly ρ':

$$\underline{u} \cdot \nabla \rho' + w(\rho_0 \beta \gamma_S - \rho_0 \alpha \gamma_T) = \kappa_E \nabla^2 \rho'$$

$$\rho' \equiv \rho_0(\beta S' - \alpha T')$$

in dimensional form, where K_E is the common eddy coefficient, T' is the temperature anomaly, S' is the salinity anomaly, α is the thermal expansion coefficient, β is the analogous coefficient for salinity and γ_T and γ_S are the mean gradients of temperature and salinity, respectively. Provided the density anomaly gradients are small relative to the mean stable density gradient, the equation can be linearized and the dynamical problem solved as in chapter II. One then has a subsidiary calculation to determine T' and S' from their conservation equations. If these fields are both strongly stratified, both conservation equations can be linearized and the calculation is simple. If only one field is strongly stratified the other must be computed by substituting the calculated velocities into its full conservation equation and solving the resulting linear problem with variable coefficients. The field in this case acts like a passive tracer, the density being influenced primarily by linearized advection of the strongly stratified field. If the unstratified field develops large gradients, advections of density anomaly become important and the dynamical problem is nonlinear at the outset.

The matter of including rotation in the model should be taken up, especially if comparisons to actual oceanic

situations are sought. The y-momentum equation must be retained in the basic set. Scaling as in chapter II then leads to a nondimensionalized Coriolis term γu in this equation and a term $-\gamma v$ in the x-momentum equation. Here $\gamma = 2\Omega/N_B$, where Ω is the (constant) rotation frequency and $N_B = \sqrt{g\alpha\gamma}$ is the Brunt-Väisälä frequency. Wunsch (1970) has shown how these terms, for $\gamma = O(1)$, can modify a nondivergent buoyancy layer. In important ocean regions, such as the main thermocline, the ratio γ may be fairly small and we can expect rotational effects to modify but not dominate the flow. This suggests one possible application of the theory. Suppose in the main thermocline a region of, say, 5 meters in depth gets mixed due to the breaking of an internal wave or some other cause and that in the surrounding fluid small-scale turbulence leads to eddy viscosity and eddy conductivity of $O(1 cm^2/sec)$. If N_B is 10^{-3} sec^{-1}, a reasonable value, we obtain $\epsilon \simeq 0.06$ and $\gamma \simeq 0.1$. $\delta = O(1)$ if the mixing is fairly complete, less if it is partial. These are values of δ and ϵ not unlike those of the laboratory experiment and γ is at least not huge. Perhaps the subsequent flow from such a region of disturbed temperature gradient would occur in a quasi-steady fashion and obey the dynamics of chapter II. We hasten to add that this is a speculation only, intended as a notion for further investigation.

The experimental apparatus should first be much improved. The basic size and operating values of stratification and forcing seem feasible enough, but a multitude of the author's errors in mechanical design make it an extremely difficult and tedious apparatus to operate. This is not the place to catalog these errors in detail but simply to note that such matters as levelling adjustments, cooling machinery occasional sidewall leakage, dye line visibility, and photographic technique all stand in need of attention and refinement if more and better data are to be collected. If a way can be devised to measure the small temperature anomalies in the presence of the large mean field it would add greatly to the experiments; the author has not been successful in finding such a method.

With an improved apparatus one could immediately drive the heat source harder and study the transition from the laminar convection cell to the turbulent plume which must occur at sufficiently strong forcing. All that is needed is to build a new, higher resistance heat source. One could try to make a salt source using a semipermeable membrane, or one could stratify the tank in salt and apply the existing heat source. It would also be interesting to study the effects of time-varible heating.

Appendix I Delta-function Sources

In previous analytical work on similar source flow problems the idea of delta-function sources has been used to simplify the mathematics. Koh (1966), in analyzing the flow from a mass source, assumed that what we have referred to as the far field balance applied everywhere and then matched a solution of the linear problem (II-74) to a condition $u(0,z) = \delta(z)$* This form of boundary condition also fixes T and w according to the far field balances and the net effect is thus to exclude any buoyancy layer. List (1971) has analyzed momentum sources simply by adding terms like $\delta(\vec{x})$ to the right sides of the momentum equations as inhomogeneous terms.

These approximations are useful, but one must use care in choosing the correct source condition to correspond to ones physical idea of how the flow is driven; the flow from the heat source is a case in point. One might reason intuitively that the localized heat source f(z) would produce, at large x, the same effects as a delta-function

---

* Koh's analytical method is different than ours. He transforms the linear far field equations into ordinary differential equations in the similarity variable τ of (II-97) and solves these numerically.

source of temperature anomaly. This is not the case; the far field should instead be approximated as being driven by a $\delta'(z)$ source of horizontal velocity. From (II-95), where we approximated $\bar{u}^{(0,1)}$ for large s:

$$\bar{u}^{(0,1)}(s,z) \simeq C_0 \int_0^\infty k e^{-k^3 s} \sin kz \, dk \quad ; \quad C_0 = \frac{\sqrt{2}}{\pi} \int_0^\infty f(z) dz$$

If this is assumed to hold for all s:

$$\bar{u}^{(0,1)}(0,z) = C_0 \int_0^\infty k \sin kz = -\pi C_0 \delta'(z)$$

which is exactly what we obtain if, like Koh, we solve (II-74) subject to $u(o,z) = -\pi C_0 \delta'(z)$. The expression (II-88) for the far field temperature anomaly, subjected to the same approximation, gives:

$$\bar{T}^{(0,1)}(0,z) = C_0 \int_0^\infty k \cos kz \, dk$$

which is not proportional to $\delta(z)$.

If we were to match a far field solution to a condition $T(0,z) = \delta(z)$ we would have:

$$T = \frac{1}{\pi} \int_0^\infty e^{-k^3 s} \cos kz \, dk$$

Then

$$u_{3z} = T_s = -\frac{1}{\pi} \int_0^\infty k^3 e^{-k^3 s} \cos kz \, dk$$

or

$$u = \frac{1}{\pi}\int_0^\infty e^{-k^3 s}\sin kz\, dk$$

From the usual rules for asymptotic estimation of Fourier transforms (Lighthill, p.56) we have for large z:

$$u \sim \frac{1}{\pi}\left[\frac{1}{z} + (\text{terms in } \frac{1}{z^n},\ n>1)\right]$$

and thus $\int_{z_0}^{\infty} u\, dz$, the net transport above some level z_0, is infinite. It is thus clear that the wrong choice of a delta-function source condition can lead to highly unphysical results. The reason of course is that the buoyancy layer is the physical agency which adjusts the far field to the actual source condition, and the far field mathematics cannot describe this adjustment. The actual source condition can be directly matched to far field solutions by a delta-function approximation only in those cases, such as Koh's, in which a buoyancy layer is not required, i.e., when the source condition is such as to introduce vertical velocities and temperature anomalies only in balance according to far field dynamics, or at least to introduce them out of such balance only at some higher order in the perturbation scheme.

Note There is a further peculiarity of Koh's solution which is not related to the use of delta-functions; the pressure anomaly is infinite at $s = +\infty$. This

fact was pointed out to the author by Dr. S. Martin. The singularity occurs because of the conflict between assuming a steady flow and assuming a steady source of mass; the "reservoir" has been "filling up" since $t = -\infty$. The singularity can be removed by specifying an equal and opposite source of mass (a sink) at $s = s_o$ and then letting s_o approach $+\infty$. The other fields are unchanged by this device.

Appendix II Full Linear Problem

It was mentioned on p.20 that the full linear problem posed by (II-23) can be solved by Fourier techniques. List (1971) has done this for certain delta-function sources by using a combination of residue theory and numerical integration to invert the Fourier integrals and has presented calculations for the case $\epsilon = O(1)$. We outline below a less subtle approach involving no contour integration. We begin with (II-23) applied to the streamfunction Φ defined by:

$$u = -\Phi_z \quad ; \quad \omega = \Phi_x$$

In the usual way we look for separable solutions proportional to cos kz and decaying in x. The general solution is a Fourier superposition of these:

$$\Phi = \int_0^\infty \left[c_1(k) e^{\lambda_1(k)x} + c_2(k) e^{\lambda_2(k)x} + c_2^*(k) e^{\lambda_2^*(k)x} \right] \cos kz \, dk \qquad \text{(AII-1)}$$

where * indicates complex conjugation. λ_1, λ_2, λ_2^* are the three roots with nonpositive real parts of the separability condition:

$$\lambda^6 - 3k^2\lambda^4 + 3k^4\lambda^2 - k^6 + \lambda^2\epsilon^{-4} = 0 \qquad \text{(AII-2)}$$

is real for $k \geq 0$.

The boundary conditions take the following forms.

$u(0,z) = 0$ gives:

$$C_1 + C_2 + C_2^* = 0 \tag{AII-3}$$

$w(0,z) = 0$ gives:

$$C_1\lambda_1 + C_2\lambda_2 + C_2^*\lambda_2^* = 0 \tag{AII-4}$$

$T(0,z) = f(z)$ gives:

$$h_1C_1 + h_2C_2 + h_2^*C_2^* = -\mathcal{F} \tag{AII-5}$$

where

$$h_i = \frac{\epsilon^2(\lambda_i^2 - k^2)^2}{\lambda_i}, \quad i = 1, 2 \tag{AII-6}$$

and

$$f(z) = \int_0^\infty \mathcal{F}(k) \cos kz \, dk \tag{AII-7}$$

(AII-5) is derived using the vorticity equation

$$\epsilon^2 \nabla^4 \Phi = -T_x \tag{AII-8}$$

obtainable from (II-16) and (II-17) with $\delta = 0$. The three simultaneous equations (AII-3) - (AII-5) give:

$$C_1 = \frac{\mathcal{F}(\lambda_2 - \lambda_2^*)}{D} \tag{AII-9}$$

$$c_2 = \frac{\mathcal{I}(\lambda_2^* - \lambda_1)}{D} \qquad \text{(AII-10)}$$

$$c_2^* = -\frac{\mathcal{I}(\lambda_2 - \lambda_1)}{D} \qquad \text{(AII-11)}$$

where

$$D = \begin{vmatrix} 1 & 1 & 1 \\ \lambda_1 & \lambda_2 & \lambda_2^* \\ h_1 & h_2 & h_2^* \end{vmatrix} \qquad \text{(AII-12)}$$

Expansion of D shows it to be imaginary, as it must be for (AII-10) and (AII-11) to hold.

With these expressions, and given a (not necessarily small) choice of ϵ and f(z), evaluation of (AII-1) is just a matter of algebra and numerical calculation of the integral. The other fields w, u, T can of course be written as similar integrals.

One reason for presenting this unwieldy, but exact, solution of the linear problem is to show that for small ϵ (AII-1) reduces to the solution found by boundary layer and perturbation methods in chapter II. From that work we know that there are two horizontal scales in the problem, the buoyancy layer scale and the far field scale. For

(AII-1) to exhibit these two scales one or more of the λ_i must be $O(\epsilon^{-1})$ and likewise one or more must be $O(\epsilon^2)$. We use this fact to find approximations for the λ_i. First let:

$$\hat{\lambda} = \epsilon\lambda$$

Then (AII-2) becomes:

$$\underline{\frac{\hat{\lambda}^6}{\epsilon^6}} - 3k^2\frac{\hat{\lambda}^4}{\epsilon^4} + 3k^4\frac{\hat{\lambda}^2}{\epsilon^2} + \underline{\frac{\hat{\lambda}^2}{\epsilon^6}} - k^6 = 0$$

and the underscored terms are the largest, for $k \lesssim O(\epsilon^{-1})$, so that we have, approximately:

$$\hat{\lambda}^6 + \hat{\lambda}^2 = 0$$

The two nontrivial roots leading to x-decay are the conjugate ones:

$$\hat{\lambda}_2 = e^{\frac{3\pi i}{4}}; \quad \hat{\lambda}_2^* = e^{-\frac{3\pi i}{4}} \qquad \text{(AII-13)}$$

The remaining root λ_1 must give the far field part of the solution. Rescale, letting:

$$\bar{\lambda} = \lambda\epsilon^{-2}$$

Thus (AII-2) becomes:

$$\epsilon^{12}\bar{\lambda}^6 - 3k^2\epsilon^8\bar{\lambda}^4 + 3k^4\epsilon^4\bar{\lambda}^2 + \underline{\bar{\lambda}^2} - \underline{k^6} = 0$$

and the underscored terms form the main balance, again for $k < O(\epsilon^{-1})$. The desired root is:

$$\bar{\lambda} = -k^3 \qquad \text{(AII-14)}$$

Alternatively we could obtain (AII-13) and (AII-14) by solving (AII-2) directly and expanding the results for small ϵ. With (AII-13) and (AII-14) (AII-12) gives:

$$D = \frac{2i}{\epsilon^2} + O(\epsilon k^3) \qquad \text{(AII-15)}$$

and (AII-9) - (AII-11) become:

$$c_1 \simeq \frac{\epsilon \mathcal{F}}{\sqrt{2}}, \quad c_2 \simeq \frac{\epsilon \mathcal{F} e^{3\pi i/4}}{2}; \quad c_2^* \simeq \frac{\epsilon \mathcal{F} e^{-3\pi i/4}}{2} \qquad \text{(AII-16)}$$

With (AII-13) - (AII-16) (AII-1) becomes:

$$\Phi \simeq \frac{\epsilon}{\sqrt{2}} \int_0^\infty \mathcal{F}(k) \left[e^{-k^3 s} - e^{-\zeta/\sqrt{2}} \left(\cos \zeta/\sqrt{2} + \sin \zeta/\sqrt{2} \right) \right] \cos kz \, dk \qquad \text{(AII-17)}$$

where s and ζ are as defined in (II-29). For $\zeta = O(1)$, $s = O(\epsilon^3)$, i.e., in the buoyancy layer, $e^{-k^3 s} \simeq 1$ until $k = O(\epsilon^{-1})$, and then $\mathcal{F}$ is very small. So approximately:

$$\Phi \simeq \frac{\epsilon}{\sqrt{2}} f(z) \left(1 - e^{-\zeta/\sqrt{2}} \left(\cos \zeta/\sqrt{2} + \sin \zeta/\sqrt{2} \right) \right) \qquad \text{(AII-18)}$$

For s= O(1), $\zeta = O(\epsilon^{-3})$, i.e., in the far field, $e^{-\zeta/r_2} \approx 0$ and (AII-17) becomes:

$$\Phi = \frac{\epsilon}{r_2} \int_0^\infty f(k) e^{-k^3 s} \cos kz \, dk \qquad \text{(AII-19)}$$

We see that (AII-18) and (AII-19) are just the linear buoyancy layer streamfunction $\hat{\psi}^{(0,1)}$ and the linear far field streamfunction $\bar{\psi}^{(0,1)}$, respectively.

Appendix III Computer Program

The computer program used to make the calculations for the plots in chapter II was one of the author's first attempts at the art; it does its job but is awkwardly written, and we present here only its essential features. The computations were performed at the MIT Information Processing Center on the IBM 360.

Values of the fields, when computed, were placed in two-dimensional arrays (array indices corresponding to values of x and z) prior to being printed out. The program begins by initializing all arrays to zero and then starts the calculation of the buoyancy layer fields; the array names correspond to the fields as follows: DLBL is $-\hat{T}^{(0,0)}$, WLBL is $\hat{w}^{(0,0)}$, ULBL is $\hat{u}^{(0,1)} + \bar{u}^{(0,1)}(0,z)$, SILBL is $\hat{\psi}^{(0,1)}$, and the same names with an "N" inserted are the corresponding nonlinear corrections in the buoyancy layer. The computation is performed for a cold source, $f(z) = -e^{-z^2}$:

```
C     NEXT WE READ LOOP PARAMETERS AND COMPUTE THE LINEAR
C     AND NONLINEAR BOUNDARY LAYER FIELDS AT THE POINTS IN
C     SPACE FIXED BY THESE PARAMETERS
   15 READ(5,2)IXLBL,IXUBL,INCXBL,IZLBL,IZUBL,INCZBL,
     1FACXBL,FACZBL
    2 FORMAT(6I10,2F10.5)
      FACXBL = FACXBL*0.70717
      DO 100 KK=IXLBL,IXUBL,INCXBL
```

```
      PHI=FACXBL*(KK-1)
      EX=EXP(-PHI)
      EXCOS=EX*COS(PHI)
      EXSIN=EX*SIN(PHI)
      DO 200 LL=IZLBL,IZUBL,INCZBL
      ZBL=FACZBL*(LL-1)
      PZLIN=EXP(-ZBL**2)
      DPZLIN=-2.0*ZBL*PZLIN
      PZNL =0.5*PZLIN*DPZLIN
      DPZNL=PZLIN*PZLIN*(4.0*ZBL*ZBL-1.0)
      DLBL(KK,LL)=PZLIN*EXCOS
      WLBL(KK,LL)=-PZLIN*EXSIN
      ULBL(KK,LL)=0.70717*DPZLIN*(1.0-EXCOS-EXSIN)
      SILBL(KK,LL)=-0.70717*PZLIN*(1.0-EXCOS-EXSIN)
      DNLBL(KK,LL)=PZNL*(EXCOS*(PHI-0.2)-0.6*EXSIN
     1+0.2*EX**2)
      WNLBL(KK,LL)=PZNL*(-0.6*EXCOS+EXSIN*(0.6-PHI)
     1+0.6*EX**2)
      UNLBL(KK,LL)=-1.41421*DPZNL*
     1(EXCOS*(0.7+0.5*PHI)+EXSIN*(0.5*PHI-0.4)-0.3*
     2EX**2-0.4)
      SINLBL(KK,LL)=1.41421*PZNL*
     1(EXCOS*(0.7+0.5*PHI)+EXSIN*(0.5*PHI-0.4)-0.3*
     2EX**2-0.4)
  200 CONTINUE
  100 CONTINUE
```

Some output statements follow and then we begin the routine which calculates the far fields by a trapezoidal rule:

```
C     WE READ LOOP PARAMETERS FIXING THE POINTS AT WHICH
C     THE FAR FIELDS WILL BE COMPUTED
   17 READ(5,7)BASE,FACZFF
    7 FORMAT(2F10.5)
      READ(5,8)IDIFF,NMAX,INC,IZLFF,IZUFF,INCZFF
    8 FORMAT(6I10)
      DO 300 MM+1,NMAX,INC
      INT=MM-IDIFF
      S=BASE**INT
      DO 400 NN=IZLFF,IZUFF,INCZFF
      ZFF=FACZFF*(NN-1)
      BIGK=0.0
      DELTAK=1.0
```

```
      COMP=0.0
C     HAVING FIXED ONE POINT, THE 50 LOOP SETS AN
C     APPROPRIATE UPPER LIMIT OF INTEGRATION AND THE
C     60 LOOP SETS AN INCREMENT OF THE INTEGRATION
C     VARIABLE T SMALL ENOUGH TO GIVE AN ACCEPTABLE
C     ERROR IN THE RESULT  THESE NUMBERS ARE ENTERED
C     IN ARRAYS AFTER STATEMENT 60 FOR REFERENCE
      DO 50 IX=1,100
      BIGK=0.5*IX
      COMP=COMP+S*BIGK**3+0.125*BIGK**2
      IF(COMP-30.0)50,55,55
   50 CONTINUE
   55 DO 60 IY=1,100
      DELTAK=DELTAK/2.0
      TESTNO=(BIGK*DELTAK**2)/12.0
      IF(TESTNO-1.0E-4)65,60,60
   60 CONTINUE
   65 NSTEP=IFIX(BIGK/DELTAK)
      UPLIMIT(MM,NN)=BIGK
      SPACE(MM,NN)=DELTAK
      LOOPNO(MM,NN)=NSTEP
      T=0.0
      SILFF(MM,NN)=-0.199471*DELTAK
C     THE ACTUAL INTEGRATION BY TRAPEZOIDS BEGINS HERE
C     AND CONTINUES THROUGH STATEMENT 300
      DO 550 III=1,NSTEP
      T=T+DELTAK
      TRIG1=COS(T*ZFF)
      TRIG2=SIN(T*ZFF)
      EXPNT=EXP(-0.125*T**2)
      AMPL=-0.398943*EXPNT**2
      AMPNL=-0.0282095*T*EXPNT
      FAC=EXP(-(T**3)*S)
      DLFF(MM,NN)=DLFF(MM,NN)-T*AMPL*FAC*TRIG1*DELTAK
      WLFF(MM,NN)=WLFF(MM,NN)-(T**3)*AMPL*FAC*TRIG1*DELTAK
      ULFF(MM,NN)=ULFF(MM,NN)+T*AMPL*FAC*TRIG2*DELTAK
      SILFF(MM,NN)=SILFF(MM,NN)+AMPL*FAC*TRIG1*DELTAK
      DNLFF(MM,NN)=DNLFF(MM,NN)+T*AMPNL*FAC*TRIG2*DELTAK
      WNLFF(MM,NN)=WNLFF(MM,NN)+T**3*AMPNL*FAC*TRIG2*DELTAK
      UBLFF(MM,NN)=UNLFF(MM,NN)+T*AMPNL*FAC*TRIG1*DELTAK
      SINLFF(MM,NN)=SINLFF(MM,NN)-AMPNL*FAC*TRIG2*DELTAK
  550 CONTINUE
```

There follow 8 statements which reduce each far field array by one half the last increment so that the area of the last trapezoid is not added twice, and then the 300 CONTINUE

and 400 CONTINUE statements terminate the loops. These far field array names have the same pattern as the buoyancy layer array names. The upper limit of integration BIGK is chosen such that the integrands are $O(e^{-30})$ there. The choice of DELTAK, the spacing in k of the bases of the trapezoids, is taken from Hildebrand's (p. 75) error criterion for this method:

$$|E| = \frac{(b-a)^3}{12n^2} |f''(x)|$$

where (a,b) is the interval of integration, n is the number of points at which the integrand is calculated, and f"(x) is the value of the second derivative of the integrand somewhere in the interval. If f" is bounded the error goes to zero as $n \to \infty$. To check that our ad hoc choice of a limit for this error was satisfactory, additional computations (not shown) were made in which the integrals were simply computed again and again at successively smaller values of DELTAK until the results stabilized. No significant differences between these results and the ones from the program listed above were observed. The amplitudes of the nonlinear corrections in the far field (proportional to AMPNL above) were computed too small by a factor of two; this has been adjusted in making the plots of chapter II.

Appendix IV Influence of a Sidewall

We write the linear equations of motion in the usual nondimensional far field form but retain y-dependence, where y is distance perpendicular to a sidewall, made nondimensional with L.

$$0 = -p_s + u_{yy} + u_{zz} + \epsilon^4 u_{ss} \tag{AIV-1}$$

$$0 = -p_y + \epsilon^2 (v_{yy} + v_{zz} + \epsilon^4 v_{ss}) \tag{AIV-2}$$

$$0 = -p_z + T + \epsilon^2 (w_{yy} + w_{zz} + \epsilon^4 w_{ss}) \tag{AIV-3}$$

$$0 = \epsilon^2 u_s + v_y + w_z \tag{AIV-4}$$

$$0 = -w + \epsilon^2 (T_{yy} + T_{zz} + \epsilon^4 T_{ss}) \tag{AIV-5}$$

We use these to find a boundary layer solution, i.e., one which vanishes as $y \to \infty$, capable of adjusting the interior velocity to zero at the sidewall. This interior velocity we take to be the linear horizontal far field velocity $\bar{u}^{(0,1)}$ of the two-dimensional problem; we ignore the much smaller two-dimensional vertical velocity. Expanding variables in power series in ϵ in the standard

way we find from (AIV-2):

$$p_y^{(0)} = p_y^{(1)} = 0 \qquad \text{(AIV-6)}$$

and thus for a boundary layer solution:

$$p^{(0)} = p^{(1)} = 0 \qquad \text{(AIV-7)}$$

Then from (AIV-3):

$$T^{(0)} = T^{(1)} = 0 \qquad \text{(AIV-8)}$$

(AIV-5) now shows that w is $O(\epsilon^4)$ at most, and thus from (AIV-4) we see that v is at most $O(\epsilon^2 u)$. $\bar{u}$ will be $O(\epsilon)$ since this is the magnitude of the interior velocity, so $v \leq O(\epsilon^3)$. (AIV-2) then shows $p \leq O(\epsilon^5)$. Thus to find $u^{(1)}$ we have only to solve the reduced form of (AIV-1):

$$u_{yy}^{(1)} + u_{zz}^{(1)} = 0 \qquad \text{(AIV-9)}$$

The appropriate solution is:

$$u^{(1)} = -\int_0^\infty f^{(a,1)}(k)\, e^{-k^3 s} e^{-ky} \sin kz \, dk \qquad \text{(AIV-10)}$$

and thus the total velocity is:

$$\bar{u}^{(0,1)} + u^{(1)} = \int_0^\infty f^{(0,1)}(k)\, e^{-k^3 s}(1-e^{-ky}) \sin kz \, dk \qquad \text{(AIV-11)}$$

Some machine calculations of (AIV-11) were made, but it is a simple matter to show analytically that (AIV-10) constitutes a small correction to $\bar{u}^{(0,1)}$ along the centerline of the tank where observations are made. Set s = 4, corresponding to the end of the tank opposite the source, and set y= 20, corresponding to the centerline. Set z = 2.5, corresponding to the level of maximum $u^{(0,1)}(4,z)$, for the e^{-z^2} source. Then (AIV-10) is:

$$u^{(1)} = -\frac{1}{\sqrt{2\pi}} \int_0^\infty k e^{-k^2/4} e^{-4k^3} e^{-20k} \sin 2.5k \, dk \qquad \text{(AIV-12)}$$

Now

$$e^{-20k} \le 1 - 6\tfrac{1}{3}k \,, \quad 0 \le k \le 0.15$$

$$e^{-20k} \le 0.05 \,, \quad k \ge 0.15$$

$$\sin 2.5k \le 2.5k \,, \quad k \ge 0$$

So an upper bound for $|u^{(1)}(4,2.5)|$ is:

$$|u^{(1)}(4,2.5)| \le \frac{1}{\sqrt{2\pi}} \int_0^{0.15} k(1-6\tfrac{1}{3}k)(2.5k)\, dk$$

$$+ \frac{1}{\sqrt{2\pi}} \int_{0.15}^\infty k e^{-k^2/4} e^{-4k^3} (0.05) \sin 2.5k \, dk$$

The first term is about 3.25×10^{-4} and the second is

obviously less than $0.05\left|u^{(0,1)}(4,2.5)\right|$, so:

$$\left|u^{(1)}(4,2.5)\right| \leq 3.25\times10^{-4} + 0.05\,\bar{u}^{(0,1)}(4,2.5)$$

Since $\bar{u}^{(0,1)}(4,2.5) = 7.5 \times 10^{-2}$, the relative error is

$$\frac{\left|u^{(1)}(4,2.5)\right|}{\bar{u}^{(0,1)}(4,2.5)} \leq 4.33\times10^{-3} + 0.05$$

i.e., less than about 5%. In short, this boundary layer makes the required adjustment of velocity while introducing small alterations of observed values of $\bar{u}^{(0,1)}$ and quite negligible alterations of the other dependent variables.

Bibliography

Defant, A. (1961) Physical Oceanography, v.1. pp. 105-108, Pergamon Press, New York.

Hildebrand, F.B. (1956) Introduction to Numerical Analysis, p. 75, McGraw - Hill, New York.

International Critical Tables (1928) v. 3, pp. 25-26, v. 5, p. 10, p. 227, McGraw - Hill, New York.

Koh, R.C.Y. (1966) Viscous stratified flow toward a sink. J. Fluid Mech., 24, 555.

Lighthill, M.J. (1962) Fourier Analysis and Generalized Functions, 79 pp., University Press, Cambridge.

List, E.J. (1971) Laminar momentum jets in a stratified fluid. J. Fluid Mech., 45, 561.

Simon, I. and P.F. Strong (1968) Measurements of static and dynamic response of the Green Building at the M.I.T. campus to insolation and wind. Bull. Seis. Soc. Amer., 58, 1631.

Sverdrup, H.U., M.W. Johnson and R.H. Fleming (1942) The Oceans, pp. 503-507, Prentice - Hall, Englewood Cliffs, N.J.

Thorpe, S.A., P.K. Hutt and R. Soulsby (1969) The effect of horizontal gradients on thermohaline convection. J. Fluid Mech., 38, 375.

Veronis, G. (1967a) Analogous behavior of homogeneous, rotating fluids and stratified, non-rotating fluids. Tellus, 19, 326.

Veronis, G. (1967b) Analogous behavior of rotating and stratified fluids. Tellus, 19, 620.

Wunsch, C.I. (1970) On oceanic boundary mixing. Deep-Sea Res., 17, 29.

Wüst, G. (1959) Remarks on the circulation of the intermediate and deep water masses of the Mediterranean Sea and the methods of their further exploration. Ann. dell'Inst. Univ. Navale di Napoli, 28, 1.

Bibliography (cont'd.)

Wüst, G. (1960) Die Tiefenzirkulation Des Mittelländischen Meeres in den Kernschichten des Zwischen- und des Tiefenwassers, D. Hydrog. Z., 13, 105.

Wüst, G. (1961) On the vertical circulation of the Mediterranean Sea. J. Geophys. Res., 66, 3261.

Biographical Note

The author was born on January 15, 1943 in Washington, D.C., and received his early education in the elementary schools of Shoreham, N.Y. and Greenwich, Conn. and in the high school of Bernardsville, N.J., from which he graduated in 1960. He attended Amherst College, majored in physics, and received his A.B. degree in 1964. After one year of graduate study as a teaching assistant in physics at the University of California at Berkeley, the effects of two summers at Woods Hole had their influence and he entered the oceanography program at M.I.T. in the fall of 1965. He is a member of Phi Beta Kappa and of Sigma Xi. In 1966 he married the former Dorothy Hall of Woodbridge, Conn. They have one daughter, Leila Elizabeth.